THE OPTICAL PROPERTIES OF HIGH-T_c SUPERCONDUCTORS GROWN BY PULSED LASER DEPOSITION

By

Robert Hughes, B.Sc., M.Sc.

A Thesis

Submitted to the Faculty of Graduate Studies

in Partial Fulfilment of the Requirements

for the Degree

Doctor of Philosophy

McMaster University

September 1992

THE OPTICAL PROPERTIES OF HIGH-T_c SUPERCONDUCTORS GROWN BY PULSED LASER DEPOSITION

DOCTOR OF PHILOSOPHY(1992) McMASTER UNIVERSITY
(Physics) Hamilton, Ontario

TITLE: The Optical Properties of High-T_c Superconductors Grown by Pulsed Laser Deposition

AUTHOR: Robert Hughes, B.Sc. (Lakehead University)
M.Sc. (McMaster University)

SUPERVISOR: Dr. T. Timusk

NUMBER OF PAGES: ix, 140

ABSTRACT

The discovery of superconductivity at temperatures in excess of 30 K has led to an unprecedented effort in both fundamental and materials research. Four separate projects will be presented here which encompass both types of research. The first two involve the deposition of superconducting thin films by the pulsed laser deposition technique. The final two projects use optical spectroscopy to probe the fundamental excitations which govern these exotic materials. All four projects are summarized below.

Superconducting $(Pb_{0.75}Cu_{0.25})Sr_2(Y_{1-y}Ca_y)Cu_2O_7$ films were successfully deposited by pulsed laser deposition. The films are grown *in situ* on (100) $LaAlO_3$ at the relatively low substrate temperature of 620 °C. The films are highly oriented with their c-axis perpendicular to the substrate and exhibit a surface morphology which is unique to the oxide superconductors. The growth procedure used yields relatively sharp superconducting transitions and a maximum T_c that exceeds all other reported values. By substituting Ca for Y it is possible to systematically vary the superconducting transition temperature from 10 K to a maximum of 86 K.

The laser deposition system was also used to deposit superconducting $Nd_{1.85}Ce_{0.15}CuO_{4+\delta}$ thin films. By carefully controlling the film's oxygen content through high temperature vacuum anneals it is possible to obtain a superconductor with a transition temperature which onsets at 21 K. The high temperature anneal can result in a film surface which is copper deficient. By optimizing the growth parameters we have been able to eliminate this layer resulting in films with superior homogeneity. The films are highly oriented with their c-axis perpendicular to the substrate and show a surface morphology of high quality.

The far infrared optical properties of the $Nd_{1.85}Ce_{0.15}CuO_{4+\delta}$ films were mea-

sured using Michelson interferometry. The reflectance spectra clearly show the presence of a ledge at 420 cm^{-1} offering further evidence that this feature is common to all the cuprate superconductors. The optical conductivity obtained from Kramers-Kronig analysis can be divided into two components. The first component, which is strongly temperature dependent, is fit to a Drude model. This fit indicates that $Nd_{1.85}Ce_{0.15}CuO_{4+\delta}$ has a constant plasma frequency and a temperature dependent scattering rate which closely follows the temperature dependence exhibited by the dc resistivity. The second component shows little temperature dependence and is described by a model which couples phonons to a midinfrared band. Comparisons between the optical conductivity and the structures seen by tunneling and inelastic neutron scattering measurements are made.

In the final project, the far infrared reflectance of partially transparent $(Pb_{0.75}Cu_{0.25})Sr_2(Y_{0.4}Ca_{0.6})Cu_2O_7$ films were measured. As was the case for $Nd_{1.85}Ce_{0.15}CuO_{4+\delta}$, the normal state results were described in terms of the two component model. Once again, the Drude component showed a constant plasma frequency and a scattering rate which closely follows the temperature dependence of the dc resistivity while the second component showed only a small change as the temperature was varied. In the superconducting state the reflectance spectra do not exhibit the clean limit behaviour that has been observed in the other oxide superconductors. A measurable fraction of the Drude component's oscillator strength does not condense into the delta function which creates the possibility of observing structure associated with a superconducting energy gap.

ACKNOWLEDGEMENTS

I would like to thank my supervisor, Dr. Timusk, for the opportunity to work in his lab and for many helpful insights and suggestions. All of the work presented here has been done in collaboration with John Preston. He has essentially been a second supervisor, providing many useful ideas that have allowed this research to progress at a much faster rate. I appreciate all of his help and am grateful for the interest he took in my research.

The two people I am most grateful to are Ho Fan Jang and Yong Lu. Ho Fan took an active interest in my research, spending countless hours helping me perform tasks and providing me with useful insights and ideas. This took place during my first few years at McMaster when the help was needed most. Lu provided much of the expertise and experience needed to make the thin film project work.

Many people have helped make the far infrared optical measurements easier to perform and understand. Maureen Reedyk and Dave Crandles have given me much help in every stage of my research and I have profited greatly from their lab work and experience. The computer expertise and technical assistance of Andy Duncan was invaluable in both the data acquisition and analysis. I am grateful to Thomas Strach for helping me with my PSYCCO analysis. I would like to thank Andrew McConnell for performing the reflectance measurement on the $LaAlO_3$ substrate. I have also benefited from the work and advice of Xiucheng Wu, Ning Cao, Chris Rymaszewski, Doug Bonn, Barb Zvan and Chris Homes. I would also like Jake Vanderwal, Tadek Olech, Gord Hewitson, Tom Krause and Yuebin Ning, who have all worked in the nearby labs and have given me a considerable amount of help.

I would like to thank Eddy Guzzo, Brian Challis, Thomas Strach, Andrew McConnell, Mark Antaya and Darcy Poulin for their tolerance of my continuous use of the excimer laser, their help, and for making the laser processing lab a very entertaining place to work. Everyone who works in this lab is indebted to Frank

Hegmann for making sure that it is never cluttered with excess equipment.

The technical nature of the projects I have undertaken has meant that I have had to rely on the expertise of a great many people. My entire project was dependent upon the construction of equipment by the machine shop. I would like to thank Gino Innocente, Venice Perno, Clee Berwick and Michael Roberts for their careful machining, helpful suggestions and for more than a few emergency repairs. I am grateful to Valdis Cers, George Zibens and Roger Periard for work done in the electronics shop. It is almost impossible to do materials research at McMaster without receiving some help from Jim Garrett. This help is greatly appreciated. I would also like to thank Bill Scott and Gord Hewitson for the many litres of liquid helium they have supplied over the years. The work of Christina Broadley and George Timko at chemical stores is also appreciated.

The characterization of the thin films produced was an invaluable service. I would like to thank W. H. Gong and K. Teeter for the x-ray work, J. Hudak for the SEM images, F. Pearson for both the TEM sample preparation and EDX analysis, J. McAndrew for the ICP results, D. Stevanovic for the RBS data and D. Poulin for the inductance measurements.

This work has benefited from discussions with some very knowledgeable people. I would like to thank Antonne Dabkowski, Hanna Dubkowska, Simon Xue, John Greedan, Jules Carbotte and John Zasadinski for their input.

I would like to thank Marg Wilby, Wendy Malerek, Rose McNiece and Jane Hammingh for keeping things organized and for helping me deal with the necessary, but much hated paperwork.

I would like to thank all of the people, past and present, who have played on the Liquid State baseball team for providing me with a great deal of entertainment. I would also like to thank Chris Rymazewski, Eddy Guzzo, Andy Duncan, Bruce Gaulin, Frank Hayes, John Preston and Bruce Takasaki for giving me the opportunity to educate them about the sport of hockey; a subject they know so very little about.

I would like to thank my family for their love and support. Their many visits and phone calls were greatly appreciated. I'd especially like to thank Karen and Bruce for providing many welcome breaks from my work and for more barbecues and show tunes than any one person deserves.

To My Family

TABLE OF CONTENTS

CHAPTER I
INTRODUCTION

I. INTRODUCTION

Superconductivity is one of solid state physics' most fascinating phenomena. When a superconductor is cooled below its critical temperature, T_c, it undergoes a phase transition which results in the complete loss of electrical resistance. In addition to this ability of allowing current to flow without dissipation, there exists one other phenomenon which sets a superconductor apart from other materials. This is the ability to expel magnetic fields passing through it once its temperature is lowered below T_c. This is referred to as the Meissner effect.

The phenomenon of superconductivity was discovered in 1911 by Kamerlingh Onnes[1] in elemental mercury for temperatures below 4.25 K. It was soon realized that superconductivity was a common phenomenon, but it was restricted to the low temperature regime. For example, almost half of the elements on the periodic table will superconduct under various conditions, but the highest superconducting transition temperature is found in niobium with $T_c = 9.26$ K. The cumbersome and expensive cryogenics required to maintain a material at these low temperatures severely limited the widespread use of superconductors in an array of technological applications. Finding a superconductor with a higher transition temperature was a very attractive prospect.

The search for higher transition temperatures turned out to be a difficult task. Thousands of superconductors were discovered, but by the end of 1985 the highest transition temperature recorded was only 23.2 K.[2] This was discovered in 1973 in Nb_3Ge, which belongs to a class of materials referred to as the A15 compounds. In the years following this discovery the search for higher critical temperatures turned to more complex materials. In early 1986, this search paid dividends. The

landmark discovery of J. G. Bednorz and K. A. Müller showed the onset of superconductivity occurring at 35 K in a multiphase La-Ba-Cu-O compound.[3] The superconducting phase was later identified as $La_{2-x}Ba_xCuO_4$[4] with the highest T_c occurring for the composition with x = 0.15. Once this discovery became known to the scientific community, many researchers began producing variations of the original compound in the hope of obtaining higher T_c's. This hope was realized when Wu *et al.*[5] discovered superconductivity above 90 K in a multiphase Y-Ba-Cu-O compound. The superconducting phase was later identified as $YBa_2Cu_3O_{7-\delta}$.[6] This compound is of greater interest since its higher T_c makes the use of inexpensive liquid nitrogen as a refrigerant feasible.

The unit cell of the $YBa_2Cu_3O_{7-\delta}$ compound is shown in Fig 1.1. It consists of three primitive perovskite cells stacked upon one another. The copper and oxygen atoms form two distinct structures within the lattice. They are commonly referred to as the planes and the chains. The CuO_2 planes seemed to be the ingredient common to all of the oxide superconductors while the chains are unique to $YBa_2Cu_3O_{7-\delta}$. Removal of oxygen from the chain sites can render $YBa_2Cu_3O_{7-\delta}$ non-superconducting while at the same time transforming the material from a poor metal to a semiconductor. Many of the other oxide superconductors also show this high sensitivity to the oxygen stoichiometry.

After the discovery of $YBa_2Cu_3O_{7-\delta}$ four other families of high temperature superconductors were found. They are the Bi-Sr-Ca-Cu-O,[7] Tl-Ba-Ca-Cu-O,[8] Pb-Sr-Y-Ca-Cu-O[9] and Nd-Ce-Cu-O[10] families, with T_c's as high as 105 K, 120 K, 85 K and 23 K respectively. The two compounds which have higher T_c's than $YBa_2Cu_3O_{7-\delta}$ have proved to be more difficult to synthesize. As a result $YBa_2Cu_3O_{7-\delta}$ has become the most widely studied superconductor for both basic and applied research.

Even though the $YBa_2Cu_3O_{7-\delta}$ superconductor is not the main focus of this research, it is impossible to discuss any results on other oxide superconductors without making direct comparisons to similar experiments performed on this com-

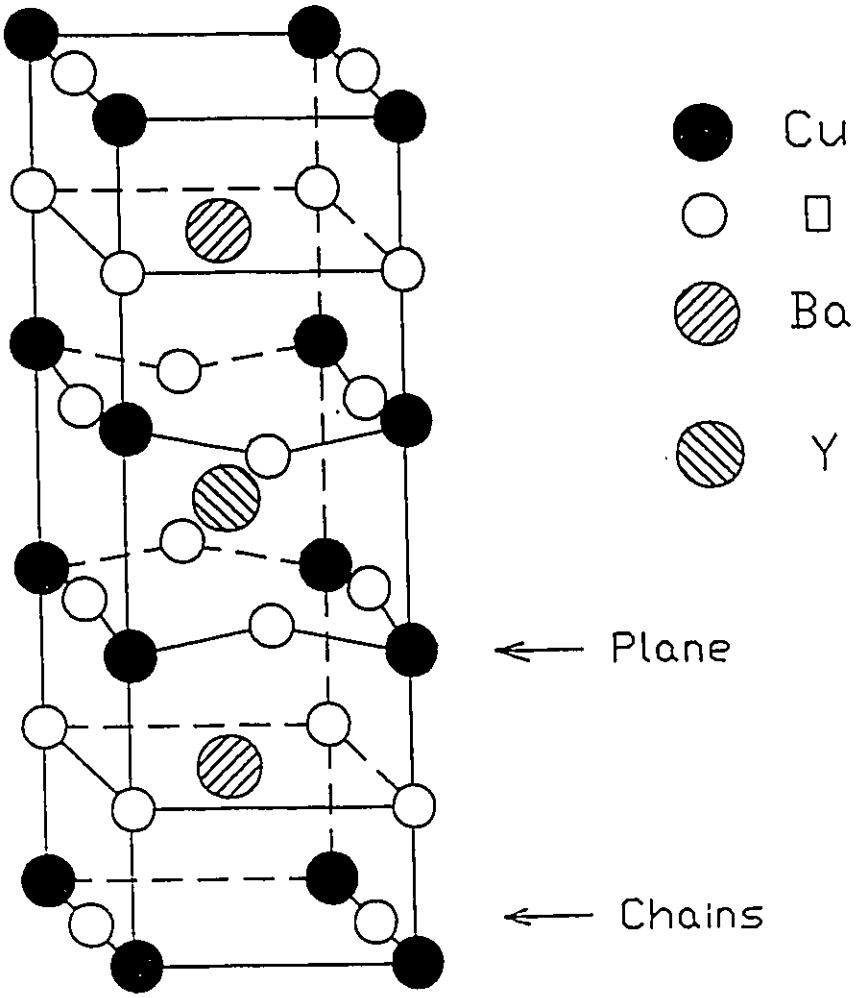

Fig. 1.1 Orthorhonıbic crystal structure of $YBa_2Cu_3O_{7-\delta}$ with lattice parameters a = 3.820 Å, b = 3.892 Å and c = 11.688 Å. Note the presence of both CuO_2 planes and CuO chains within the stucture.

pound. As a result, much of this chapter will be devoted to reviewing the research performed on $YBa_2Cu_3O_{7-\delta}$ in the areas of interest. The two areas of interest are the optical properties of the oxide superconductors and the growth of high temperature superconducting thin films by pulsed laser deposition. The remainder of the chapter will provide the necessary background for the analysis of optical data as well as a brief description of the materials studied.

II. THE OPTICAL PROPERTIES OF THE HIGH TEMPERATURE SUPERCONDUCTORS

EXTRACTING INFORMATION FROM REFLECTANCE SPECTRA

For a material to reflect or absorb light the incident electromagnetic radiation must interact with it. Thus, the extent to which the light interacts at a particular frequency must provide information about the material. This is the essence of optical spectroscopy. The optical conductivity is the most direct measure of the processes governing these interactions between light and matter. The type of information which can be extracted from this parameter will be discussed in future sections. Here we will develop the formalism for extracting this parameter from reflectance spectra.

The optical conductivity $\sigma(\omega)$ and the dielectric function $\epsilon(\omega)$ are related by the formula,

$$\epsilon(\omega) = \epsilon_\infty + \frac{4\pi}{\omega} i\sigma(\omega) \tag{1.1}$$

where, ϵ_∞ is the high frequency dielectric constant and ω is the frequency of the light. Both, the optical conductivity and the dielectric function are comprised of real and imaginary parts:

$$\sigma(\omega) = \sigma_1(\omega) + i\sigma_2(\omega) \tag{1.2}$$

$$\epsilon(\omega) = \epsilon_1(\omega) + i\epsilon_2(\omega) \tag{1.3}$$

The reflectance at normal incidence is related to the dielectric function by,

$$R = \frac{\sqrt{\epsilon_1^2 + \epsilon_2^2} + 1 - \sqrt{2(\sqrt{\epsilon_1^2 + \epsilon_2^2} + \epsilon_1)}}{\sqrt{\epsilon_1^2 + \epsilon_2^2} + 1 + \sqrt{2(\sqrt{\epsilon_1^2 + \epsilon_2^2} + \epsilon_1)}}. \tag{1.4}$$

$\epsilon_1(\omega)$ and $\epsilon_2(\omega)$ (or $\sigma_1(\omega)$ and $\sigma_2(\omega)$) describe the underlying excitations governing the optical properties. The fact that they are related to the reflectance in such a complex manner gives some indication of the difficulty in obtaining information directly from the reflectance spectra.

It is obvious that additional information is required to extract $\epsilon_1(\omega)$ and $\epsilon_2(\omega)$ from the reflectance spectra since they represent two unknowns in Eqn. 1.4. This information comes from the Kramers-Kronig transformations. They arise from the causality condition being imposed upon a linear response function. The result is a relationship which relates the real and imaginary parts of a linear response function. The Kramers-Kronig transformation used here provides a means of calculating the phase difference between the incident and reflected light. It is given by,

$$\theta(\omega) = -\frac{\omega}{\pi}\int_0^\infty \frac{\ln R(\omega') - \ln R(\omega)}{\omega'^2 - \omega^2} d\omega'. \tag{1.5}$$

It is immediately evident that the reflectance and phase are related in an intricate manner. The phase at a particular frequency is not only dependent on the reflectance at that frequency, but depends on the reflectance at all other frequencies. Thus, the far infrared optical properties are partly governed by the optical properties in the ultraviolet. This effect is minimized by the fact that the denominator is essentially a weighting factor which is biased towards nearby frequencies. Eqn.

1.5 demands that the reflectance must be known at all frequencies in order to calculate the phase at a single frequency. Obviously, a measurement of this kind is impossible. To circumvent this problem appropriate extrapolations must be used. It is found that these approximations effect the magnitude of the phase, but have little effect upon the shape or position of the frequency dependent features. Once $\theta(\omega)$ has been calculated $\epsilon_1(\omega)$ and $\epsilon_2(\omega)$ can be determined using,

$$\epsilon_1 = n^2 - k^2 \tag{1.6}$$

and

$$\epsilon_2 = 2nk \tag{1.7}$$

where,

$$n = \frac{1-R}{1+R-2\sqrt{R}cos\theta} \tag{1.8}$$

and

$$k = \frac{-2\sqrt{R}sin\theta}{1+R-2\sqrt{R}cos\theta}. \tag{1.9}$$

n and k are the real and imaginary parts of the index of refraction. Once, $\epsilon_1(\omega)$ and $\epsilon_2(\omega)$ are known the real part of the optical conductivity, which is the parameter of most interest here, can be calculated using Eqn. 1.1. A comprehensive analysis of these fundamental concepts is given by Wooten[11] and Palik.[12]

THE OPTICAL PROPERTIES OF CONVENTIONAL SUPERCONDUCTORS

Before presenting a brief review of the optical properties of the oxide superconductors it is worthwhile to present a summary of the optical properties of conventional superconductors. This provides a comparison which will illustrate the exotic nature of the high-T_c superconductors. This section will begin with a

description of the normal state properties of simple metals followed by an examination of the changes the material undergoes as it becomes a superconductor.

THE NORMAL STATE

The fact that free electrons strongly interact with electromagnetic radiation accounts for the high reflectivity in metals. This behaviour can be adequately described by the classical Drude model. It treats the conduction electrons as free electrons subject to a scattering mechanism. When these electrons are accelerated by light's oscillating electric field they will undergo forced oscillations described by the equation of motion:

$$m\frac{d^2x}{dt^2} + m\Gamma\frac{dx}{dt} = eE \tag{1.10}$$

where m is the mass of the electron, Γ is the scattering rate, e is the charge on the electron and E is the time dependent electric field of the incident light. By solving for x, the polarization (P) can be calculated using,

$$P = nex \tag{1.11}$$

where n is the electron carrier density. Now, all of the optical constants can be calculated, since the dielectric constant is equal to:

$$\epsilon = 1 + 4\pi\frac{P}{E} \tag{1.12}$$

Solving for the real part of the optical conductivity gives,

$$\sigma_1^{DR}(\omega) = \frac{\sigma_o}{1 + \omega^2/\Gamma^2} \tag{1.13}$$

Thus, a fit to $\sigma_1(\omega)$ obtained from reflectance measurements gives values for the scattering rate (Γ) and the dc conductivity (σ_o). From this information the plasma frequency can be calculated using,

$$\omega_p = \sqrt{4\pi\Gamma\sigma_o} \tag{1.14}$$

which also yields the ratio of the carrier concentration to the effective mass (m^*) since,

$$\omega_p = \sqrt{\frac{4\pi ne^2}{m^*}}. \tag{1.15}$$

A measurement of the reflectivity as a function of temperature should yield the temperature dependence of all these quantities.

Often the optical properties of simple metals do not adhere to the predictions set forth by the Drude model. The cause of this is usually interband transitions. These transitions can be described by an oscillator where there exists forced vibrations of bound electrons. The equation of motion is given by,

$$m\frac{d^2x}{dt^2} + kx + m\Gamma\frac{dx}{dt} = eE. \tag{1.16}$$

The second term is a restoring force where k is the spring constant and the third term describes the damping of the oscillations. Solving the above equation and using the result to calculate the real part of the conductivity gives,

$$\sigma_1^{OSC}(\omega) = \frac{1}{4\pi}\frac{\Gamma\omega_p^2\omega^2}{(\omega_o^2 - \omega^2)^2 + \Gamma^2\omega^2}. \tag{1.17}$$

Γ, ω_p and ω_o describe the oscillators width, strength and center frequency respectively. When both oscillator(s) and free electrons are present the total conductivity is the sum of the components:

$$\sigma_1^{TOT}(\omega) = \sigma_1^{DR}(\omega) + \sigma_1^{OSC}(\omega) \tag{1.18}$$

Phonon structure can also appear in the far infrared spectra of simple metals. Even though they show up as weak features, they are significant, since phonons are responsible for superconductivity in conventional superconductors. The phonon

features originate from the Holstein process,[13,14,15] whereby a charge carrier absorbs a photon and emits a phonon. Both an electron and a phonon are required in this absorption process if momentum is to be conserved.

THE SUPERCONDUCTING STATE

The superconducting phase transition transforms a metal to a state which is more energetically favourable than the free electron Fermi gas. Bardeen, Cooper and Schrieffer proposed a theory describing this state in 1957.[16] They postulated the existence of an ordered state which arises from the attractive interaction between pairs of electrons. These so-called Cooper pairs are comprised of two electrons with equal and opposite momentum and spin. The source of attraction which binds them is the electron-phonon interaction. An electron moving through a crystal will cause a lattice deformation due to the coulombic interaction between the positive ions and negative electron. The electron quickly vacates this region leaving behind ions which oscillate in phase around their equilibrium position; a phonon has been created. As the ions approach each other, they will produce a region of enhanced positive charge. A second electron will be attracted towards this region. The net result is an attractive interaction between two electrons mediated by a phonon.

By examining the predictions of Bardeen, Cooper, Scrieffer (BCS) theory, it is easy to see why far infrared spectroscopy has become an important tool in the study of the superconducting state. One of the most fundamental predictions of BCS theory is the existence of an energy gap, whereby the ratio of the size of the energy gap (2Δ) to the critical temperature is equal to a constant. This is given by,

$$\frac{2\Delta}{k_B T_c} = 3.54 \tag{1.19}$$

where, k_B is Boltzmann's constant. Conventional superconductors, more or less,

adhere to this prediction with strong coupling materials such as mercury showing the most deviation ($2\Delta/k_BT_c = 4.6$). The energy required to excite carriers across this gap lie at the lower extreme of the energies accessible to far infrared spectroscopy. Thus, a feature associated with the energy gap should be visible in the infrared spectrum. In addition, the Holstein absorption process described above, should become sharper and shift to higher energies by an amount 2Δ. The Holstein process requires this additional energy in order to break a Cooper pair.

The pioneering work of Tinkham showing the far infrared transmission[17,18] spectra of lead and tin films provided part of the experimental basis needed to confirm BCS theory. Performing this task required a comprehensive analysis of the optical properties using the BCS formalism. This work was done by D. C. Mattis and J. Bardeen.[19] They calculated the optical conductivity for the superconducting state which provides enough information to calculate all of the optical properties. When this calculation is performed at zero kelvin it shows distinct features in the real part of the optical conductivity. At zero frequency there is a delta function which describes the infinite conductivity observed in dc resistivity measurements. Between zero frequency and 2Δ the conductivity is equal to zero. Zero conductivity implies that no absorption is possible which is the expected result since there are no states in the gap to excite carriers into. For energies in excess of 2Δ excitation states become available and as a result the conductivity rises rapidly and then slowly merges to the values observed in the normal state. For frequencies well above the energy gap the optical properties of the superconducting and normal states are identical.

Any changes to the optical conductivity that a sample undergoes as its temperature is varied must conform to the restrictions set forth by the oscillator strength sum rule given by,

$$\int_0^\infty \sigma_1(\omega')d\omega' = \frac{\omega_p^2}{8} \tag{1.20}$$

where ω_p is the plasma frequency. It demands that the area under the σ_1 versus

frequency curve remain constant. Thus, as the sample becomes superconducting the area removed due to the formation of the energy gap must reside underneath the delta function at zero frequency. Likewise, in the normal state when the sample undergoes a reduction in its free carrier scattering rate resulting in a Drude peak of reduced width, the height of the peak must increase so that there is no lost area. In addition, a partial oscillator strength sum rule is defined in an equivalent manner except that the integral is calculated from zero to ω. It is used as a measure of the spectral weight for frequencies up to ω. By substituting Eqn. 1.15 into Eqn. 1.20 the partial sum rule can be written as,

$$N_{eff}(w) = \frac{2mV_{cell}}{\pi e^2} \int_0^{\omega} \sigma_1(\omega')d\omega' \tag{1.21}$$

In this form $N_{eff}(\omega)$ can be thought of as the number of carriers involved in excitations up to a frequency ω.

The reflectance, transmission and absorption spectra can all be derived from this optical conductivity. Only the reflectance will be discussed here since it is the experimental quantity of interest. Since no absorption is possible for frequencies below 2Δ, the reflectance must equal 100 %. The onset of absorption processes at the gap frequency give rise to a ledge in the reflectance. At higher frequencies the normal and superconducting state spectra merge.

Figure 1.2 summarizes the optical properties presented in this section. The normal state properties were calculated using a Drude model while the superconducting state properties were calculated using BCS theory. The values for the scattering rate, plasma frequency and energy gap were chosen arbitrarily. It should be pointed out that the description of the optical properties presented here has been made as simplistic as possible. There exist many subtleties which have been the source of many investigations for many years. However, this description presents some of the necessary framework needed to appreciate the optical spectra of the high temperature superconductors.

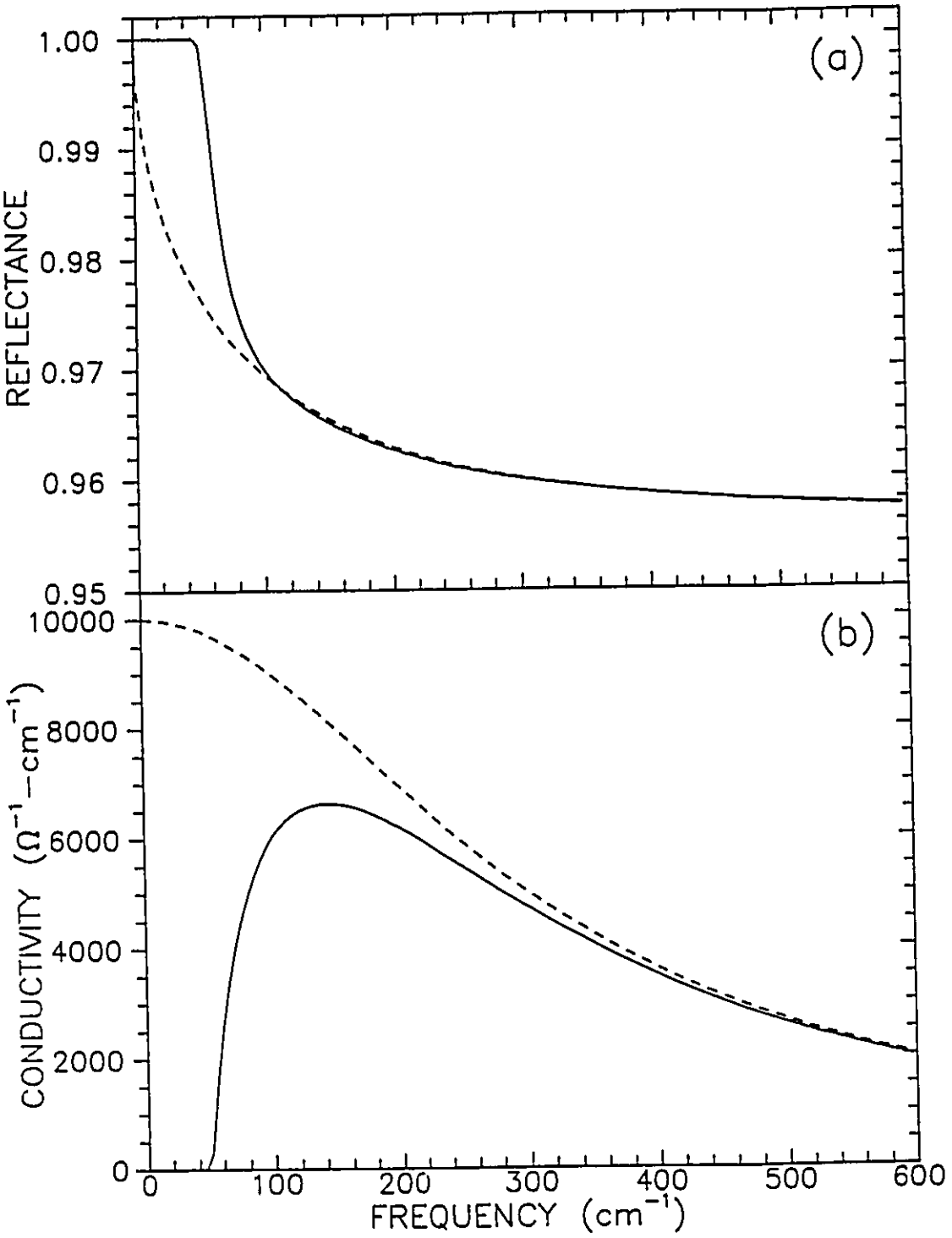

Fig. 1.2 The (a) reflectivity and (b) real part of the optical conductivity for a conventional superconductor. The normal state properties (dashed) are calculated using a Drude model (σ =10000 $\Omega^{-1}cm^{-1}$, Γ = 300 cm^{-1}) while the superconducting state properties (solid) were calculated using BCS theory (2Δ = 50 cm^{-1}).

THE HIGH TEMPERATURE SUPERCONDUCTORS

Since the discovery of high-T_c superconductors, optical measurements have been used to gain insight into the fundamental excitations governing the superconductivity. It is not the intent of this section to present a comprehensive review of this work. Its purpose is to provide the basics, summarize the key issues and describe the models used in the interpretation of the data presented in Chapter III. Most optical measurements have been performed on $YBa_2Cu_3O_{7-\delta}$ due to the availability of high quality and well characterized single crystals and films. Thus, the results quoted here, to a large extent, will concentrate on this compound. They will deal exclusively with the optical measurements performed on the ab-plane.

Through a series of comprehensive measurements the reflectance representing the intrinsic behaviour of $YBa_2Cu_3O_{7-\delta}$ has emerged.[20-27] Figure 1.3a shows typical far infrared spectra for twinned crystals at temperatures above and below the superconducting transition. The inset shows the normal state reflectance at higher frequencies. Figure 1.3b shows the corresponding optical conductivity obtained through Kramers-Kronig analysis. There exist some similarities between these results and those shown in Fig. 1.2, but upon close inspection it becomes obvious that neither Drude or BCS theory adequately describes the reflectivity.

THE NORMAL STATE

Fits to the reflectance provided the first test of whether or not the normal state obeys the predictions set forth by the Drude model. Over a finite spectral region the fits are quite good.[21] Fits to the far infrared give reasonable values for both the scattering rate and the plasma frequency, but when it is extended to higher frequencies the quality deteriorates dramatically. Fits to the reflectance at just midinfrared frequencies are also of reasonable quality, but yield a scattering rate in excess of 8000 cm^{-1}. This scattering rate is unreasonably high. It yields a mean free path of only a few angstroms which is on the same scale as the interatomic

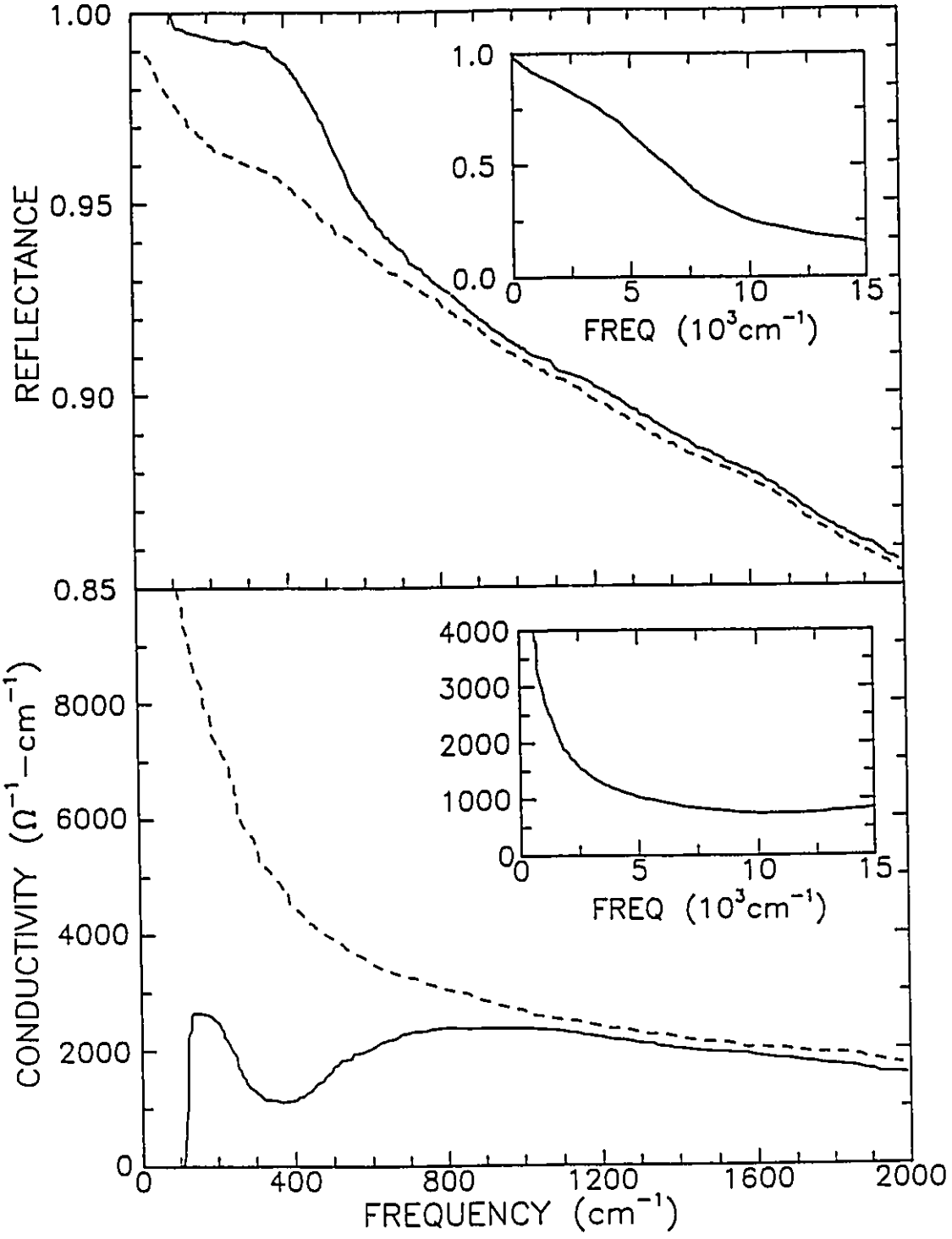

Fig. 1.3 The reflectivity and the real part of the optical conductivity for $YBa_2Cu_3O_{7-\delta}$ for both the superconducting (solid) and normal (dashed) states. The insets show optical response at higher frequencies. The spectra were taken from the work of Orenstein *et al.*[26]

spacing.[28]

Even more compelling evidence that the normal state's reflectivity is non-Drude in nature originates from an examination of the temperature dependence of the optical conductivity. Between 100 K and room temperature the dc resistivity of $YBa_2Cu_3O_{7-\delta}$ changes by a factor of three. According to the Drude model this should manifest itself in the optical conductivity by alterations in both the width and height of the Drude peak. What is found is that the midinfrared response is largely unaffected by changes in the temperature while the far infrared conductivity, more or less, adheres to Drude theory.[21] This led many researchers to describe the optical conductivity in terms of two component models. This will be discussed in more detail below.

The carrier concentration of $YBa_2Cu_3O_{7-\delta}$ can be changed appreciably by removing oxygen from the chain layer. Optical measurements[23,26] on such samples have been very revealing. When enough oxygen is removed from a sample to make it insulating the optical conductivity shows only phonon structure at low frequencies and a charge transfer gap at 1.5 eV. As carriers are added the charge transfer gap looses oscillator strength and both the midinfrared and Drude components start to develop. Both of these components continue to gain strength as the oxygen concentration is increased to its highest value. For many of these oxygen concentrations there appears to be a plasma edge with a minimum near 1.25 eV. The fact that this minimum does not move as the carrier concentration is varied casts further doubt upon describing the midinfrared reflectance in terms of a Drude model.

The first attempts at describing the optical spectra resorted to simple two component models.[20,21] A Drude component (Eqn. 1.13) was used to describe the low frequency response while a broad Lorentzian oscillator (Eqn. 1.17) centered near 1500 cm^{-1} was used to describe the midinfrared optical conductivity. It was found that the scattering rate of the Drude component followed the linear temperature dependence exhibited by the dc resistivity while the plasma frequency remained

unchanged.[22] The strength of the midinfrared band showed significant variation under various doping configurations, but showed little temperature dependence.

Subsequent work on other oxide superconductors began to show the deficiencies in this simple two component model. It became apparent that the minimum in the optical conductivity near 400 cm^{-1} exhibited by $YBa_2Cu_3O_{7-\delta}$ for temperatures below T_c (see Fig. 1.3b) was a feature associated with the normal state excitation spectrum. This conclusion was based on the observation of similar features in the normal state spectra of the $Bi_2Sr_2CaCu_2O_8$,[29] $Tl_2Ba_2CaCu_2O_8$[30] and $Pb_2Sr_2(Y/Ca)Cu_3O_x$[31] superconductors as well as in $YBa_2Cu_3O_{7-\delta}$[23] samples with reduced T_c's. The simple two component model could not provide adequate fits to this data. Some attempts were made to introduce more oscillators to improve the quality of the fits,[22] but they provided little knowledge regarding the underlying excitations governing the optical conductivity. It became apparent that new models were needed.

Time of flight neutron spectroscopy offered the first insight into this structure. The data showed the existence of phonons at energies coincident with the minimum in the optical conductivity that were not present for non-superconducting samples.[32,33] This prompted Timusk and Tanner[34,35] to propose that the minimum was caused by phonons which were coupled to a broad midinfrared band whereby these phonons created a Fano-like antiresonance.[36] Further support for this proposal came from comparisons between optical[31] and Raman[37] measurements on $Pb_2Sr_2(Y/Ca)Cu_3O_x$. Again, phonon structure observed in the Raman spectra was at the same energies as the minima in the optical conductivity. Recently, it has been observed that the longitudinal optic modes extracted from optical measurements with the light polarized along the c-axis was also coincident with the minima in the ab-plane optical conductivity for a wide variety of oxide superconductors.[38]

A model, which was first developed by Rice[39] for organic superconductors, has been successfully used to describe this coupling between the broad midinfrared

band and phonons. It yields a dielectric function given by,

$$\epsilon = [1 - \frac{\omega_{PD}^2}{\omega^2 + i\omega\Gamma_D}] + \frac{\omega_{Pe}^2}{\omega_e^2 - D - \omega^2 - iw\Gamma_e} + \epsilon_\infty \qquad (1.22)$$

where,

$$D = \sum_k \frac{\omega_{Pk}^2}{\omega_k^2 - \omega^2 - iw\Gamma_k}. \qquad (1.23)$$

The first term describes the free electron behaviour in terms of a simple Drude model which has the plasma frequency (ω_{PD}) and scattering rate (Γ_D) as the adjustable parameters. The second term describes how the midinfrared band with its position (ω_e), strength (ω_{Pe}) and width (Γ_e) is coupled to phonons described in a similar manner by ω_k, ω_{Pk} and Γ_k . The final term gives the high frequency dielectric constant (ϵ_∞). This model will be used in Chapter III to fit the reflectance data.

THE SUPERCONDUCTING STATE

The most fundamental quantity associated with the superconducting state is the energy gap. Much effort has gone into determining its existence and size, but it has remained an illusive quantity. Both the reflectance and the optical conductivity shown in Fig. 1.3 seem to show a gap-like feature near 100 cm^{-1}. The observation of unity reflectance followed by the onset of absorption has been observed by a number of researchers,[22,24,26] but the frequency where the absorption onsets is sample dependent and many spectra show no such feature.[21,25,40] There is even some evidence that the feature is present in the normal state.[22] These facts give reason to believe that it is not the energy gap. Furthermore, it should be recognized that the unity reflectance level is only accurate to within $\frac{1}{2}$ % . The zero conductivity at low frequencies originates only because the reflectance was arbitrarily set to 100 % before performing the Kramers-Kronig analysis. Any small deviations from unity reflectance in this frequency range would have produced

dramatic fluctuations in the conductivity. Absorption measurements provide superior accuracy, but are technically more demanding. The few measurements performed on $YBa_2Cu_3O_{7-\delta}$ indicate that there is a finite absorption level ($\frac{1}{3}$ %) at these low frequencies.[41,42]

The development of the ledge at 450 cm^{-1} as the sample is cooled below T_c led a number of researchers to label this feature as the energy gap.[43,44] As stated above, the observation of a similar ledge in the normal state optical properties of other cuprates and its insensitivity to T_c provided convincing evidence that it was not associated with the superconducting energy gap.

It became apparent that all of the features observed in the optical spectra of the cuprate superconductors could not be directly attributed to an energy gap. Even though the size of the gap is still unknown, much progress has been made in determining why it has been so difficult to measure. It was pointed out by Kamerās *et al.*[22] that an energy gap will not be seen for a superconductor in the clean limit where the scattering rate is much smaller than the energy gap (i.e. $2\Delta \gg \Gamma$). In the clean limit, essentially all of the spectral weight associated with the normal state's Drude peak collapses to form the superconducting state's zero frequency delta function. Thus, the rapid rise in the conductivity for frequencies just above 2Δ seen in Fig. 2b is nonexistent for a clean limit superconductor. Without it, there is no ledge in the reflectance spectra at 2Δ to provide evidence for the existence of an energy gap.

The clean limit scenario was appealing, but there were some difficulties with it. Simple calculations showed that if the scattering rate continued to drop off linearly below T_c then a small gap feature should still be present in the optical spectra if its size is comparable to the BCS value.[45,46] This implied that either the energy gap was very large or that the scattering falls off much faster than linear below T_c. Recent microwave surface impedance measurements on high quality $YBa_2Cu_3O_{7-\delta}$ single crystals show that the scattering rate does decline dramatically below T_c.[47] Far infrared transmission measurements on $Bi_2Sr_2CaCu_2O_8$ [48,49]

seem to be consistent with this result. The size of the energy gap is still unknown.

III. THE MATERIALS OF INTEREST

$(Pb_{1-x}Cu_x)Sr_2(Y_{1-y}Ca_y)Cu_2O_{7+\delta}$

The discovery of the lead based superconductor, $Pb_2Sr_2(Y/Ca)Cu_3O_x$[9] (2213 PSYCCO), with a T_c of 85 K has led to the discovery of an entire family of superconductors. Most notably is the $(Pb_{1-x}Cu_x)Sr_2(Y_{1-y}Ca_y)Cu_2O_{7+\delta}$ phase (1212 PSYCCO) which was independently discovered by Subramanian *et al.*[50] and Lee *et al.*[51] Both of these groups reported that the 1212 phase was non-superconducting. However, it was later demonstrated that superconductivity could be induced in polycrystalline samples by carefully manipulating the oxygen stoichiometry through such procedures as high pressure oxygen anneals[52] (T_c=67 K) or liquid nitrogen quenches[53](T_c=60 K). The superconducting properties of these samples were poor when compared to the standards set by the YBCO, BSCCO, TBCCO and NCCO families of superconductors. The stringent conditions required to produce even poor quality superconductors has not deterred interest in this system, since chemical substitutions have led to superconducting transitions which onset at temperatures in excess of 100 K.[54]

The tetragonal crystal structure of the $(Pb_{1-x}Cu_x)Sr_2(Y_{1-y}Ca_y)Cu_2O_{7+\delta}$ phase is shown in Fig. 1.3. This structure is similar to $YBa_2Cu_3O_{7-\delta}$ (compare with Fig. 1). Both materials have two CuO_2 planes per unit cell. The Y and BaO layers in $YBa_2Cu_3O_{7-\delta}$ are analogous to the (Y,Ca) and SrO layers in $(Pb_{1-x}Cu_x)Sr_2(Y_{1-y}Ca_y)Cu_2O_{7+\delta}$. The main difference lies in the fact that the CuO chain layer in $YBa_2Cu_3O_{7-\delta}$ is replaced by a (Pb,Cu)-O layer in the 1212 PSYCCO material. Thus, an investigation of the optical properties of PSYCCO could lead to some interesting comparisons between a superconductor with and without a chain layer. At this time, no optical investigations have been reported.

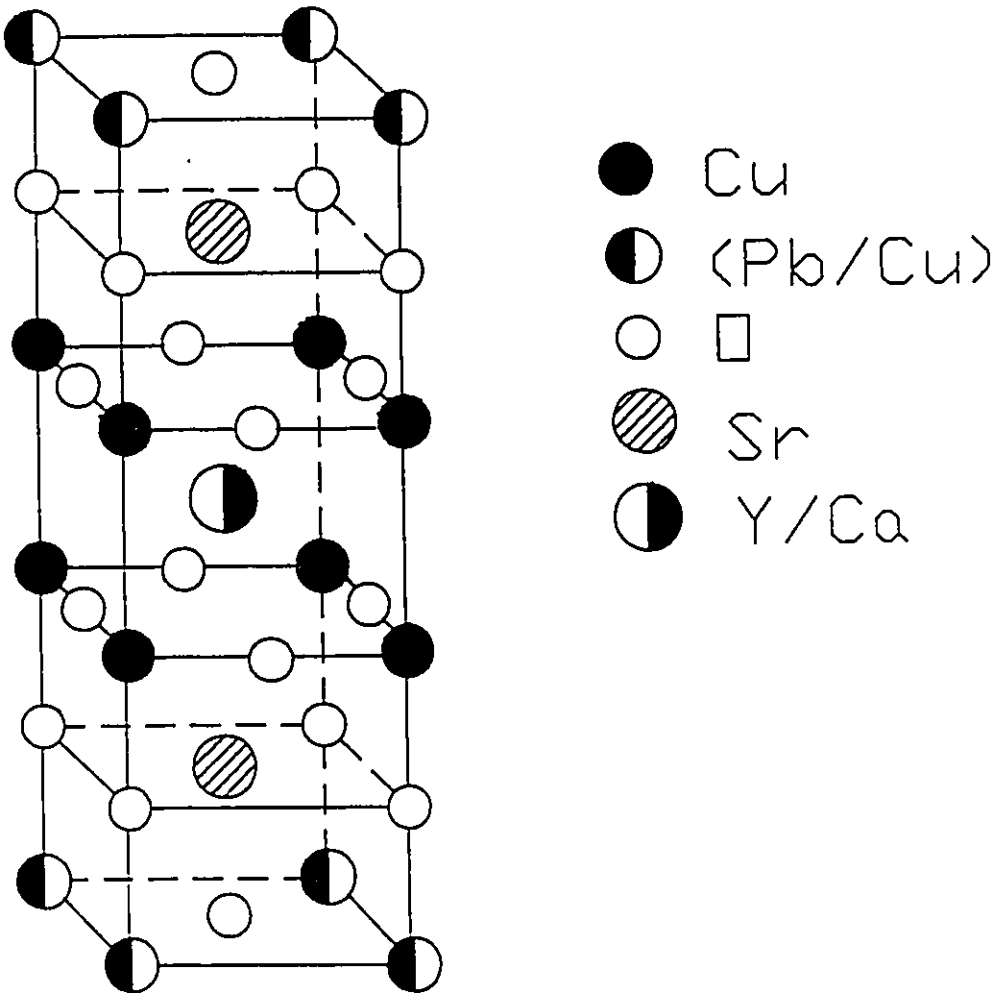

Fig. 1.3 Tetragonal crystal structure of the 1212 PbSrYCaCuO superconductor with lattice parameters a = 3.82 Å and c = 11.90 Å. Note the resemblance of this crystal structure to that of $YBa_2Cu_3O_{7-\delta}$ shown in Fig. 1.1.

$Nd_{2-x}Ce_xCuO_{4+\delta}$

The $Nd_{2-x}Ce_xCuO_{4+\delta}$ system[10] has received a considerable amount of attention despite the fact that its transition temperatures never exceed 23 K. It gained immediate notice due to the fact that superconductivity could be induced in Nd_2CuO_4 by substituting Ce^{4+} on the Nd^{3+} site which made this material the first candidate for n-type superconductivity among the cuprate superconductors. Negative Hall coefficients[55] confirmed this behaviour although these results have been questioned.[56] The normal state ab-plane resistivity also proved to be distinct as it shows a T^2 – like[57] temperature dependence rather than the more common linear behaviour. The onset of superconductivity is strongly dependent upon both the cerium and oxygen concentration. The cerium concentration which gives the optimum T_c is $x = 0.15$.[55] Below this value the transition temperature drops off rapidly, while above it T_c drops off at a more gradual rate. The optimum superconducting transition temperature can only be achieved by carefully optimizing the oxygen content as a small excess can render the material non-superconducting. This material is usually grown in an oxygen rich state and superconductivity is induced by removing the oxygen through a high temperature anneal in either argon or helium. Figure 1.4 shows the crystal structure of this material. It is unique to the oxide superconductors in that there exists no oxygen atoms above or below the copper atoms. The absence of these so-called apical oxygen atoms makes the CuO_2 planes structurally more two dimensional than any other high temperature superconductor.

These unique transport and structural properties make $Nd_{2-x}Ce_xCuO_{4+\delta}$ an attractive candidate for detailed investigations of its optical properties. These investigations will allow direct comparisons to the more well established oxide superconductors to determine if the unique properties displayed by $Nd_{2-x}Ce_xCuO_{4+\delta}$ manifest themselves in the optical spectra. Thus far, most of the optical investigations have focused upon the effects of adding electrons to the CuO_2 planes through the substitution of cerium on the neodymium site.[58–62] These measure-

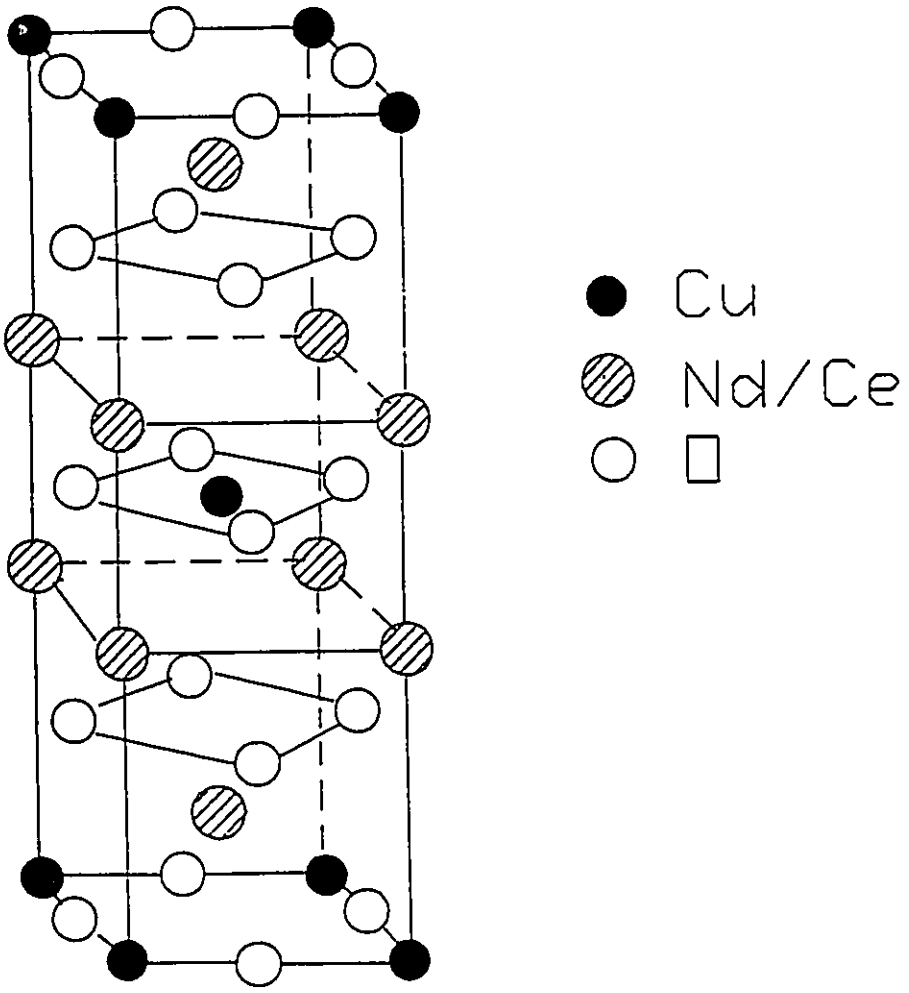

Fig. 1.4 The tetragonal crystal structure of $Nd_{1.85}Ce_{0.15}CuO_{4+\delta}$ with lattice parameters a = 3.95 Å and c =12.07 Å. The structure of this cuprate superconductor is unusual in that no apical oxygen atoms are present.

ments clearly show the development of the midinfrared band as carriers are added to the planes. This is accompanied by a decrease in the oscillator strength at energies above 1.5 eV associated with a charge transfer band. For cerium concentrations in excess of the optimum for superconductivity the spectra become more Drude like and the reflectance becomes more metallic. This behaviour is reminiscent of that obtained for $La_{2-x}Sr_xCuO_4$[63] as the number of holes is varied by adjusting the value of x. The only two measurements which show the temperature dependence of the far infrared reflectance have been performed on polycrystalline samples. One measurement[64] showed an enhancement in the reflectivity as the sample was cooled below T_c with a reflectance edge at 50 cm^{-1}. They interpreted this ledge as the superconducting energy gap. The second measurement[65] showed similar results, but they demonstrated that the ledge could also be explained by a plasma edge. Similar controversies occurred when reflectance measurements were performed on polycrystalline $La_{2-x}Sr_xCuO_4$ samples.[66,67] These measurements demonstrate the inherent difficulties in interpreting the results obtained from polycrystalline pellets of highly anisotropic materials. Past experience with the other oxide superconductors has shown that these problems are resolved as the availability of high quality single crystals and highly oriented thin films improves.

IV. PULSED LASER DEPOSITION

INTRODUCTION

The process of using a laser to deposit a thin film is a relatively straightforward procedure. The light from a pulsed or continuous wave laser is focused onto a material commonly referred to as the target. If the resulting energy density is large enough the material will be evaporated or vaporized. This material can then be collected on a substrate forming a thin film. The definition of pulsed laser deposition is more specific. As the name suggests it is restricted to pulsed

lasers. This distinction is not simply a matter of creating classifications, but implies a fundamentally different process. A continuous wave laser can heat the target material until a state of equilibrium sets up where each element in the target evaporates according to its own partial pressure. In contrast, laser pulses will expose the target to a short period of rapid heating followed by a quiescent interval which allows it to return to its original temperature. In this scenario, the equilibrium process of evaporation does not occur. Instead, a process referred to as laser ablation takes place. The physics of this process is not well understood, but it is recognized that it is a far from equilibrium process where the incident laser pulse vaporizes the first few thousand angstroms of the target forming a short lived plasma which expands away from the target surface. Obviously, laser ablation cannot occur for any target fluence. The minimum fluence required defines the ablation threshold and is a quantity which strongly depends upon the thermal and optical properties of the target material.

The greatest advantage pulsed laser deposition has over other film growth techniques is a consequence of this difference between evaporation and ablation. Because evaporation depends upon the partial pressure of the elements contained within the target, preferred evaporation of an element can occur resulting in a film with the incorrect stoichiometry. On the other hand, laser ablation removes the surface of target with little regard for its composition. This congruent removal of material greatly simplifies the growth process as it reduces the number of growth parameters that must be optimized. This is especially true for high temperature superconductors which can contain as many as eight elements.

The mechanism behind laser ablation's unique ability to congruently vaporize a multielement target can be understood by considering the properties of a typical target material. The duration of laser pulses used in the ablation process is usually between 10 and 50 nsec. This time period is large when compared to electronic relaxation rate which is typically 10^{-14} seconds.[68] The electrons lose energy to the lattice via phonon emission. Hence, when the light is absorbed its energy is

quickly distributed throughout the crystal lattice resulting in the intense heating and subsequent ejection of material to a depth of several thousand angstroms from the target surface. It will only take a few milliseconds for the target to disperse the remaining heat during the quiescent period following the laser pulse. Even though the atoms contained near the target surface have sufficient energy during this time interval to diffuse, possibly forming a layer which does not represent the initial stoichiometry, the brevity of cooling period severely limits the distance which an atom can travel. The next laser pulse will remove material to a depth greater than the diffusion layer and the material removed will, on average, be vaporized congruently.

Pulsed laser deposition is both a simple and versatile film growth technique, but it is not without its shortcomings. From the practical viewpoint the laser purchase and operation is expensive. Technically there exist two major problems. First, the ejection of material from the target is strongly forward directed. This makes it difficult to produce uniform large area films ($\geq$1 cm^2). As a research tool this limitation is not that important, but on an industrial scale it is the major drawback of the technique. Second, the surface morphology of the films can be poor with micron size spherical particulates dispersed throughout the film. This is undesirable when growing multilayer film structures as the particulates can short-circuit two metallic layers separated by an insulating layer. They can also corrupt the results obtained from such characterization techniques as Rutherford backscattering (RBS) and inductively coupled plasma mass spectrometry (ICP/MS). These problems will be discussed in detail below with specific reference to the high-T_c superconductors.

GROWTH OF HIGH-T_c SUPERCONDUCTING FILMS BY LASER ABLATION

Superconductivity above 77 K generated a great deal of interest as it created the possibility of fabricating SQUIDS, Josephson junctions, bolometers, and various microwave devices which operate at liquid nitrogen temperature. The deposition of high quality films was the obvious first step in their production. This effort was spearheaded by Dijkkamp *et al.*[69] who were the first investigators to produce $YBa_2Cu_3O_{7-\delta}$ thin films by pulsed laser deposition. These films were deposited in a two-step process. In the first step the material from a stoichiometric target was deposited in vacuum on a $SrTiO_3$ substrate heated to 450 °C. The resulting film was amorphous and oxygen depleted. The samples became superconducting in the second step which involved a 1 hour, 900 °C anneal in flowing oxygen. These films were comparable to the best superconducting material available at the time. With subsequent improvements highly oriented films were routinely deposited with a transition temperature of 93 K and transition widths of less than 1 K. The critical current densities were as high as $1x10^6$ amps/cm^2 which was two orders of magnitude greater than the values observed for polycrystalline pellets. Other film growth techniques such as sputtering, molecular beam epitaxy (MBE), coevaporation and metalorganic chemical vapor deposition (MOCVD) lagged behind. This early success resulted in the emergence of pulsed laser deposition as the dominant technique for depositing high-T_c superconducting films.

A significant improvement to the above growth procedure was to introduce a few hundred millitorr of oxygen into the growth chamber while maintaining the substrate at a temperature of 750 °C.[70] Films produced in this manner required no post anneal and were superior in every respect. Most of the oxygen released from the target does not end up as part of the film due to its volatility. The added oxygen compensates for this loss allowing a stable crystal structure to form during the deposition. Since films produced in vacuum at these temperatures are copper deficient, the addition of oxygen must also have a stabilizing influence. Further

improvements originate from the fact that the film is never exposed to the high temperatures required in the annealing process. These temperatures can cause film cracking, interdiffusion at the film/substrate interface and the formation of precipitates. The production of films by this one-step process is referred to as *in situ* growth.

A detailed investigation of the film properties resulting from the various growth parameters must be made if high quality superconducting films are to be grown. Growth parameters such as the laser wavelength, laser repetition rate, laser energy density, substrate, target, deposition temperature, deposition rate, annealing conditions and the oxygen pressure all play a key role in determining the transport properties, surface morphology and structural orientation of the films produced. As an introduction to the p ·lsed laser deposition process it is best to give an overview of the growth parameters and film properties of $YBa_2Cu_3O_{7-\delta}$. It is the most widely studied compound of any material grown by this technique, while the literature dealing with other superconductors is rather sparse. Many of the growth parameters listed above are associated with either the laser or substrate properties. The next two sections will discuss the role they play in the production of $YBa_2Cu_3O_{7-\delta}$ thin films.

THE EFFECTS THE LASER PARAMETERS HAVE ON THE GROWTH OF $YBa_2Cu_3O_{7-\delta}$ FILMS

Excimer lasers have emerged as the laser of choice in the growth of $YBa_2Cu_3O_{7-\delta}$ films. This laser emits short bursts (FWHM $\approx$ 30 nsec) of ultraviolet light with energies that are typically a few hundred millijoules. The light pulses have spatial dimensions (i.e. width and height) that are in the centimeter range and are focused to obtain the desired energy density. The frequency of the light emitted from the laser cavity depends upon the active medium. The most common frequencies used are 193 nm (ArF), 249 nm (KrF) and 308 nm (XeCl).

The laser can be pulsed at repetition rates that exceed 100 Hz, but the values used for film growth rarely exceed 10 Hz. The laser's frequency, repetition rate and energy density determine the stoichiometry, growth rate and the severity of the particulate problem.

The laser energy densities used in the growth of $YBa_2Cu_3O_{7-\delta}$ films are usually between 1 and 3 J/cm^2. Values outside this optimized range result in a deterioration in film quality. The ablation threshold for $YBa_2Cu_3O_{7-\delta}$ is in the range of 0.1 to 0.3 J/cm^2.[71] Near the threshold the laser heating, which results in evaporation and diffusion, still plays an important role as the ablation process only removes a depth of 10's of angstroms. Here the film growth is more aptly described as a mixture of ablation and evaporation. As a result, yttrium which is the least volatile element contained in $YBa_2Cu_3O_{7-\delta}$ does not leave the target as readily as barium and copper. Thus, the surface of the target becomes yttrium rich leaving the film deficient in this element.[72] As the energy density is increased the ablation process dominates resulting in the congruent removal of material from the target. If the energy density is too high the film remains stoichiometric, but more particulates begin to appear on the surface of the film.[73]

The particulates are usually spherical in shape and are of the order of 1 μm in size. Energy dispersive x-ray analysis shows a stoichiometry which is near that of $YBa_2Cu_3O_{7-\delta}$.[73] The exact origin of the particulates is not well understood. The uncertainty originates from the fact that it is difficult to study interactions occurring on the nanosecond timescale. It is thought that the particulates form as a result of deep target heating followed by the explosion of bubbles causing the spitting of molten material. The factor which most strongly influences the number of particulates is the laser wavelength. Kautek *et al.*[74] compared the density of particulates using lasers with wavelengths varying from the far infrared to the ultraviolet. The work clearly demonstrated that using a smaller wavelength laser minimized the number of particulates on the film surface. This result has contributed a great deal to the popularity of excimer lasers in the pulsed laser

deposition technique.

In addition to using an excimer laser with a low energy density many procedures have been devised to reduce the number of particulates. It has been empirically determined that a dense target with a surface that has not been exposed to a large number of laser pulses is beneficial.[75] Thus, it has become commonplace to remove the surface of the target between depositions. The more elaborate scheme of using a second laser pulse travelling parallel to the target surface to vaporize the particulates as they travel to the substrate has also been tried with some success.[76] A final method exploits the fact that the particulates travel at velocities two orders of magnitude smaller than the atoms and molecules. This makes it possible to use a shutter which is syncronized to the laser pulses to selectively block out the particulates.[77]

Controlling the film growth rate can be a delicate task as it is dependent upon many parameters. The parameters associated with the laser have the largest influence. The quantity of material removed from the target surface with each laser pulse depends upon the laser energy density and the laser spot size. The amount of material ejected increases rapidly above the ablation threshold and saturates at an energy density near 2 J/cm^2.[71] The material leaving the target is strongly forward directed with a $\cos^n\theta$ dependence where n can be as high as 11.[78] The substrate-target distance and the pressure of the background gas determine how much material becomes part of the film. Typically, 1 Å per pulse is deposited for $YBa_2Cu_3O_{7-\delta}$. By adjusting the laser's repetition rate the growth rate can be increased to the desired level. This procedure seems relatively straightforward, but complications arise. A fresh target surface can result in a growth rate which is five times greater than one which has been exposed to many laser pulses.[79] This result is somewhat surprising considering the nature of the ablation process. Insight into this phenomenon comes from studies of the target surface.

When a spot on the target is hit with hundreds of laser pulses it undergoes a metamorphosis in both morphology and composition. Four independent

studies[72,74,79,80] using scanning electron microscopy have shown that the surface of the target develops conical features with diameters between 1 and 10 μm and depths as large as 25 μm. These cones are always at an angle with respect to the target surface that is identical to the angle of incidence of the laser pulses. The features become larger as the laser wavelength is increased. This phenomenon may be associated with the increase in the severity of the particulate problem at longer wavelengths. Energy dispersive x-ray analysis indicates that the cones have a yttrium rich surface layer. These observations present two possible origins for the reduction in the growth rate as a target is repeatedly hit with laser pulses. The development of cones increases the surface area that the laser pulses strike effectively lowering the energy density and hence the amount of material removed with each pulse. An alternative explanation is that the thermal and optical properties of the yttrium rich surface layer results in the removal of less material. It is important to recognize that even though the target surface is undergoing continuous change the films produced remain stoichiometric.

THE EFFECTS THE SUBSTRATE PARAMETERS HAVE ON THE GROWTH OF $YBa_2Cu_3O_{7-\delta}$ FILMS

The material ejected from the target is comprised of a diverse collection of species which include atoms, ions, metal oxides, clusters, and particulates. These species are collectively referred to as the plume. It appears as a bright flash due to the deexcitation of excited states. The plume is short lived as the species comprising it travel at velocities ranging from 10^4 to 10^6 cm/sec.[77,81] These velocities give the atomic species energies between 40 and 70 eV which is the ideal range for film deposition. The energy gives the atoms increased mobility once they strike the target surface. It supplements the mobility provided by a heated substrate and thus allows for a reduction of its temperature. The high energies are also beneficial in the early stages of film growth as they can remove loosely bound

contaminants from the substrate surface. These energies are not high enough to sputter the substrate or the growing film.

Once the species in the plume strike the substrate they must migrate along its surface until they settle in the correct lattice position. The heated substrate provides sufficient mobility for atoms and simple molecules, but more complex species must decompose or will end up as defects in the film. As atoms migrate along the substrate surface there exists the possibility that a particular atomic species will preferentially evaporate resulting in a film with the incorrect stoichiometry. This process is quantitatively described by the sticking coefficient which is defined as the ratio of the amount of an element which condenses on the substrate to that which is incident upon it. For the deposition parameters used in $YBa_2Cu_3O_{7-\delta}$ film growth the sticking coefficients are unity for all elements except oxygen. This oxygen deficiency is easily compensated for by the oxygen leaked into the deposition chamber.

The island growth mechanism describes the formation of $YBa_2Cu_3O_{7-\delta}$ films.[82] In the initial stages of growth, species land on the substrate and begin to migrate along its surface. Eventually enough material will collect on the surface to form more complex structures. Soon afterward islands of $YBa_2Cu_3O_{7-\delta}$ begin to appear. This process is called nucleation and is often triggered by substrate defects. The islands grow in size until they coalesce to form a continuous film. The resulting film clearly shows the grain boundaries where the islands met. The island size is strongly influenced by the physical properties of the substrate, the substrate's temperature and deposition rate. They are typically 1μm wide.

The early stages of film growth are profoundly influenced by the properties of the substrate. It can determine whether the resulting film is polycrystalline or highly oriented . If the lattice parameters of its exposed surface are close to those of the material being deposited then it can provide a template for the growing film. Thus, in the initial stages of growth the crystallographic orientation of the islands will be determined by the orientation which best matches the substrate's

lattice parameters. The lattice mismatch describes the quality of the template provided by the substrate. It is given by,

$$\text{lattice mismatch} = \frac{b - c}{c} \times 100\% \qquad (1.24)$$

where, b and c are the film and substrate lattice constants respectively. When the superconducting film's orientation is governed by the substrate it is referred to as epitaxial growth. The more strict definition of epitaxial growth, which is often applied to semiconducting supperlattice structures, demands that the film takes on the lattice constant of the substrate rather than its bulk value. For $YBa_2Cu_3O_{7-\delta}$, this only occurs in the initial stages of film growth. As the film gets thicker defects relieve the strain.

Many different materials have been used as substrates for $YBa_2Cu_3O_{7-\delta}$, but none have met all the desired criteria. Initially, the high quality and technological importance of silicon and GaAs substrates made them the most desirable choice. Even though these materials provided an excellent lattice match to the a-axis of $YBa_2Cu_3O_{7-\delta}$, the quality of the films were poor due to interdiffusion at the substrate/film interface.[82-85] Sapphire (Al_2O_3), which is another commonly used substrate, presented similar difficulties in that the aluminum diffused into the superconductor resulting in a severe deterioration of its properties.[87] A high quality film using the above substrates can only be produced by depositing a thin film of a more desirable material onto the surface of the substrate. This buffer layer must eliminate the diffusion problem and must also be suitable for the growth of high quality $YBa_2Cu_3O_{7-\delta}$. At the present time CeO_2 is the material most commonly used for this purpose.[88,89]

The failure to deposit $YBa_2Cu_3O_{7-\delta}$ directly on the more common substrates resulted in the use of more exotic materials such as $SrTiO_3$,[78] $LaAlO_3$[90] and $NdGaO_3$[91] which were usually oriented in the (100) orientation. $SrTiO_3$ substrates result in the deposition of films with the highest quality. The major drawback is its high dielectric constant, which makes it unsuitable for many microwave

applications. $LaAlO_3$ has a low dielectric constant and the $YBa_2Cu_3O_{7-\delta}$ films deposited on it are of comparable quality. Its main deficiency is the twinning induced by a cubic to rhombohedral phase transition which occurs at 550 °C.[92] $NdGaO_3$ has shown much promise in that it can be grown without the formation of twins and it has a low dielectric constant. Further research is needed to determine how useful this substrate will be.

The high temperature superconductors show a strong correlation between film quality and lattice match. This is somewhat of a problem for $YBa_2Cu_3O_{7-\delta}$ since it is an orthorhombic superconductor. The ideal substrate would also be orthorhombic with lattice constants equal to those of $YBa_2Cu_3O_{7-\delta}$. A substrate such as this is difficult to find. It is obviously advantageous to have a tetragonal superconductor.

It would not be surprising if the substrates which have been the most successful in the growth of $YBa_2Cu_3O_{7-\delta}$ also prove to be successful in the growth of other cuprate superconductors. These substrates have been chosen for their chemical inertness as well as a small lattice mismatch. It is likely that the other cuprates will share similar chemical properties and as a result remain chemically inert. To a large extent the size of the ab-plane lattice parameters is determined by the CuO_2 planes. Since this is a common feature to the cuprates a small lattice mismatch will result for all of them. Table 1.1 summarizes the lattice parameters of the relevant substrates and superconductors.

As mentioned previously the film's crystallographic orientation can be defined by the substrate. The substrates described above were chosen to give a small lattice mismatch to the ab-plane lattice parameters of $YBa_2Cu_3O_{7-\delta}$. Thus, a highly oriented superconductor with its CuO_2 planes parallel to the substrate can be formed. These so-called c-axis films show the best transport properties with critical current densities in excess of 10^6 amps/cm^2. The surface morphology of the best films do not show particulates, but two problems still exist. During the early stages of film growth the islands coalesce leaving pockets which are absent

Compound	Lattice Parameter (Å)
Si	a = 5.430
GaAs	a = 5.654
MgO	a = 4.211
CeO_2	a = 5.411
$SrTiO_3$	a = 3.905
$LaAlO_3$	a = 3.788
$NdGaO_3$	a = 5.426 b = 5.496 c = 7.707
$YBa_2Cu_3O_{7-\delta}$	a = 3.820 b = 3.892 c = 11.688
$(Pb_{0.75}Cu_{0.25})Sr_2(Y_{0.5}Ca_{0.5})Cu_2O_7$	a = 3.821 c = 11.896
$Nd_{1.85}Ce_{0.15}CuO_{4+\delta}$	a = 3.946 c = 12.067

Table 1.1 - The lattice parameters of substrates used in high-T_c research as well as those of the superconductors of interest. Even though some of these substrates have a-axis lattice parameters in excess of 5 Å they still provide an excellent lattice match to the oxide superconductors since the CuO_2 plane lattice parameters are approximately equal to $\frac{\sqrt{2}}{2}$a.

of material. As the film grows thicker they rapidly fill in with non-stoichiometric material and misoriented $YBa_2Cu_3O_{7-\delta}$ grains and eventually protrude from the film surface.[93,94] The density of these outgrowths varies dramatically between various researchers. Further study is required. The second problem exists on a much finer scale and can only be seen with the high resolution of a scanning tunneling electron microscope. These images indicate that each superconducting grain has a terrace structure centered around a screw dislocation.[95,96,97] Each terrace has a height of one or two unit cells. The film grows by attaching material to the ledge of the terrace. Much effort has gone into the deposition of multilayer structures consisting of alternating layers of superconducting $YBa_2Cu_3O_{7-\delta}$ and semiconducting $PrBa_2Cu_3O_7$ with periodicities as small as one unit cell.[98,99,100] This growth pattern can disrupt these structures.

Another field of active research is the growth of films with the c-axis parallel to the substrate. These so-called a-axis films are useful in the formation of multilayer structures, since it takes advantage of the longer coherence length in the ab-plane allowing easier coupling between superconducting layers separated by an insulator. Films with this orientation can be grown simply by lowering the growth temperature below 700 °C, but this results in a poor morphology consisting of a basket weave structure with needle-like grains growing perpendicular to each other.[101] This morphology is not a consequence of a poor lattice match. The c-axis lattice parameter of $YBa_2Cu_3O_{7-\delta}$ is almost identical to three times that of the b-axis. Thus, any substrate which offers a good lattice match to the b-axis also offers an equally good match to the c-axis. The most successful attempt at depositing a-axis films takes advantage of the excellent surface morphology provided by a-axis $PrBa_2Cu_3O_7$ films grown at low temperatures.[102] Because of the closeness of the two structures a $PrBa_2Cu_3O_7$ film can provide a template of such perfection that its orientation and excellent morphology is mimicked by the growing $YBa_2Cu_3O_{7-\delta}$ film at the high temperatures where c-axis growth is usually more favorable. High resolution transmission electron microscopy indicates that these

films are structurally superior to c-axis films as they exhibit far fewer defects.[103] However, they show a slightly reduced T_c. This has been attributed to an oxygen deficiency which relieves stress induced by the substrate. An alternative method of growing a-axis films uses (110) oriented perovskites as substrates.[104,105]

V. CONCLUSIONS

Materials problems have been one of the major stumbling blocks in the understanding of high temperature superconductivity. Thus, combining materials preparation and characterization with fundamental research is a necessity. Far infrared optical measurements have proved their usefulness in determining the basic processes governing superconductivity while pulsed laser deposition has become the dominant technique for producing large area, optically smooth high temperature superconductors. Thus, these two techniques are well suited to each other. The experimental procedures involved in performing far infrared optical measurements have been developed over many years and are now well established. On the other hand, pulsed laser deposition is a relatively new technique whose physics is not well understood. As a result, empirical information is often the most reliable guide in the production of high quality material. The work presented here describes how pulsed laser deposition was used to produce superconducting $(Pb_{0.75}Cu_{0.25})Sr_2(Y_{1-y}Ca_y)Cu_2O_7$ and $Nd_{1.85}Ce_{0.15}CuO_{4+\delta}$ films and there subsequent use in the investigation of their far infrared optical properties.

CHAPTER II
GROWTH OF HIGH – T_c FILMS BY PULSED LASER DEPOSITION

I. PULSED LASER DEPOSITION APPARATUS

INTRODUCTION

The system used to grow high-T_c thin films by pulsed laser deposition was designed with two objectives:

- to construct a versatile system that would allow the user to freely vary the maximum number of growth parameters and
- to gain control of the deposition parameters in order that reproducible results could be obtained.

Figure 2.1 shows a schematic of the deposition system. Its two main components are the deposition chamber and the optics required to focus and manipulate a high energy laser pulse. For the purpose of clarity the two components will be discussed separately.

THE OPTICS

The laser used in the ablation process was a Lumonics 308 nm XeCl excimer laser. The ultraviolet light emitted was in the form of pulses which have a full width at half maximum of 30 nsec and a maximum energy of 210 mJ. The pulses are rectangular (1.8 cm x 3.6 cm) in shape, but lack spatial uniformity as illustrated by Fig. 2.2. The laser had the ability to be pulsed at frequencies as high as 200 Hz, but the frequencies used in these experiments rarely exceeded 2 Hz.

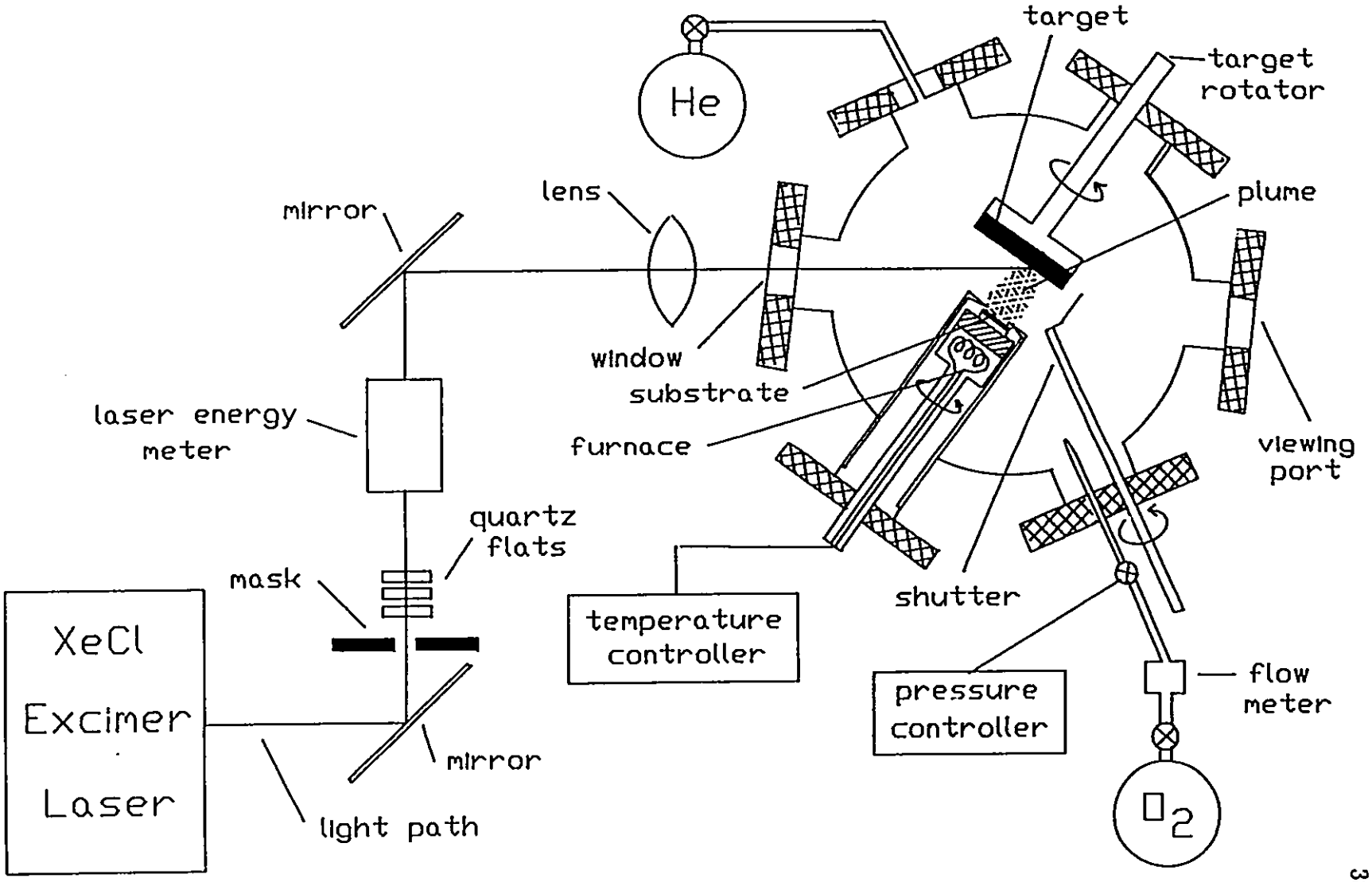

Fig. 2.1 Schematic of the laser deposition system.

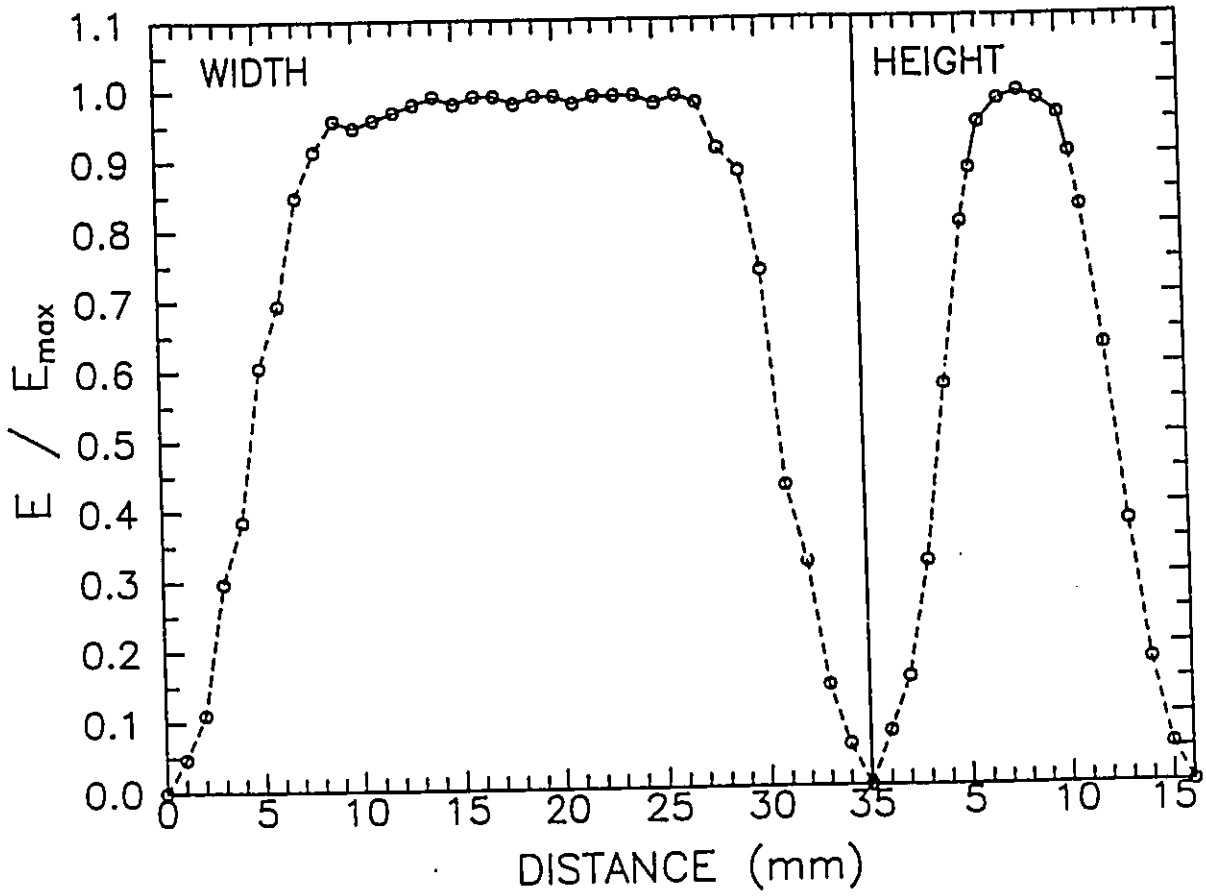

Fig. 2.2 Spatial profile of the laser pulse energy (E) emitted from the excimer laser. The solid lines indicate the light which is ultimately focused onto the target while the dashed lines denote the light blocked by the mask.

Once the pulses exited the laser cavity they were manipulated in three ways. First, the pulse is reflected off of a series of two mirrors (fused silica with a dielectric coating) whose purpose is to rotate the laser pulse 90°. The reasoning behind this rotation will be discussed below. Second, the light is passed through a mask whose function is to block the non-uniform parts of the laser pulse as indicated by the dashed lines in Fig. 2.2. The mask is simply a rectangular hole (0.5 cm x 1.8 cm) constructed from stainless steel shim stock. It is placed on a xz-stage to simplify the alignment procedure. If the mask were removed a non-uniform laser pulse would be focused upon the target resulting in an energy density gradient. Obviously, this is not a desired effect since the energy density is one of the key parameters in the laser ablation process. Also, the edges of the laser pulse do not contain a sufficient amount of energy to exceed the ablation threshold which can introduce errors to the film stoichiometry. Thirdly, the pulses are passed through a series of quartz flats which are used to regulate the energy density incident upon the target. Each quartz flat attenuates approximately 10 % of the incident energy. The pulse energy continuously drops due to the highly reactive nature of the HCl gas contained within the laser cavity and must be replaced periodically. Thus, immediately after the gas is changed the laser pulses are too intense and must be attenuated. As the pulse energy falls the quartz flats are gradually removed. The pulse energy is monitored by a Scientech laser energy meter which can be removed from the light path allowing the light to strike a third mirror which reflects the laser pulse onto a lens.

A fused silica plano-convex lens (focal length = 30 cm) with an antireflection coating was used to focus the image of the mask onto the target. It is mounted on an xyz-stage for alignment purposes. The magnification (M) must be chosen to give the desired energy density. It is given by,

$$M = -\frac{S_i}{S_o} \tag{2.1}$$

where, S_i and S_o are the image and object distances respectively. Once it is set,

the positions of the mask and lens are dictated by the Gaussian lens formula given by,

$$\frac{1}{S_o} + \frac{1}{S_i} = \frac{1}{f} \tag{2.2}$$

where, f is the focal length of the lens. In practice, the lens and mask are placed in approximately the correct positions and fine adjustments are made empirically. Several laser pulses are directed at a piece of plastic situated in the target position. Properly aligned optics will yield a damage spot which is both rectangular and uniform.

As a final remark, it is noteworthy that the light path is at an angle of 45° with respect to the target. Thus, a perfect focus is not possible with a simple lens as the image on the target is not parallel to the focal plane. The rotation of the laser pulse by the first two mirrors limits this effect, since a rectangular spot whose width is greater than its height sustains the most distortion while a pulse rotated 90° suffers the least distortion.

THE DEPOSITION CHAMBER

The chamber is constructed out of stainless steel and is 9 inches in diameter. It contains six ports onto which flanges can be attached that contain the various chamber components such as the furnace and target rotator. All of the flanges are the same size and are therefore interchangeable. This design simplifies the process of making modifications and revisions to the chamber. A removable lid provides easy access to the chamber and contains a 2 inch viewing port which is used to observe the plume and film during the growth process. The pumping system is connected to the bottom of the chamber. It consists of a Alcatel 3 inch diffusion pump backed up by a Edwards E2M12 roughing pump. The base pressure of the system is 1×10^{-6} Torr as measured by an ionization gauge. Although this is a relatively poor vacuum, high-T_c superconductors are forgiving in the sense that

high quality material can grow under these conditions.

The targets are mechanically clamped to a holder which allows both translational and rotational motion. The shaft of the target holder is fed through a double o-ring seal and is rotated by gears which are driven by an AC motor. The target, which is typically $1\frac{1}{4}$ inches in diameter, completes one revolution every 25 minutes. The translational motion allows the distance between the target and furnace to be varied. This distance is typically 3 cm. Because of this close proximity the target can reach temperatures in excess of 200 °C. To prevent this the target holder is air cooled from behind and is constructed out of copper to expedite the cooling process.

The furnace consists of a resistively heated Kanthal wire encapsulated in a metallic cylinder. The cylinder is constructed out of Inconel since it is resistant to oxidation at high temperatures. To reduce the heat loss the entire furnace is surrounded by radiation shielding. With the shielding in place it takes approximately 200 watts of power to maintain a temperature of 750 °C. The plume is allowed to reach the furnace through a $\frac{1}{2}$ inch diameter hole in the radiation shielding which can be blocked off by a manual shutter. The temperature of the furnace is measured by a type S Pt/PtRh thermocouple clamped to the surface of the furnace. It is important to recognize that the thermocouple is measuring the temperature of the furnace block which can be as much as 50 °C higher than the substrate. The temperature is regulated by a Thermo Electric Tempstar II temperature controller which maintains a constant temperature to an accuracy of ± 1 °C.

The final growth parameters which require attention are those involving gases released into the chamber. *In situ* growth of oxide superconductors require the presence of oxygen within the chamber. During the deposition process oxygen is leaked into and out of the chamber while maintaining a constant pressure. Because of the important role played by the deposition parameters involving oxygen they have been quantified and automated as much as possible. The oxygen pressure

which is measured by a Granville-Phillips convectron vacuum gauge, is controlled by an automatic pressure controller which regulates a servo driven valve. The flow is continuously monitored by a Sierra Top Trak flow meter. In some cases, helium gas was released into the chamber to accelerate the cooling process once the film growth was complete.

II. GROWTH AND CHARACTERIZATION OF 1212 PSYCCO FILMS

INTRODUCTION

For the most part, the growth of high-T_c thin films has been devoted to the production of highly oriented material with excellent transport properties of well established compounds. New superconductors are usually first seen in multiphase polycrystalline pellets. This initial discovery is followed by a determination and purification of the superconducting phase and the production of single crystals. In this process the compound undergoes an array of characterization procedures as well as a myriad of substitutional chemistry. Only after this storehouse of information is gathered are thin films grown. Our growth of 1212 PSYCCO thin films proceeded in a different manner in that the discovery, the purification of the superconducting phase and the investigation of the substitutional chemistry were all done in concert with the polycrystalline work. Our initial discovery stemmed from our attempts to grow the 2213 PSYCCO phase. It was soon realized that the growth kinetics and substrate interaction involved in the laser deposition process strongly favoured the growth of a new superconducting phase. The $(Pb_{0.75}Cu_{0.25})Sr_2(Y_{1-y}Ca_y)Cu_2O_{7+\delta}$ phase was established through the variation of the target stoichiometry and comparisons to new work on polycrystalline samples. Even with this realization, the growth of this compound presented many challenges as the effects of x, y and δ on the superconducting properties were

not well established. The work presented here will discuss the variation of these parameters and will only show our most recent results where the stoichiometry of the target has been optimized.

THE TARGETS

The process of laser ablation results in the stoichiometry of the target being transferred to the substrate. Thus, the composition of the target is chosen to match that of the film to be produced. Deviations from this behaviour arise when the sticking coefficient of an element at the substrate temperature used is less than unity rendering the film deficient in that element. Pb is such an element and to counteract this effect all targets must be Pb enriched. The extent to which the target must be enriched is intimately connected to other growth parameters such as substrate temperature, repetition rate and the oxygen partial pressure within the chamber. For the optimized growth parameters approximately 5 % of the Pb incident upon the substrate ends up in the film as measured by inductively coupled plasma mass spectrometry (ICP/MS). A degree of uncertainty exists in the ICP/MS results since this characterization technique cannot distinguish between particulates and the superconducting film as it treats all atoms on an equal footing. The particulates can constitute a significant percentage of the overall film volume, but are not representative of the true nature of the surrounding film. ICP/MS can either overestimate or underestimate the film's Pb content depending upon whether the particulates are Pb rich or Pb poor.

The target was prepared in a two step process in a manner similar to that described by Cava *et al.*[9] A precursor of $Sr_2Y_{0.5}Ca_{0.5}Cu_2O_x$ was made from stoichiometric amounts of $SrCO_3$, Y_2O_3, $CaCO_3$ and CuO. The precursor was sintered at 900 °C for 12 hours in air, after which the furnace was shut off and allowed to cool to room temperature. The precursor was then reground and PbO was added. The target was then annealed at 700 °C for 12 hours in flowing nitrogen

and allowed to cool to room temperature. Because of the lead enrichment, the targets are not superconducting and are often insulating.

A PSYCCO target which is hit repeatedly with laser pulses undergoes a slow change. Initially the plume is pink in colour and has a length of approximately 3 cm. Its length gradually decreases as more laser pulses strike the target. Eventually the pink plume develops a green halo. All of these effects, which occur over the course of thousands of laser shots, are a clear indication that the target is undergoing a metamorphosis which may effect both the stoichiometry and growth rate of the film. Obtaining reproducible results under these conditions was impossible. To alleviate this problem two measures were taken. First, the target was rotated to limit the number of laser pulses hitting a single spot. Thus, over the course of a single film growth neither of these effects were seen. Second, before each film deposition the surface of the target was removed to provide a reproducible surface. This removal process could result in the contamination of the target surface. The contaminants are removed immediately before the growth process by allowing laser pulses (repitition rate = 2 Hz) to strike the target as it rotates through one complete revolution. Throughout this process the shutter is kept closed to protect the substrate. Once the contaminants have been removed the shutter is opened allowing the ablated material to reach the substrate.

THE SUBSTRATES

Of all the substrates commonly used for the growth of oxide superconductors (100) $LaAlO_3$ was found to be the most suitable for the deposition of 1212 PSYCCO films. It is not surprising that the best films grow on this substrate since it has the smallest lattice mismatch (0.87 %) to PSYCCO's tetragonal unit cell. Even though $LaAlO_3$ is the only substrate used in this work it is not ideal. Its major deficiency is that it contains twins formed during a cubic to rhombohedral phase transition occurring at 550 °C. PSYCCO's tetragonal unit cell presents the

opportunity of having improved transport properties associated with the epitaxial growth of an untwinned superconductor. The twins exhibited by the substrate destroy this opportunity. The search for new substrates is an active field of research and should result in a substitute for $LaAlO_3$.

Before the film deposition takes place, the substrate undergoes a cleaning procedure to remove any residues left over from the polishing and cutting processes. The substrate is placed in an ultrasonic bath where it is exposed to soap, distilled water, methanol and acetone. The clean substrate is attached to the furnace with a uniform layer of silver paint to promote good thermal contact. The substrate temperature used to grow these films was 620 °C. This is a relatively low substrate temperature for growing laser ablated films. As a comparison our $YBa_2Cu_3O_{7-\delta}$ films on MgO grown in the same chamber gave an optimal T_c of 93 K for a furnace temperature of 760 °C which is in agreement with previous work.[106] This is of some significance, since much effort has gone into lowering the substrate temperature in order to facilitate the growth of $YBa_2Cu_3O_{7-\delta}$ on more reactive substrates such as silicon, GaAs and sapphire without the presence of a buffer layer. At best, these attempts have resulted in poor quality superconductors with the c-axis oriented parallel to the substrate.

THE OXYGEN ENVIRONMENT

In order to obtain *in situ* growth it was necessary to leak oxygen into the chamber as the film was deposited. This was done at a flow rate of 4 standard cubic cm per minute (SCCM) while maintaining a constant pressure of 300 mTorr. At the end of the growth period the furnace was shut off and the chamber was filled with half an atmosphere of oxygen. Optimization of these growth parameters involving oxygen revealed that PSYCCO, like $YBa_2Cu_3O_{7-\delta}$, grows best in an oxygen rich environment. The ease with which the oxygen environment was chosen to yield the best transport properties is somewhat surprising when it is realized

that most of the difficulties in growing polycrystalline samples are attributed to an incorrect oxygen stoichiometry. The differences between the polycrystalline and thin film results may be due to the much lower processing temperatures used in the laser deposition process.

The pulsed laser deposition technique allows for easy variation of δ in the $(Pb_{0.75}Cu_{0.25})Sr_2(Y_{1-y}Ca_y)Cu_2O_{7+\delta}$ compound, but it is difficult to quantify the amount and position of the oxygen atoms entering and leaving the crystal structure. Thus, our aim was to optimize the oxygen growth parameters to obtain the value of δ which would yield the best transport properties. It was found that the removal of oxygen from a fully oxidized sample results in drop in T_c of 10 to 15 K.

THE FILM GROWTH RATE

In order to obtain the highest quality films it was necessary to lower the deposition rate to approximately 500 Å/hour which is an extremely small value even when compared to the standards set by molecular beam epitaxy (MBE). The film deposition rate is dependent upon the amount of material incident upon the substrate per laser pulse and the laser pulse frequency. Each pulse (fluence = 1.5 J/cm^2) results in an average deposition of 0.28 Å which is a factor of three to four smaller than typical values for other oxide superconductors. The low value can be accounted for by the fact that most of the lead incident upon the heated substrate is not incorporated into the film. Initially, the laser pulse frequency was set to 2 Hz, but it was found that each drop in this value improved film quality. Ultimately, the frequency was set at $\frac{1}{2}$ Hz and the film was grown over a period of 4 hours resulting in a thickness of 2000 Å.

FILM STRUCTURE AND ORIENTATION

The standard $\theta - 2\theta$ x-ray diffraction scan has been performed on approximately 40 samples using Cu K_α radiation. Each of these samples shows a high degree of orientation with the c-axis perpendicular to the substrate as illustrated by Fig. 2.3. These (00l) reflections yield a lattice parameter of 11.90 Å. The x-ray scans show no evidence of other orientations or phases.

The main deficiency of the $\theta - 2\theta$ x-ray diffraction characterization technique is that it results in the acquisition of only one lattice parameter for an oriented film. Even though the c-axis lattice parameter obtained is identical to that of the 1212 PSYCCO phase, more information is needed to conclusively identify the material. The ideal method for determining structural information is to use powder x-ray diffraction. This is not feasible for a film under normal circumstances since a powder consisting of both substrate and film will only show the overwhelming response of the substrate. However, if the film is removed from the substrate in a manner which maintains its integrity then there is more than enough material to perform powder x-ray diffraction using a Guinier camera with Cu K_{α_1} x-rays. Film removal can be a difficult task as high quality films have excellent adherence to the substrate. Lasers have been used to remove metallic films for the purpose of patterning[107] and for film adhesion studies.[108] The process involves the passage of an excimer laser pulse through the back surface of the substrate which induces a shock at the film/substrate interface that is intense enough to liberate the film. We have adopted this simple procedure to remove the PSYCCO films from the substrates in the form of small flakes which are suitable for powder x-ray work.

The apparatus used for film removal is shown in Fig. 2.4. The laser beam is masked so that it is spatially uniform. It is then reflected by a mirror onto a lens which focuses the beam to a 0.5 mm diameter spot size which corresponds to a laser energy density of less than 0.5 J/cm^2. Small pieces (≤ 10 μm) of the film fall from the substrate and are collected onto a holder which is suitable for Guinier camera work. By scanning the laser beam over the film surface the entire film

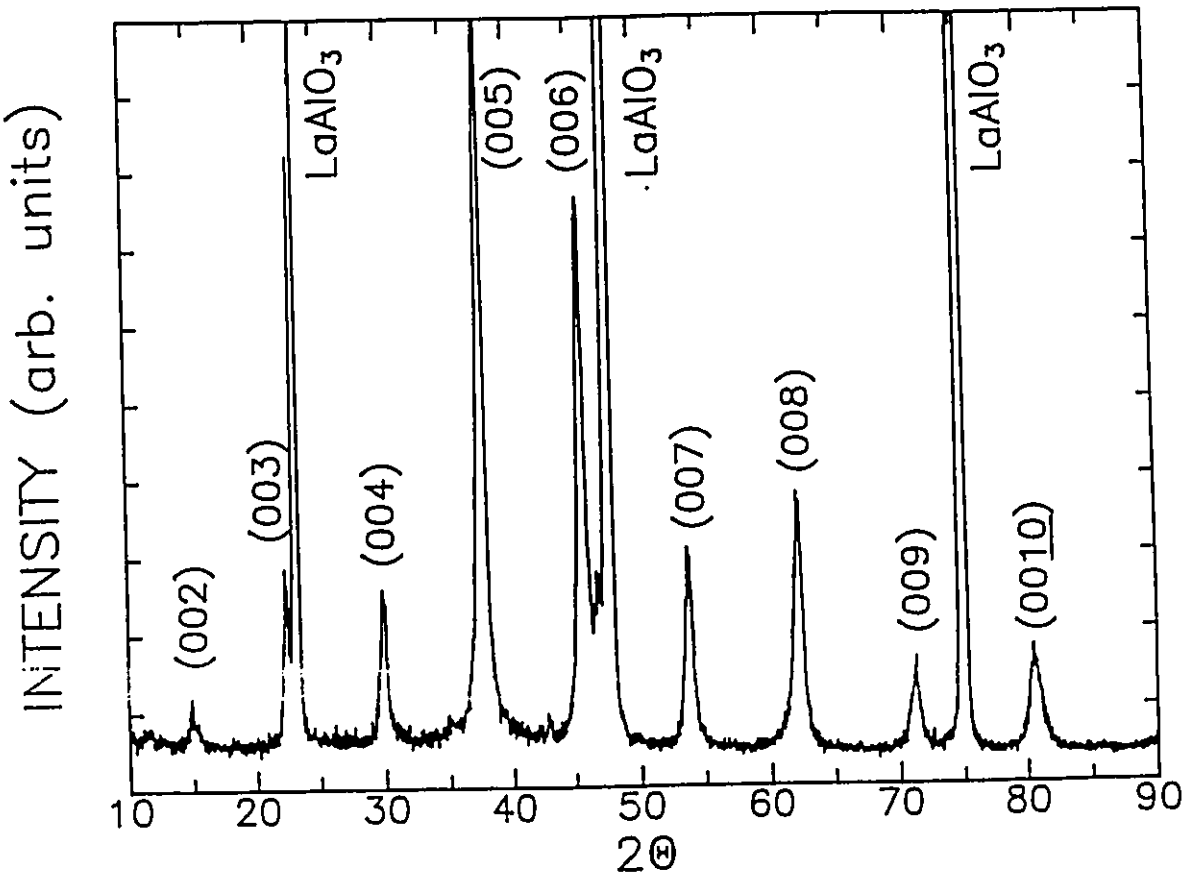

Fig. 2.3 $\theta - 2\theta$ diffraction scan for a 1212 PSYCCO film which indicates that the film is oriented with the c-axis perpendicular to the substrate with c=11.90 Å.

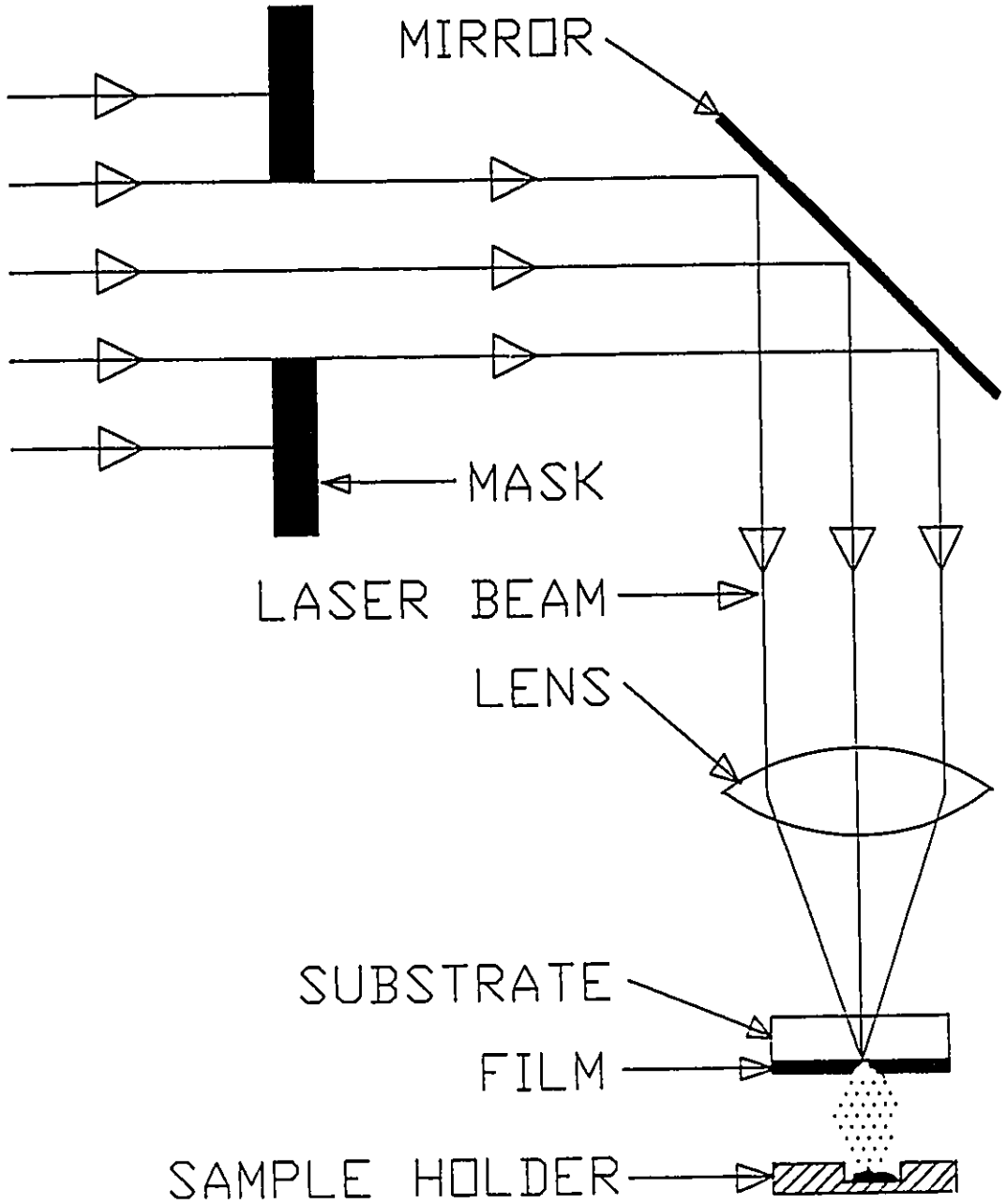

Fig. 2.4 Schematic of the film removal apparatus. An image of the mask is focused by the lens onto the film/substrate interface resulting in a shock wave that is intense enough to liberate the film. The film flakes are collected on a sample holder suitable for Guinier camera work.

can be removed. The obvious limitation of this technique is that it is only useful when the substrate is transparent to the laser wavelength used. A 308 nm XeCl excimer laser fulfills this requirement for $LaAlO_3$, but does not for silicon and $SrTiO_3$ which are substrates commonly used in the growth of high temperature superconductors. This however, does not rule out the possibility of using longer wavelength laser pulses for the film removal process.

The above technique was an instrumental part in the characterization of our 1212 PSYCCO films. In our attempts to grow the 2213 PSYCCO phase we obtained a highly oriented film with a transition temperature in excess of 70 K, but the c-axis lattice parameter obtained from the $\theta - 2\theta$ diffraction scan indicated that we were growing a different phase. Thus, we resorted to the powder x-ray diffraction technique to obtain more structural information. The x-ray lines obtained from the powder originating from a film with dimensions of 7 mm x 7 mm x 2000 Å are shown in Table 2.1. There exist 21 lines which fit to a tetragonal unit cell of a=3.821(5) Å and c=11.896(2) Å . These lattice parameters match those derived from the polycrystalline 1212 PSYCCO phase given by $(Pb_{1-x}Cu_x)Sr_2(Y_{1-y}Ca_y)Cu_2O_{7+\delta}$. This allowed us to adjust the target composition so as to obtain the correct stoichiometry resulting in an improvement in film quality.

This method of characterization has two drawbacks. First, it is a destructive technique, but this is not a major concern since it results in the acquisition of information which would otherwise be unavailable. Second, it is unclear if the film undergoes changes in the removal process where it is subject to intense heating at the film/substrate interface. The fact that the c-axis lattice parameter obtained from the $\theta - 2\theta$ diffraction scan is unaltered in the process suggests that this is not a problem for PSYCCO films. By contrast, removal of $YBa_2Cu_3O_{7-\delta}$ films from the substrate showed a change in colour, which is most likely due to a loss of oxygen.

h	k	l	d(observed) (Å)	d(calculated) (Å)
0	0	1	11.9178	11.8964
0	0	3	3.9607	3.9655
1	0	0	3.8257	3.8212
1	0	1	3.6425	3.6381
1	0	2	3.2134	3.2149
0	0	4	2.9738	2.9741
1	0	3	2.7514	2.7516
1	1	0	2.6992	2.7020
1	1	1	2.6329	2.6349
0	0	5	2.3786	2.3792
0	0	4	2.3485	2.3470
1	1	4	2.0014	1.9999
2	0	0	1.9104	1.9106
1	1	5	1.7858	1.7857
0	0	7	1.6989	1.6994
2	1	1	1.6920	1.6915
2	1	3	1.5687	1.5694
2	0	5	1.4905	1.4897
2	2	0	1.3512	1.3510
2	2	2	1.3175	1.3174
3	1	0	1.2079	1.2084

Table 2.1 - The x-ray lines obtained from the powder originating from a 1212 PSYCCO film. These lines can be fit to a tetragonal unit cell with a=3.821(5) Å and c=11.896(2) Å. The third column shows the values associated with the fit.

THE SURFACE MORPHOLOGY

The PSYCCO films are black in colour and have optically smooth surfaces. Scanning electron microscopy (SEM) has been used to look at the surface morphology of the films. Figure 2.5 shows a typical SEM micrograph for a PSYCCO film on a 10 μm scale. It exhibits the spherical particulates which are common to the laser ablation process. These particulates are of the order of 1 μm in size and are similar in shape and number to those found on $YBa_2Cu_3O_{7-\delta}$ films. These larger particulates are dispersed in a sea of precipitates with irregular shapes and sizes whose origin will be discussed below.

Figure 2.6 shows an SEM micrograph on a 1 μm scale corresponding to a film with a stoichiometry of $(Pb_{0.75}Cu_{0.25})Sr_2(Y_{0.4}Ca_{0.6})Cu_2O_7$. It exhibits an array of well defined squares approximately 700 Å on a side. X-ray analysis shows that the film is highly oriented with c-axis perpendicular to the substrate. Thus, the squares originate from the tetragonal crystal structure and indicate the presence of columnar grains. The alignment of the columns is a clear indication that the films are growing epitaxially. This surface morphology is distinct among the cuprate superconductors and may indicate the presence of a growth process different from that seen in $YBa_2Cu_3O_{7-\delta}$ films. The size of the columns may originate from the relief of stress caused by the lattice mismatch between the substrate and film.

The thickness of the film shown in Fig. 2.6 is approximately 2000 Å as measured by a Tencor α-step profilometer. As the film thickness is increased the columnar growth becomes unstable resulting in a deterioration in the surface morphology. Figure 2.7 shows a micrograph of a 1 μm thick film which is characterized by surface growths with random orientations. X-ray analysis on this film indicates the presence of lines which cannot be attributed to the 1212 PSYCCO phase. In order to avoid the complications associated with thick films all of the results presented here are for films with a thickness of 2000$\pm$500 Å.

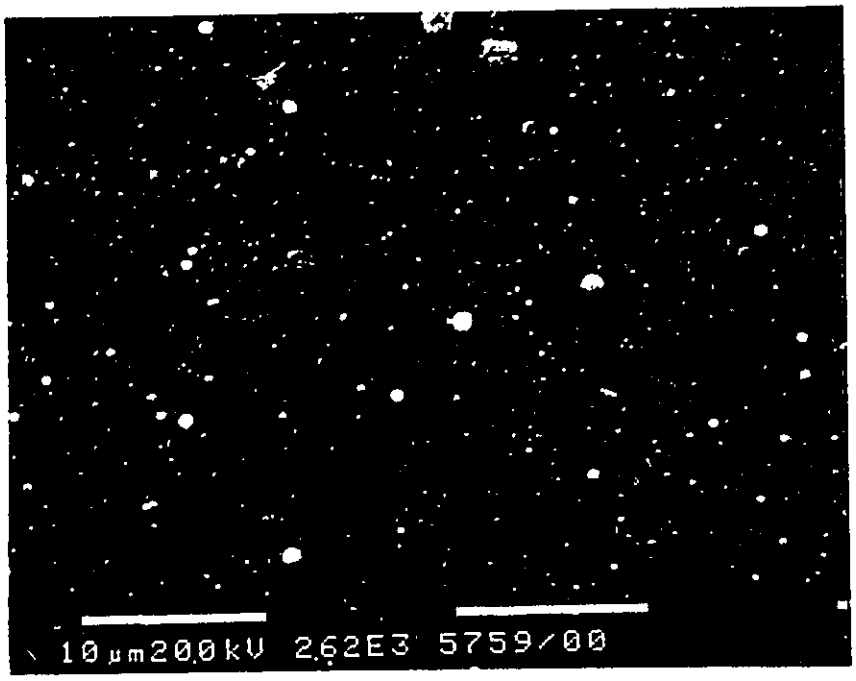

Fig. 2.5 SEM micrograph showing the surface morphology of a PSYCCO film on a 10 μm scale. There exists two types of features (1) large spherically shaped particulates and (2) small irregular shaped precipitates.

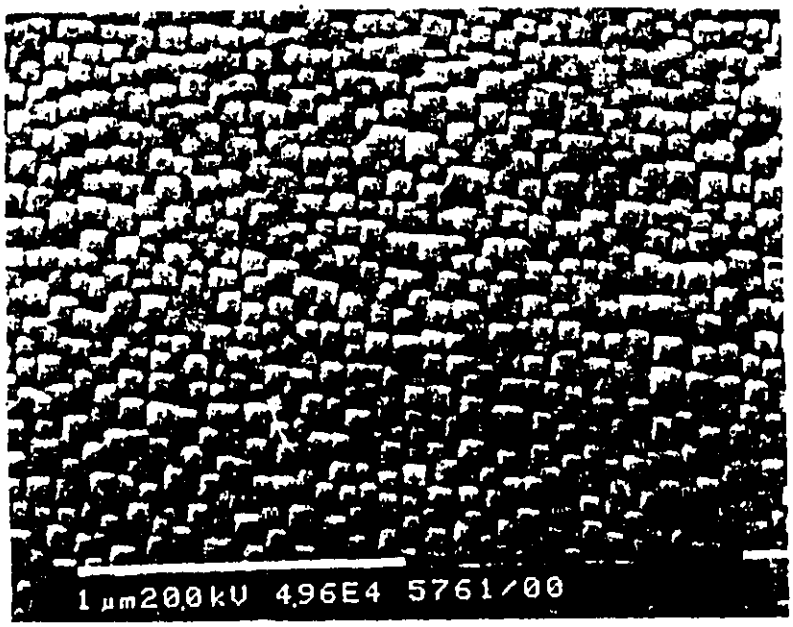

Fig. 2.6 SEM micrograph of a 1212 PSYCCO film on a $LaAlO_3$ substrate. The surface is characterized by well aligned squares indicating the presence of epitaxial growth.

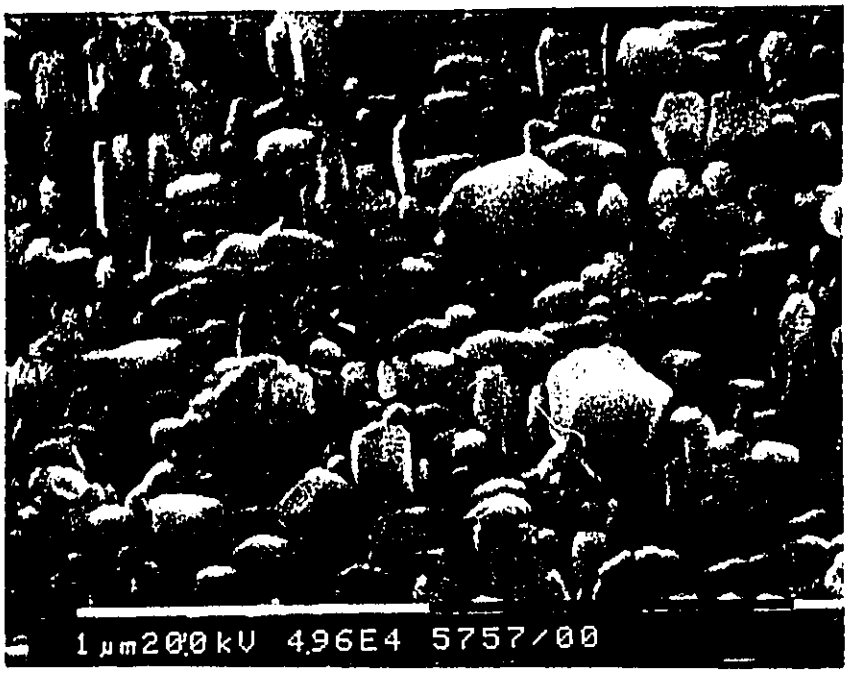

Fig. 2.7 SEM micrograph of a 1 μm thick film showing the presence of surface growths that develop for thick films.

THE TRANSPORT PROPERTIES

Figure 2.8 shows the resistivity as a function of temperature, as measured by the van der Pauw method, for a 1212 PSYCCO film with a stoichiometry of $(Pb_{0.75}Cu_{0.25})Sr_2(Y_{0.4}Ca_{0.6})Cu_2O_7$. The onset of the superconducting transition at 86 K with zero resistance at 80 K is the highest reported value for a 1212 PSYCCO superconductor. The normal state resistivity deviates slightly from the usual linear behaviour. At this time it is unclear whether these deviations are intrinsic, but two factors suggest that it is not. First, the extent of these deviations have steadily decreased as the sample quality improves. Second, similar deviations have been seen for many $YBa_2Cu_3O_{7-\delta}$ films[109–113] where the linear resistivity is intrinsic.

THE EFFECT OF VARYING x AND y IN THE $(Pb_{1-x}Cu_x)Sr_2(Y_{1-y}Ca_y)Cu_2O_{7+\delta}$ COMPOUND

The 1212 PSYCCO compound offers many opportunities to investigate the effect of varying the stoichiometry. This section is devoted to a discussion of the effects of varying the values of x and y in the $(Pb_{1-x}Cu_x)Sr_2(Y_{1-y}Ca_y)Cu_2O_{7+\delta}$ compound. As the Y/Ca ratio was varied the value of x was held constant at x=0.25 for reasons which will be discussed below. The effect of varying this ratio is very pronounced as indicated by the resistivity curves given in Fig. 2.9 and the variation in the superconducting transition temperature given in Fig. 2.10. It is clearly seen that as Ca is substituted for Y there is a systematic increase in T_c. In addition, there is an obvious progression from semiconducting to metallic behaviour. The above results can be explained by an increase in the hole carrier concentration in the CuO_2 planes arising from the substitution of Ca^{2+}on the Y^{3+} site. Tang *et al.*[52] shows similar results on polycrystalline samples, except that the transition temperatures of our films are consistently higher, and our T_c versus Ca content plot shows a more well defined trend. This

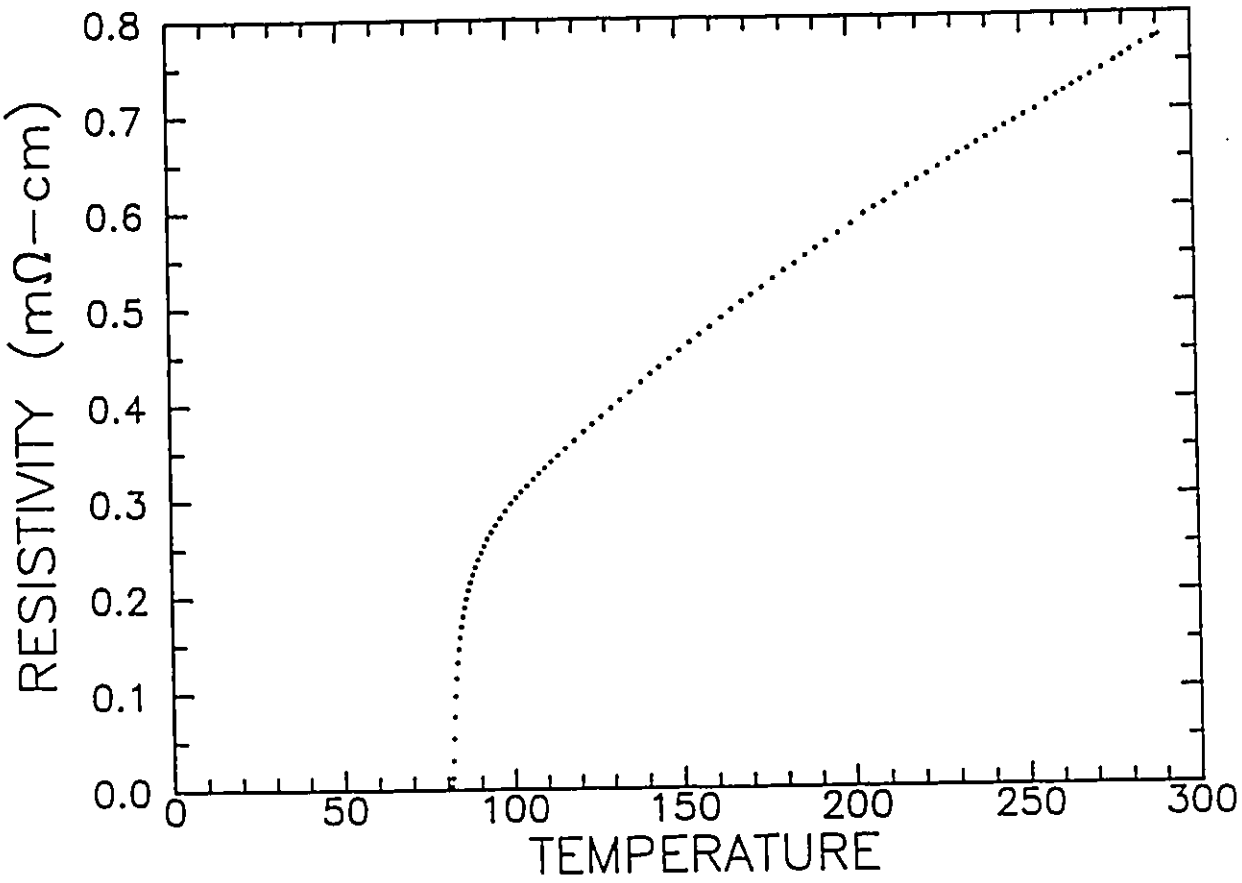

Fig. 2.8 Resistivity vs temperature for a $(Pb_{0.75}Cu_{0.25})Sr_2(Y_{0.4}Ca_{0.6})Cu_2O_7$ film. The superconducting transition onsets at a temperature of 86 K with a width of 4 K.

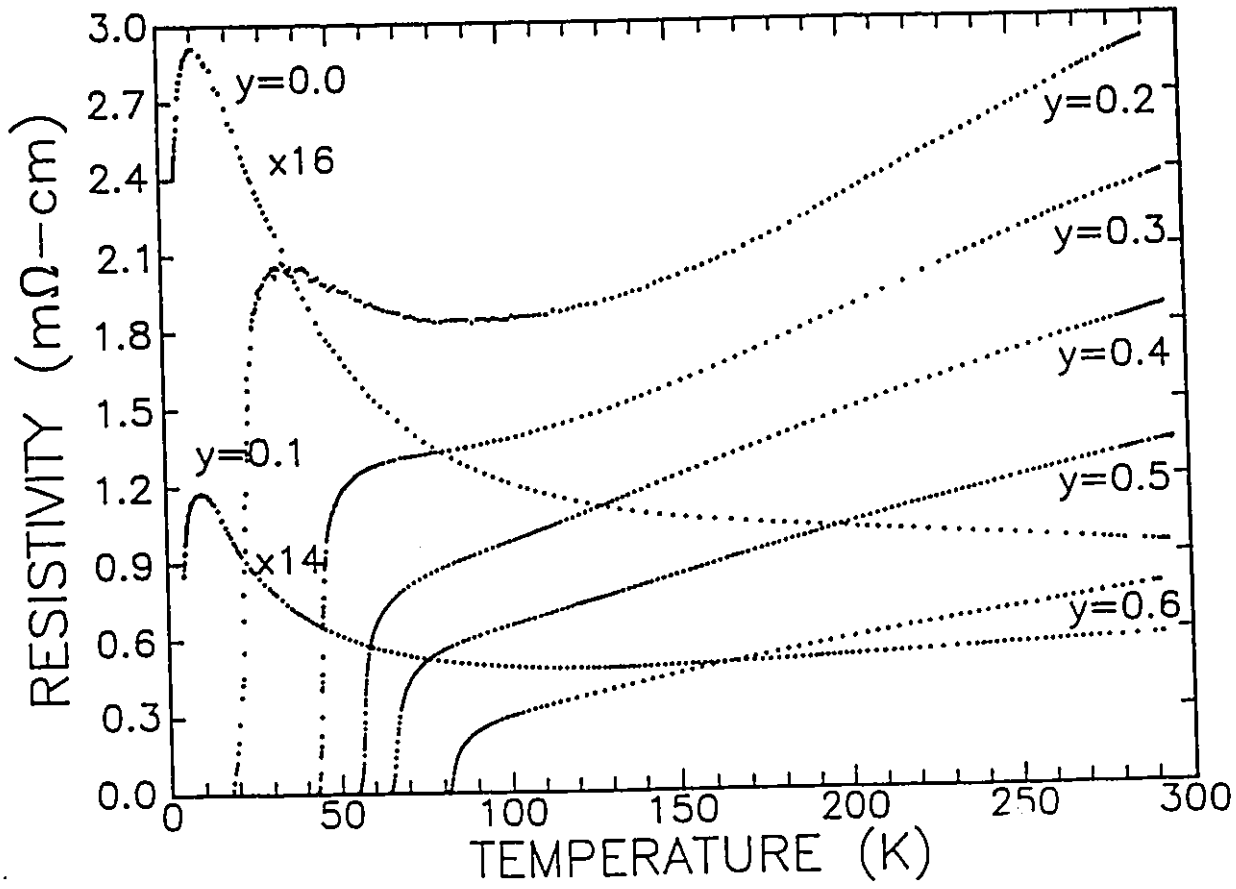

Fig. 2.9 Resistivity vs temperature for $(Pb_{0.75}Cu_{0.25})Sr_2(Y_{1-y}Ca_y)Cu_2O_7$ films for various values of y. There is a progression from semiconducting to metallic behavior as well as a systematic rise in T_c as the Ca content is increased.

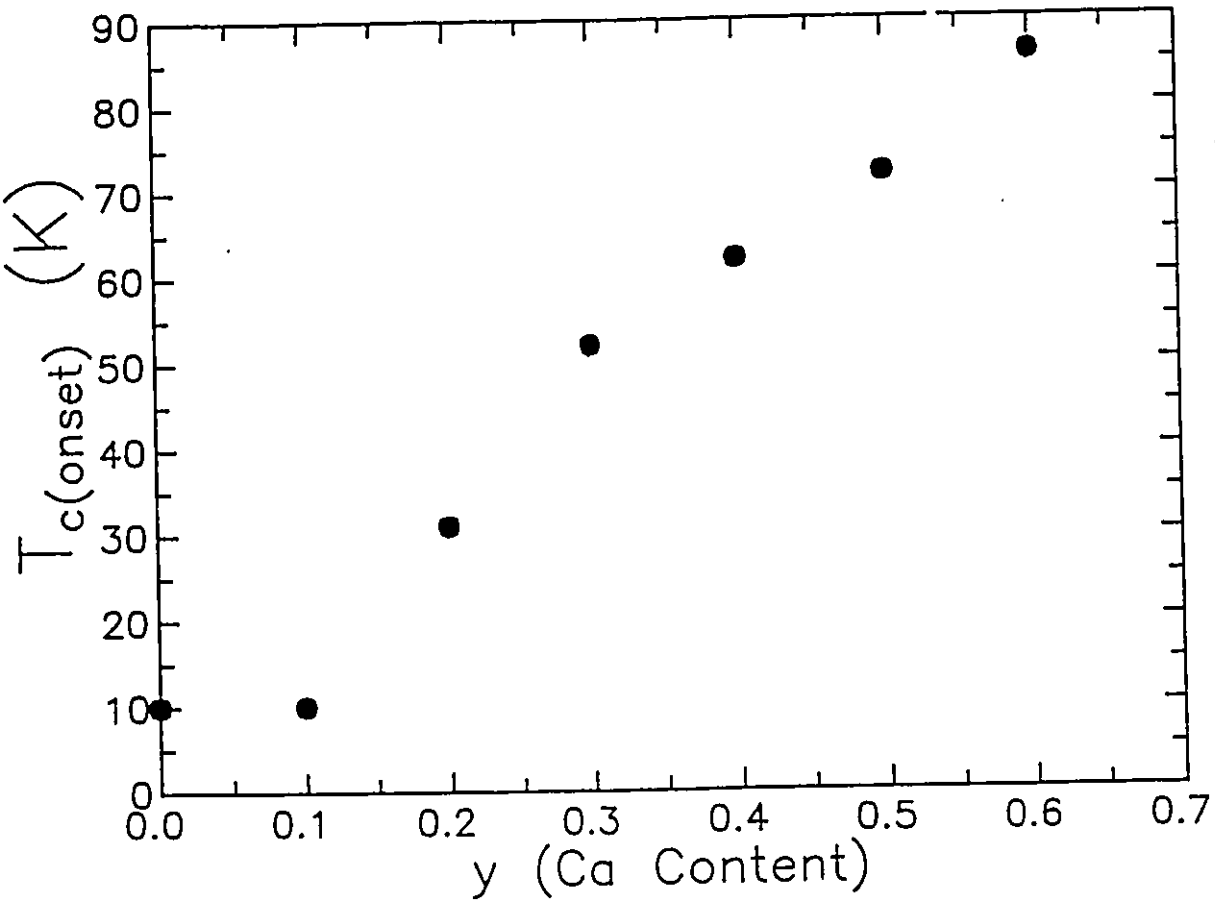

Fig. 2.10 Onset of the superconducting transition temperature as a function of Ca content within the film.

disagreement may originate from differences in the oxygen content between the films and polycrystalline samples. There is, however, agreement in the fact that the solubility limit of Ca in this structure is reached for $y \geq 0.7$ as indicated by a deterioration in both the resistive transitions and x-ray spectra. It is worthwhile to point out that films which contain no calcium (y=0) still show the onset of a superconducting transition. A short vacuum anneal destroyed the transition implying that oxygen is the source of the remaining carriers.

Variations of the Pb/Cu ratio showed no effect on the onset of the superconducting transition except for the composition corresponding to an all Pb layer (i.e. x=0). This sample had a marked decrease in its transition temperature. In addition, there were no variations in the c-axis lattice parameter which is the expected result only if Pb exists in the 4+ oxidation state which has an ionic radius close to Cu^{2+}. The width of the superconducting transition did show a narrowing for compositions corresponding to ($Pb_{0.8}Cu_{0.2}$) and ($Pb_{0.7}Cu_{0.3}$). These two facts may indicate that the film's copper concentration in the (PbCu) plane can only exist within the narrow range of approximately 0.2 to 0.3, and any extra copper added to the target ends up in an impurity phase which is not detectable with the $\theta - 2\theta$ x-ray analysis performed on the films. Verifying the existence of a copper rich impurity phase is a difficult task considering the small amount of material available in a thin film, but two facts lend credibility to its existence. First, scanning electron microscope (SEM) images of film surfaces show the presence of precipitates which are easily distinguishable from the superconducting grains (Fig. 2.11). These precipitates may be the copper rich impurity phase as they have become less numerous (compare with Fig. 2.6) as we have optimized the film stoichiometry. Second, detailed x-ray work on non-superconducting single crystals with a stoichiometry of $(Pb_{.71}Cu_{.29})Sr_2(Y_{.73}Ca_{.27})Cu_2O_7$ by Lee *et al.*[51] indicate the presence of a lattice distortion which moves the copper atom in the (PbCu) plane off of its site. It is unlikely that the distortion will exist for all concentrations of Cu within the plane. If the distortion is necessary for a stable crystal

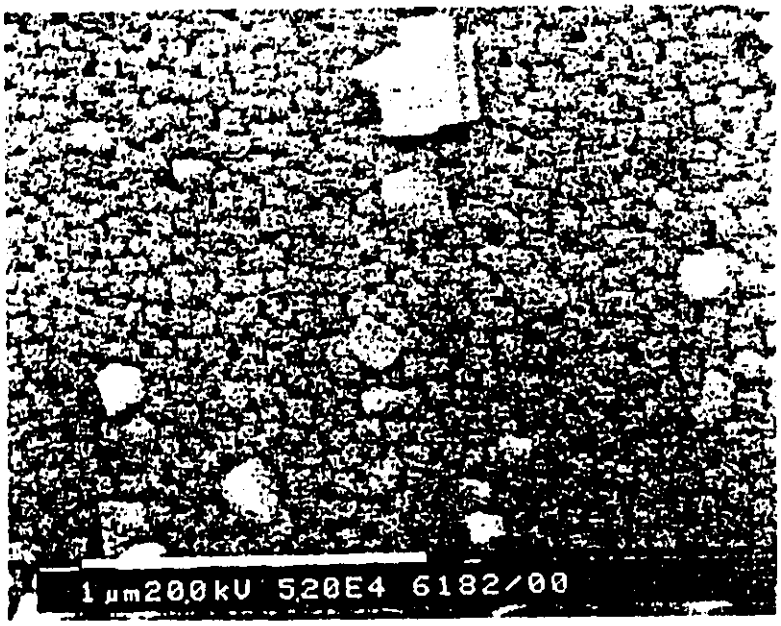

Fig. 2.11 SEM micrograph of a 1212 PSYCCO film showing the presence of surface features which become more numerous as the value of x in $(Pb_{1-x}Cu_x)Sr_2(Y_{1-y}Ca_y)Cu_2O_{7+\delta}$ is increased.

structure, and hence film growth, then excess copper must end up in an impurity phase. This problem requires further study which is more suited to single crystal and polycrystalline samples.

CONCLUSIONS

1212 PSYCCO superconducting films grown by pulsed laser deposition show much potential from many perspectives. From the point of view of film growth it shows much promise in that (1) it is tetragonal with a close lattice match to $LaAlO_3$ and (2) it can be grown *in situ* at the relatively low substrate temperature of 620 °C. In addition, its unique surface morphology is worthy of further study. As a relatively new superconductor it offers the opportunity to explore a wide range of substitutional chemistry. From the point of view of fundamental physics it has great potential as it is a completely unexplored material. The ability to systematically vary the superconducting transition temperature in a highly oriented thin film should prove to be a useful tool in the understanding of high temperature superconductivity.

III. GROWTH AND CHARACTERIZATION OF $Nd_{1.85}Ce_{0.15}CuO_{4+\delta}$ FILMS

INTRODUCTION

A preliminary investigation of the feasibility of growing $Nd_{1.85}Ce_{0.15}CuO_{4+\delta}$ by pulsed laser deposition suggests that it would be a rather simple process. With the exception of oxygen, all of the elements contained in the compound are relatively stable. Also, there exists only one stable phase containing these elements. Thus, obtaining the correct crystal structure is easily accomplished with a stoichiometric target. This turns out to be a correct assumption, but the stringent conditions imposed on the oxygen content needed to induce superconductivity turns out to

be a major obstacle. Obtaining the correct stoichiometry cannot be achieved by choosing an appropriate oxygen pressure during the deposition process. Lowering the pressure to the required levels results in a reduction of copper's sticking coefficient at the substrate temperatures necessary for epitaxial growth.[114] In order to stabilize the copper it is required that the film be grown in an oxygen rich environment, but in this scenario the films end up with an excess of oxygen. To rid the crystal structure of this excess oxygen without damaging the film is the main challenge experienced in the production of superconducting $Nd_{1.85}Ce_{0.15}CuO_{4+\delta}$ films.

THE TARGET

The target was prepared in the same manner as a superconducting polycrystalline pellet except that it was not exposed to the reducing atmosphere required to induce superconductivity. Briefly, appropriate amounts of Nd_2O_3, CuO and CeO_2 were ground together to form a powder with a nominal composition of $Nd_{1.85}Ce_{0.15}CuO_{4+\delta}$. The powder mixture was fired at 900 °C for 12 hours in air. It was then reground and pressed into a cylindrical pellet with a diameter of $1\frac{1}{4}$ inches. The pellet was then heated to 1000 °C in air for 48 hours followed by a cooldown to room temperature.

As the target was hit repeatedly with laser pulses the plume, which is blue in colour, began to decrease in size in a manner very similar to $YBa_2Cu_3O_{7-\delta}$ and $(Pb_{0.75}Cu_{0.25})Sr_2(Y_{1-y}Ca_y)Cu_2O_7$. Thus, it was deemed necessary to remove the surface of the target before each film growth to produce films with the same thickness. Keeping the film thickness constant between consecutive film growths is important from the standpoint of reproducibility as the vacuum anneal time is dependent upon this parameter.

THE GROWTH PARAMETERS

The growth parameters involving the laser are fairly typical of the ablation process. The laser was pulsed at 2 Hz for a period of 1 hour at a fluence of 2 J/cm^2. TEM cross-sections indicated that this resulted in a film thickness of 5000 Å. This corresponds to a growth rate of 0.7 Å/pulse which is a value comparable to $YBa_2Cu_3O_{7-\delta}$.

The a-axis lattice parameter of 3.946 Å for $Nd_{1.85}Ce_{0.15}CuO_{4+\delta}$ is unusually large compared to other cuprate superconductors. This makes (100) $LaAlO_3$ an unsatisfactory substrate for the growth of this material. On the other hand, (100) $SrTiO_3$ is a more appealing substrate with a lattice parameter of 3.905 Å. Gupta *et al.*[115] have shown that $SrTiO_3$ is suitable for epitaxial growth when maintained at a temperature of 780 °C. We have adopted this growth parameter and have made no attempt at further optimization.

During the growth of the film the oxygen pressure was maintained at 300 m'Torr while maintaining a flow rate of 4 SCCM. Any reduction in this pressure renders the film deficient in copper.[116] After the growth period is complete the excess oxygen contained in the film must be removed. Work with bulk and single crystal samples show that homogeneously reducing $Nd_{1.85}Ce_{0.15}CuO_{4+\delta}$ is a delicate task. The anneal is usually performed in an argon environment at temperatures in excess of 900 °C over a period of hours. The excess oxygen in the laser ablated films grown by Gupta *et al.*[115] was removed by evacuating the chamber once the film growth was complete while allowing the sample to remain at the growth temperature of 780 °C for 45 minutes. Even though the anneal was performed at lower temperatures for a shorter period of time it was found to be effective since the films large surface area to volume ratio provides optimal conditions for its reduction. The main drawback of this procedure is that it left the surface of the film deficient in copper as measured by Auger depth profiling.[116] To prevent the formation of this dead layer we have resorted to annealing the films for longer periods of time at a lower temperature. This eliminates the possibility of copper

loss from the surface. The anneal proceeds as follows:

- After the film growth was complete the substrate temperature was reduced to 600 °C while maintaining an oxygen pressure of 300 mTorr.
- The chamber is then evacuated leaving the film in a reducing environment for a period of 4 hours.
- Once this time period is complete the furnace is shut off allowing the sample to cool to room temperature. The chamber was often filled with helium to accelerate the cooling process.

The goal of this procedure was to obtain a homogeneous film with high quality transport properties.

TRANSMISSION ELECTRON MICROSCOPY

Transmission electron microscopy (TEM) provides the spatial resolution necessary to investigate the homogeneity of these samples. We have prepared TEM cross-sections by the standard techniques of mechanical polishing followed by ion milling. The cross-sections showed a sharp interface between the film and underlying substrate. Through the use of the energy dispersive x-ray analysis (EDX) mode on the transmission electron microscope it is possible to perform chemical analysis on a circular area with a diameter of approximately 50 Å. Thus, by moving the spot along the sample's cross-section a profile of the copper content can be obtained. If there exists a substantial surface layer which is copper depleted it should appear in this measurement. Fig. 2.12 shows the ratio of the intensities of the Cu K_α to the Nd K_α transitions for two samples. Sample A, which was prepared with the low temperature anneal as described above, yields a ratio which is approximately constant as expected for a homogeneous sample. In contrast sample B, which was annealed under non-optimum conditions (780 for 25 minutes), shows a decline in the ratio characteristic of a copper depleted surface.

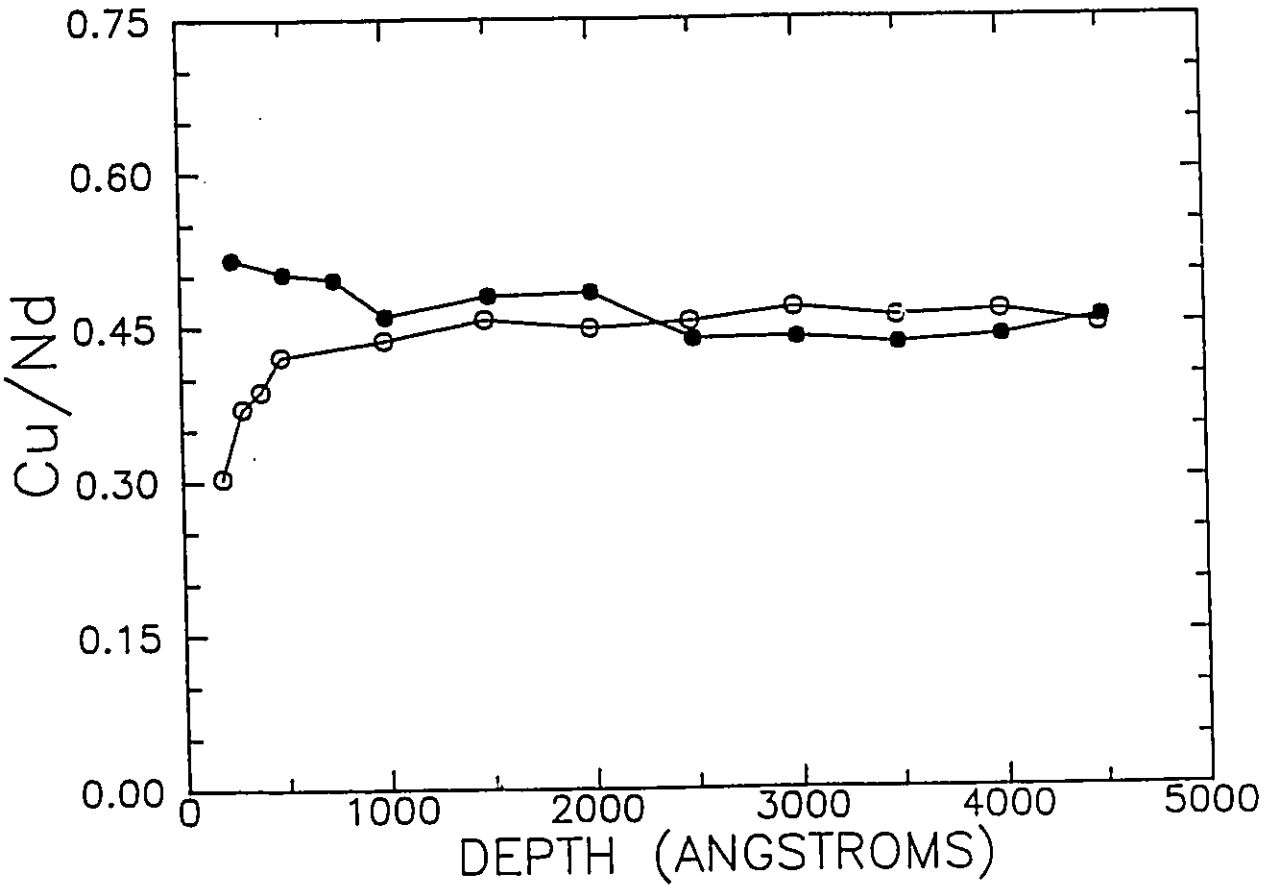

Fig. 2.12 The ratio of the intensities of the Cu K_α and Nd K_α transitions extracted from EDX spectrum versus the depth from the film surface. Sample A (•) was annealed at low temperatures while sample B (o) was annealed at high temperatures.

Thus, the low temperature anneal has been successful in minimizing the copper depleted surface to the extent that it is not observed in the EDX analysis.

THE TRANSPORT PROPERTIES

As expected the transport properties strongly depend upon the annealing procedure. Figures 2.13 and 2.14 show the transformation from semiconducting to superconducting behaviour that the film undergoes during the anneal process. The semiconducting sample was grown in an oxygen rich environment and was allowed to cool to room temperature without a vacuum anneal. It exhibits a sharp rise in its resistivity for temperatures below 60 K. The annealed sample shows a metallic response for temperatures above the superconducting phase transition. The onset of superconductivity at 21 K is consistent with the best results on bulk samples for the cerium concentration chosen. The inset to Fig. 2.14 shows that the film exhibits a sharp superconducting transition with a width of 1.5 K. The resistive transition is not the best test of sample quality. A superior test is the diamagnetic transition which was measured by a non-contact inductive technique[117] (Fig. 2.15). It shows a sharp transition at a somewhat reduced temperature. Even though the transition is quite sharp, it is still broader than the best $YBa_2Cu_3O_{7-\delta}$ films. Thus, it is felt that some oxygen inhomogeniety remains.

FILM STRUCTURE AND ORIENTATION

The $\theta - 2\theta$ x-ray diffraction scans show that the samples are highly oriented with the c-axis perpendicular to the substrate as illustrated by Fig. 2.16. These (00l) reflections yield a lattice parameter of c=12.07 Å which is consistent with single crystal results for the cerium concentration used. Two lines corresponding to (110) and (220) reflections indicate the presence of non-c-axis growths which were also apparent in other laser ablated[115] and sputtered[118] films. These x-ray diffraction scans give the impression that these growths are quite prominent, but

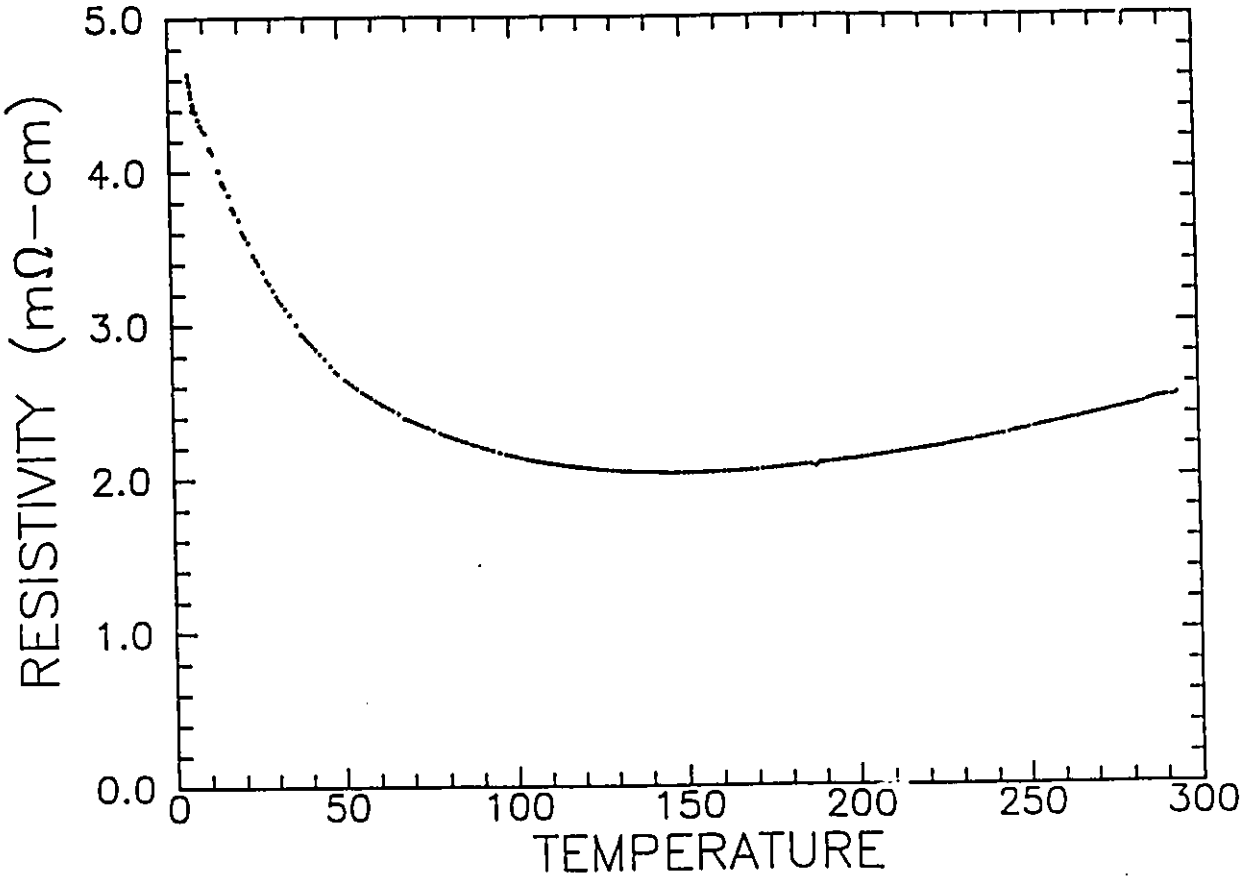

Fig. 2.13 Resistivity versus temperature for a $Nd_{1.85}Ce_{0.15}CuO_{4+\delta}$ film which has not been exposed to a vacuum anneal. The film exhibits semiconducting behavior.

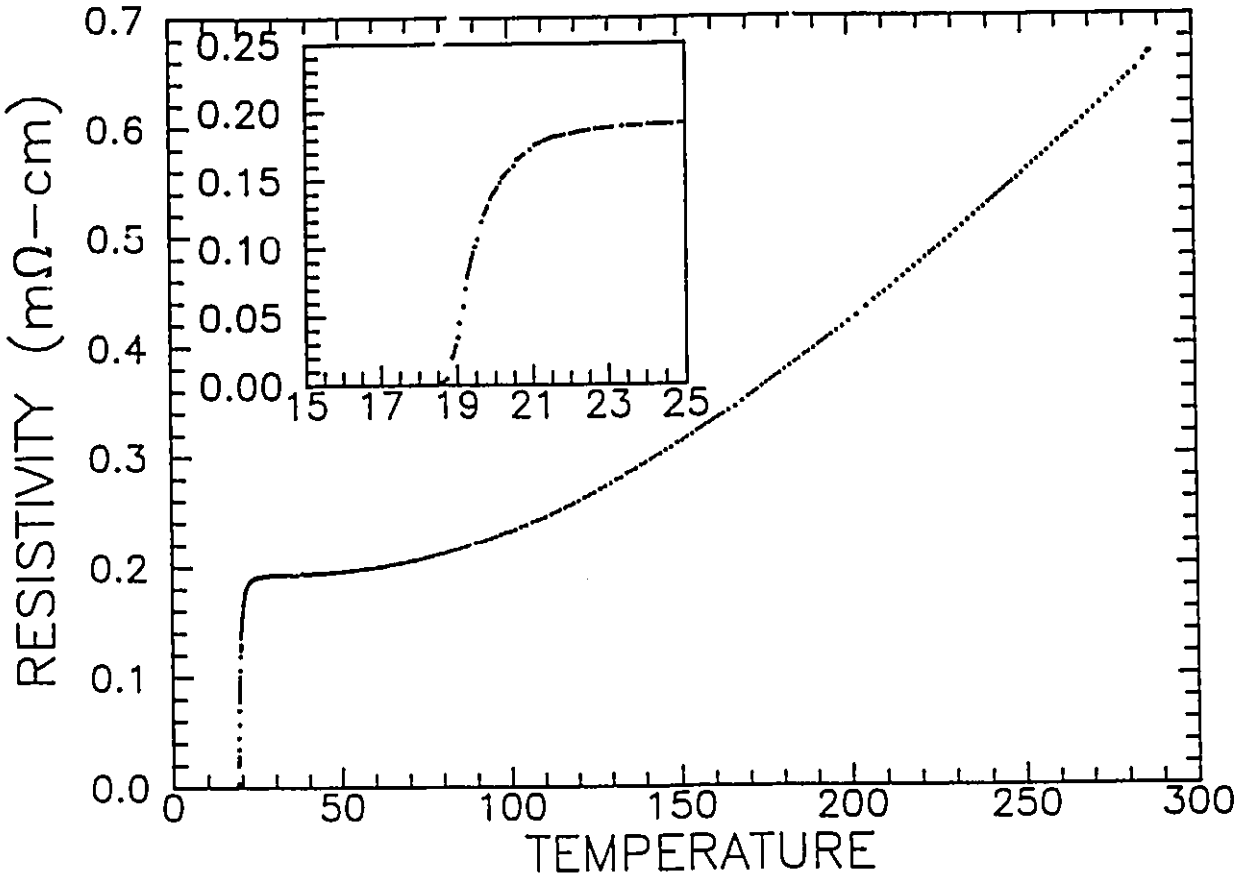

Fig. 2.14 Resistivity versus temperature for a $Nd_{1.85}Ce_{0.15}CuO_{4+\delta}$ film annealed in vacuum for 4 hours at 600 °C. The film shows metallic behavior above the superconducting transition temperature of 21 K. The inset shows an expanded view of the superconducting transition which displays a transition width of 1.5 K.

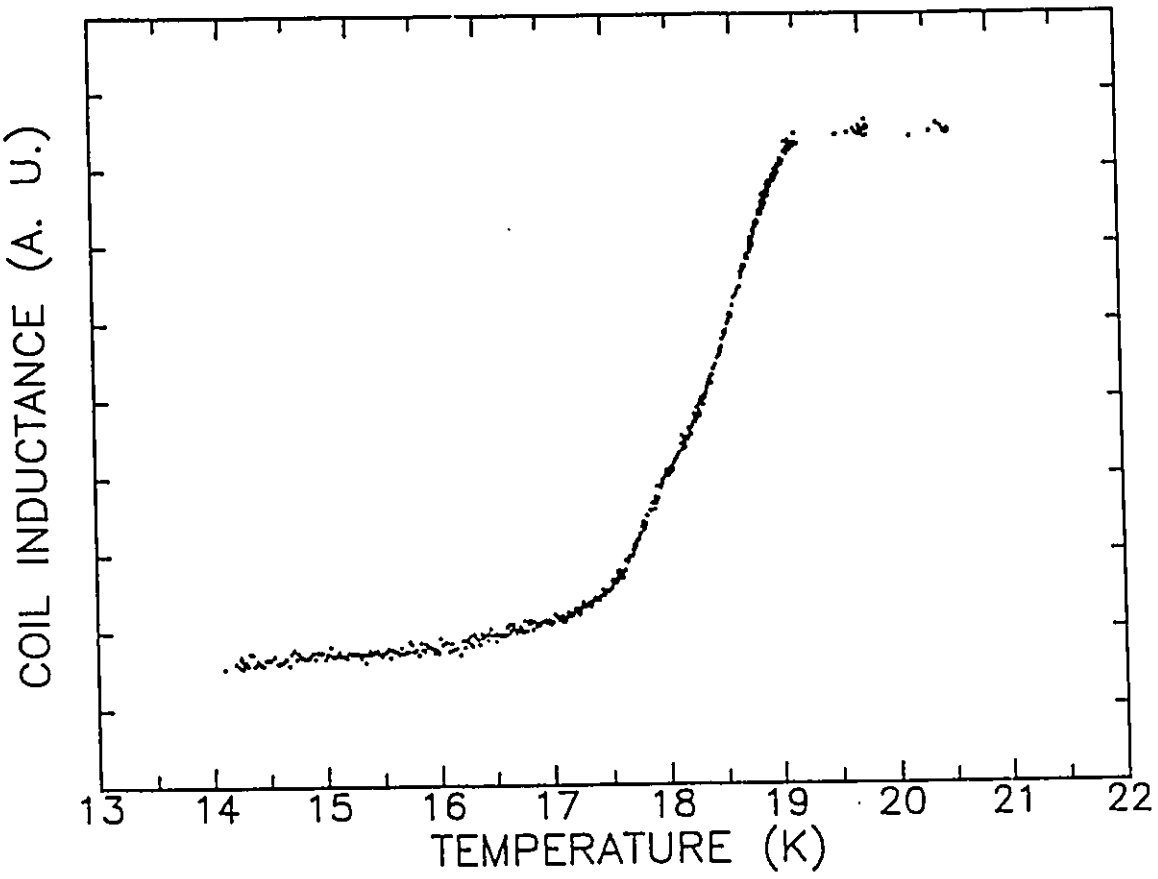

Fig. 2.15 The superconducting transition as measured by an inductive method.

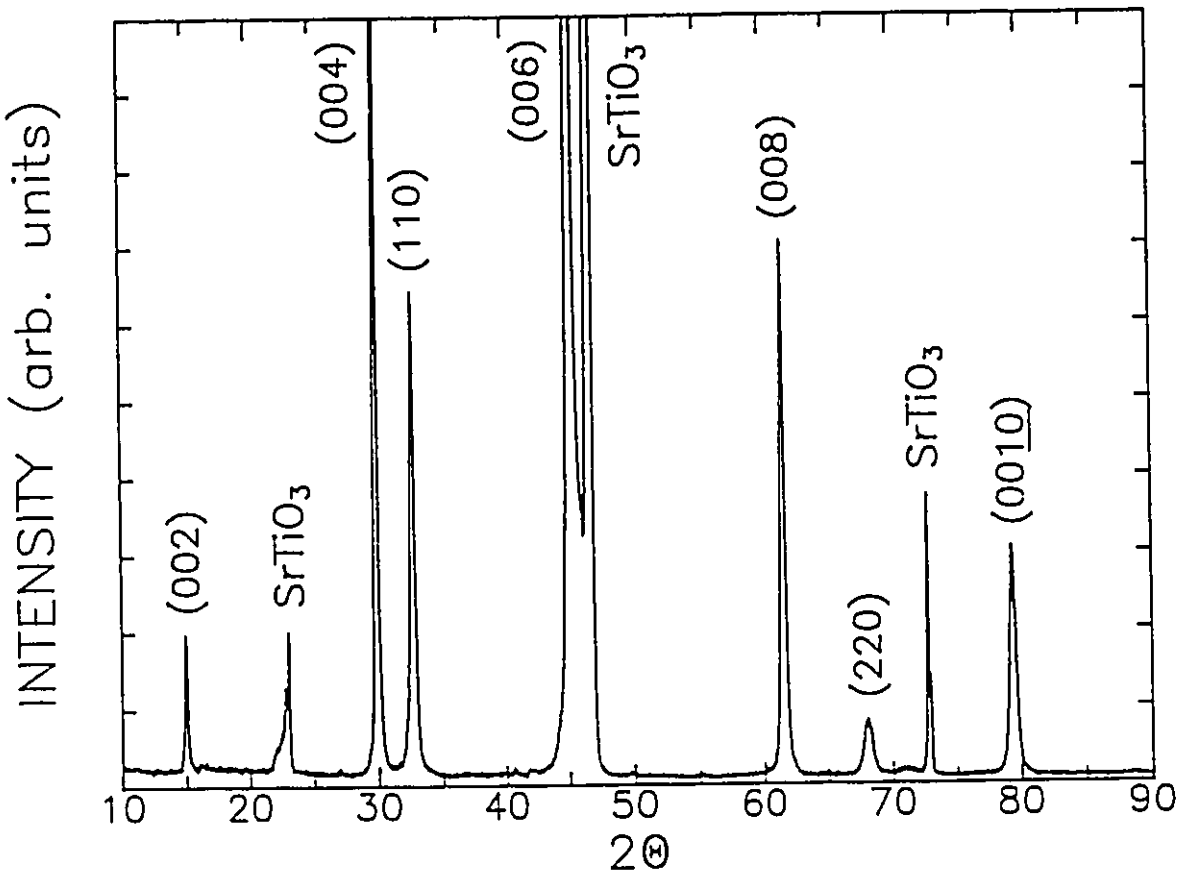

Fig. 2.16 $\theta - 2\theta$ scan for a $Nd_{1.85}Ce_{0.15}CuO_{4+\delta}$ film grown on $SrTiO_3$. The film shows predominantly (00l) lines indicating that the film is oriented such that the c-axis is perpendicular to the substrate. These lines yield a lattice constant of c=12.07 Å. The (110) and (220) lines indicate the presence of some misoriented grains.

it should be realized that the (110) reflections have a much larger intensity in x-ray powder patterns.[119]

SURFACE MORPHOLOGY

The films are similar in appearance to $YBa_2Cu_3O_{7-\delta}$ films in that they are black in colour and have mirror-like surfaces. Scanning electron microscope images are also reminiscent of $YBa_2Cu_3O_{7-\delta}$ films in that the most pronounced feature exhibited by the films are the spherical particulates as shown in Fig 2.17. An expanded view (Fig. 2.18) shows a high quality surface which is superior to $YBa_2Cu_3O_{7-\delta}$ films in two respects. First, the films do not show the presence of the outgrowths often seen in $YBa_2Cu_3O_{7-\delta}$. Second, it does not show a deterioration in its surface morphology when its thickness exceeds 3000 Å. $YBa_2Cu_3O_{7-\delta}$ films of comparable thickness to the $Nd_{1.85}Ce_{0.15}CuO_{4+\delta}$ film shown here usually show the presence of needle-like structures characteristic of c-axis growth parallel to the substrate. Apart from the particulates the main deficiency in the surface morphology of $Nd_{1.85}Ce_{0.15}CuO_{4+\delta}$ films is the presence of a few pinholes. Figure 2.19 shows an example of this feature.

CONCLUSIONS

In summary, pulsed laser deposition has been used to prepare highly oriented $Nd_{1.85}Ce_{0.15}CuO_{4+\delta}$ thin films. By maintaining a high oxygen pressure during the deposition and lowering the anneal temperature as much as possible we have produced films with superior surface homogeneity while maintaining the transport properties and surface morphology associated with high quality films.

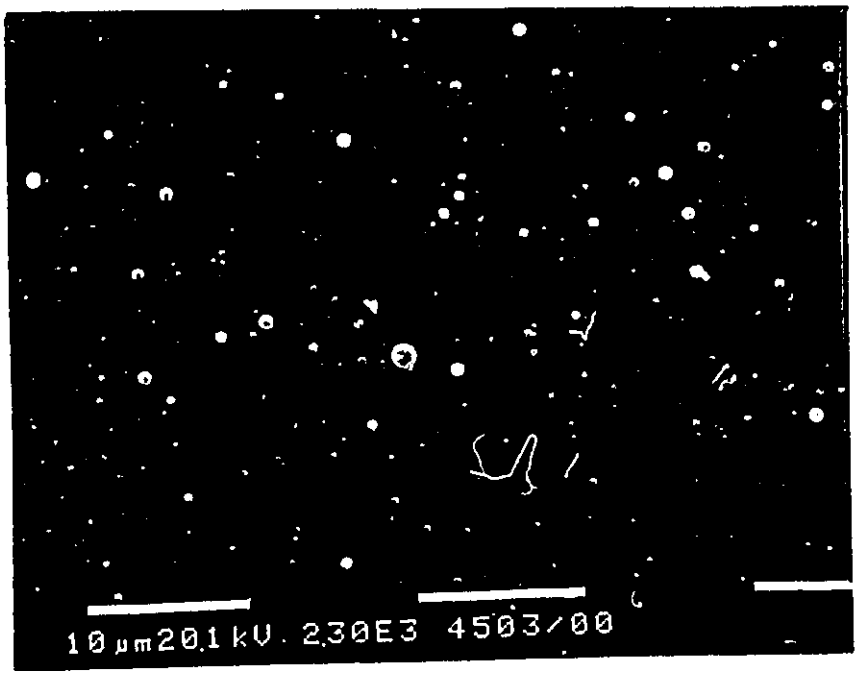

Fig. 2.17 SEM micrograph showing the surface morphology of a superconducting $Nd_{1.85}Ce_{0.15}CuO_{4+\delta}$ film. It shows the spherical particulates common to the laser deposition process.

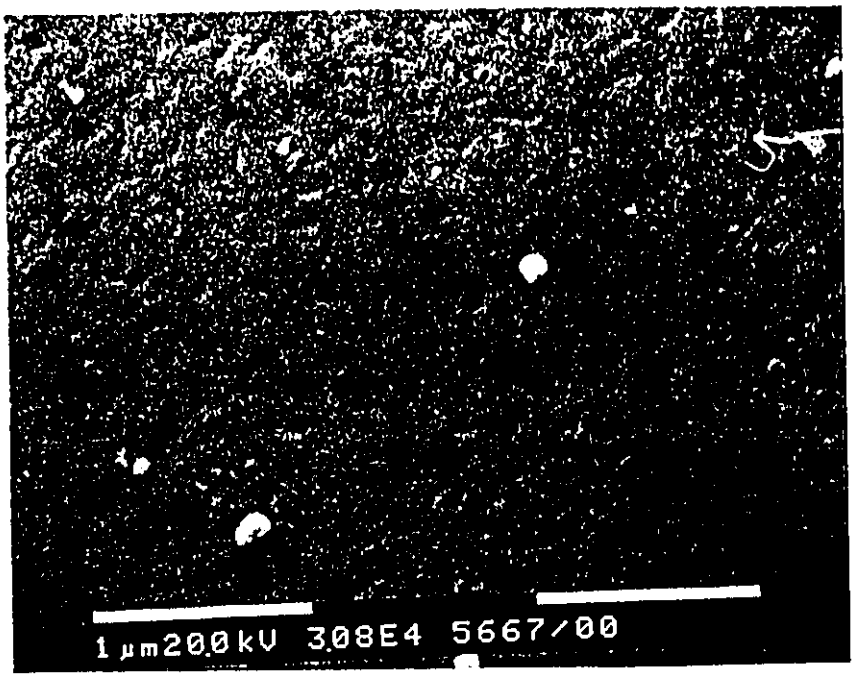

Fig. 2.18 SEM micrograph showing an expanded view of the superconducting grains for a $Nd_{1.85}Ce_{0.15}CuO_{4+\delta}$ film.

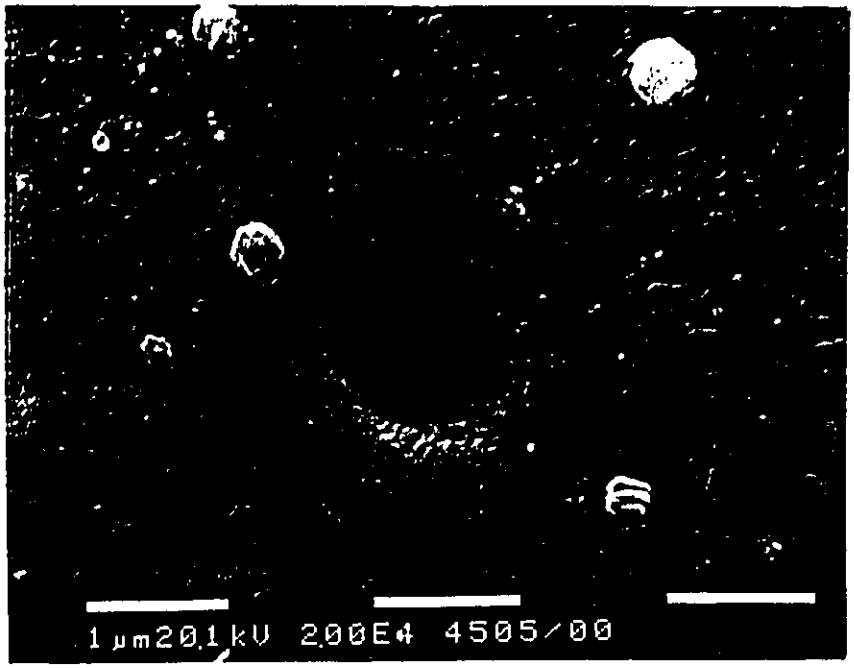

Fig. 2.19 SEM micrograph of a 1 μm size pinhole found in a $Nd_{1.85}Ce_{0.15}CuO_{4+\delta}$ film.

CHAPTER III
THE OPTICAL PROPERTIES OF HIGH-T_c SUPERCONDUCTORS

I. EXPERIMENTAL TECHNIQUE

One of the most obvious properties exhibited by a metal is its high reflectivity. Measuring this quantity can be a delicate task since it is the deviations from unity reflectance which give insight into the underlying excitations governing the transport properties. Thus, an accurate determination of the absolute value is of paramount importance. Superconductors accentuate the importance of this task since it is a unity reflectance which characterizes a true energy gap. In the normal state the oxide superconductors are poor metals and show substantially more absorption than conventional superconductors such as lead or aluminum. This makes single bounce reflectance measurements a viable means of investigating these materials. Still, the absolute value is essential in the quantitative description of the reflectance spectra as well as in substantiating the existence of a superconducting energy gap. Most optical investigations on the high-T_c materials have measured the temperature dependent reflectance spectra of the CuO_2 planes where the free carriers reside. The superconducting thin films described in the previous chapter are valuable in such studies as they provide large mirror-like surfaces whereby the film is highly oriented with the c-axis perpendicular to the substrate. Light at normal incidence will probe the CuO_2 planes since this is the direction where its oscillating electric field resides.

From the above discussion it is evident that the apparatus used to measure the infrared reflectance spectra of oxide superconductors must contain the necessary light sources and detectors as well as provide the cryogenic environment needed to vary the sample temperature over a wide range. In addition, the optics must

be precise and sensitive enough to achieve a reflectance with an accurate absolute value. Figure 3.1 shows a schematic of such an apparatus.

The key element of this apparatus is the Michelson interferometer. It provides a means of distinguishing between the various frequency components emitted by a broad source of infrared radiation (mercury arc lamp or ceramic element). The light emitted from this source is directed onto a mylar beamsplitter which divides the beam into two components. The first component strikes a stationary mirror and is reflected back towards the beamsplitter. The second component is also directed at a mirror which reflects the beam back at the beamsplitter, but in this case the mirror is allowed to move. When the two beams recombine they will interfere with each other. Whether this interference is constructive or destructive depends upon the path difference between the two beams as well as the frequency of the light. The plot of detector signal versus mirror position, known as the interferogram, can be Fourier transformed to give the frequency dependence of the light exiting the interferometer. The sample's reflectance can be determined by allowing this light to strike the sample and comparing the resulting spectrum to one obtained from a reference mirror.

The light exiting the interferometer is incident upon a circular aperture whose diameter can be adjusted to the desired value. Its size is chosen to restrict the amount of light incident upon the detector. Illuminating the entire film surface results in so much signal that the detector is overloaded. Typically the aperture has a diameter of 2 to 3 mm. A vibrating blade light chopper is inserted into the light path during the alignment procedure, but plays no role in obtaining actual spectra. The light is reflected off of a plane mirror onto a concave mirror (f/8) which focuses the image of the aperture onto the sample. The reflected light is collected by a toroidal mirror (f/2.25) and is focused onto the detector. The angles of incidence and reflection are approximately 5°. Reflectance measurements at normal incidence are not feasible since the light source and its detector would have to lie on the same axis. Fresnel's equations show that the small angle provided

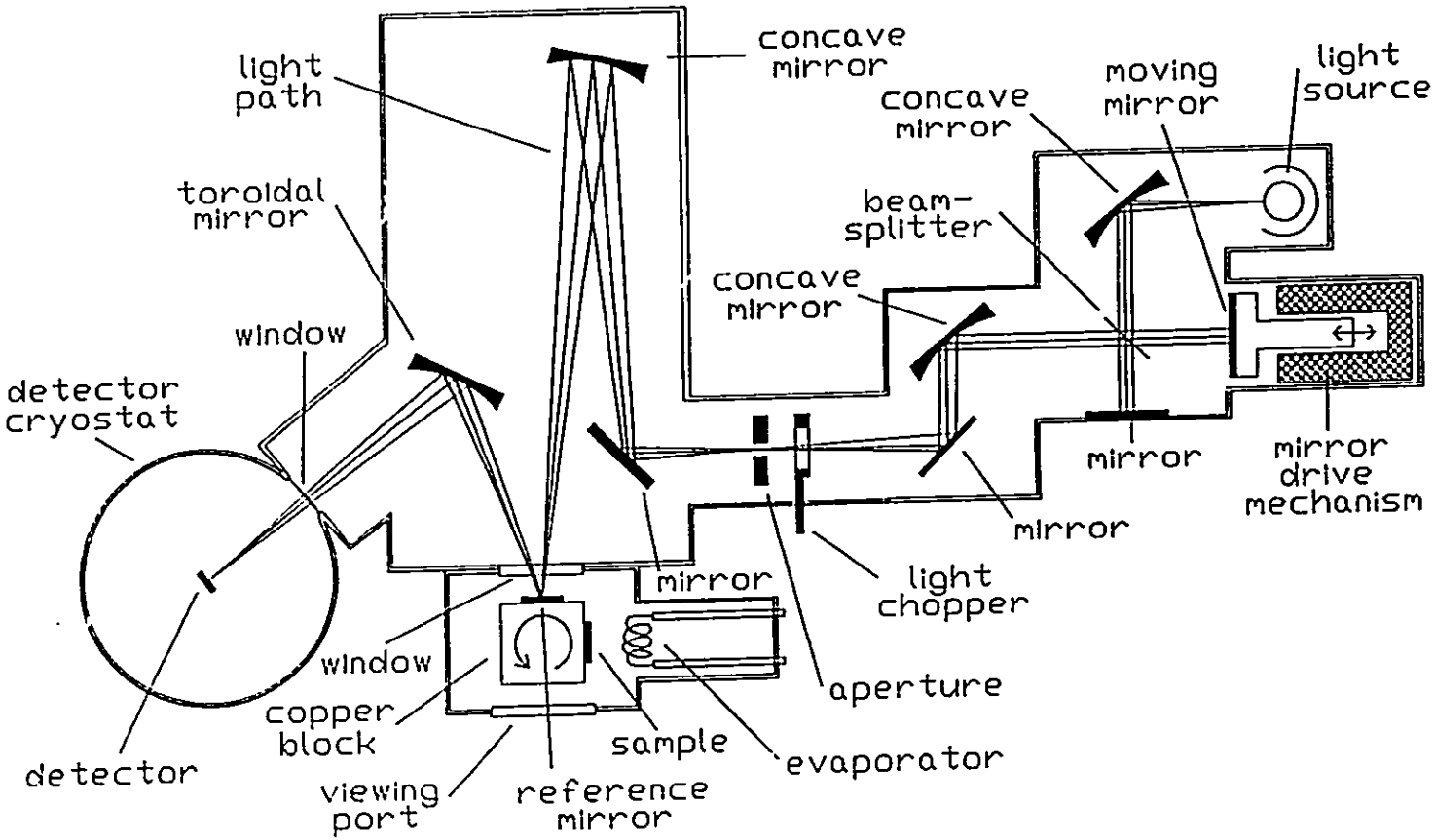

Fig. 3.1 Schematic of the apparatus used to measure the far infrared optical reflectivity.

by this configuration results in a close approximation to normal incidence.

The temperature of the sample was controlled by an R. G. Hansen continuous flow cryostat. The temperature could be adjusted to any value between 15 K and 300 K by resistively heating a copper block cooled by a continuous flow of gas from a helium dewar. The temperature of interest is that of the surface of the sample being measured optically. The nature of optical measurements preclude the possibility of placing a thermometer in direct contact with this surface. The best alternative is to attach the thermometer (silicon diode) to the copper block while thermally anchoring the sample to it. Silver paint was used to attach the sample to the block. Because the film is sitting on an insulating substrate, a direct thermal link to the copper block was made by placing silver paint on the edge of the film surface and down the sides of the substrate. An estimate of the uncertainty in the temperatures quoted in the remainder of this chapter is ± 2 K.

The cryostat is designed such that it is able to rotate the copper block 90°. This rotation allows both the sample and the stainless steel reference mirror to be placed into the optical path. By alternating between the sample and reference mirror every few minutes, the effects on the signal of long term drifts in the detector response or in the output of the light source can be eliminated. The rotation also allows the sample to be placed into a position such that it directly faces a small evaporator. Near the end of an experiment it is used to deposit a thin film of gold onto the sample surface. The reasoning behind this evaporation will be discussed below. The evaporator is simply a helix of tungsten wire (dia. = 0.005 in.) which acts as filament onto which three small pieces of gold wire (dia. = 0.01 in.) are attached. By passing a few amperes through the filament the melting gold will wet the tungsten and slowly evaporate. In order to proceed with the gold evaporation and to prevent the condensation of water onto the sample, the cryostat is evacuated using a diffusion pump backed by a roughing pump. Even though the spectrometer is evacuated, a polypropylene window is placed between it and the cryostat since the restrictions imposed on its vacuum are far

less stringent. This window is angled to scatter the light reflected off of it out of the light path. It is important to remove this light since a proper reference mirror will not eliminate its influence on the final spectrum. A second polypropylene window is used to maintain the vacuum in the cryostat housing the detector.

The reflectance measurements described in subsequent sections were derived from two separate experiments. The first experiment was performed using a 4.2 K silicon bolometer as the detector. With the appropriate filtering, reflectance spectra for frequencies ranging from 140 cm^{-1} to 800 cm^{-1} could be measured. To obtain spectra at lower frequencies required a second experiment using a 1.2 K silicon bolometer. The lower operating temperature of this detector gives it greater sensitivity. This is needed since the intensity of the light source drops off dramatically at these low frequencies. The intensity of the signal is further increased by choosing the Michelson interferometer beamsplitter that most effectively splits the light beams low frequency components. In this configuration, the spectra for frequencies ranging from 40 cm^{-1} to 230 cm^{-1} were obtained. The values for the reflectance in the overlaping spectral range of these two experiments rarely differed by more than $\frac{1}{2}$ % . This clearly demonstrates that the absolute value of the reflectance is reproducible.

Obtaining an accurate absolute value requires an elaborate experimental procedure. At each temperature approximately 600 scans are averaged together for both the sample and reference. The ratio of the two is taken to obtain the reflectivity. It is extremely difficult to accurately place the reference mirror into the exact position previously occupied by the sample. The resulting geometrical differences between the two light paths will distort the spectrum. Further distortions will be caused by any deviations the reference mirror has from unity reflectance or from surface irregularities which cause diffuse scattering. The gold evaporation described earlier eliminates these effects. Once gold is evaporated onto the sample its reflectance spectrum can be measured using the same stainless steal reference mirror. Multiplying the inverse of this spectrum by the sample's spectrum gives,

$$\frac{R_{sample}}{R_{reference}} \; X \; \frac{R_{reference}}{R_{gold}} = \frac{R_{sample}}{R_{gold}}. \tag{3.1}$$

The gold film now acts as the reference. Since it was evaporated *in situ* it is subject to the same alignment as the sample. In addition, any surface irregularities on the sample will be mimicked by the gold film. Thus, the distortions to the sample's spectrum due to these effects will also be present in the gold film's spectrum. Using the gold film as the reference will cause these effects to cancel out. Note, that the spectra obtained from the actual reference mirror used throughout the experiment divide out in the calculation. Thus, within reasonable limits, the quality of the reference mirror has no bearing on the experiment. Gold is not a perfect reflector, but its reflectivity is well known. In the final step appropriate corrections are made which take this effect into account.

The gold film does not adhere very well to the film surface due to the relatively poor vacuum in the cryostat (10^{-5} Torr). Thus, after the experiment is complete the gold film is easily removed and the sample can be cleaned in methanol and acetone. It is now available for further experimentation.

II. THE OPTICAL PROPERTIES OF $Nd_{1.85}Ce_{0.15}CuO_{4+\delta}$

INTRODUCTION

As described in the previous chapter, $Nd_{2-x}Ce_xCuO_{4+\delta}$ thin films having the cerium and oxygen concentration that give the optimum T_c were grown by pulsed laser deposition. Here, optical work will be presented which focuses upon the temperature dependence of the normal state reflectivity in the CuO_2 planes. The goal of this research was to gain some insight into the normal state excitation spectrum. This work is important because the normal state is not well understood and this is one of the main obstacles in understanding the mechanisms governing

high temperature superconductivity.

REFLECTANCE MEASUREMENTS

The room temperature midinfrared (1000 - 5000 cm^{-1}) optical properties of all the films produced were examined using a Spectra-Tech infrared microscope. Only those samples which displayed a reflectivity which was both high and homogeneous over the entire film surface were used for detailed optical investigations. This proved to be an effective method of screening samples since the films with the highest reflectivities were among those with the sharpest resistive transitions. Five films were ultimately used for temperature dependent far infrared measurements. The sample to sample variation in the reflectance spectra were quite small. The same features were exhibited by each of the samples and the absolute value of the reflectance differed by no more than 5 % . Thus, the results and analysis presented here will originate from a single sample where an extensive temperature dependent study was undertaken.

Figure 3.2 shows the temperature dependence of the reflectance spectra. Measurements were made at 30 K, 60 K and for every 25 K ranging from 100 K to 300 K. Some of the reflectance spectra are not shown for the sake of clarity. It is evident that the sample exhibits a systematic increase in the reflectivity as the temperature is lowered where, on average, the extent of the change becomes smaller at low temperatures. The magnitude of the reflectance at low frequencies is quite high and is comparable to that of $YBa_2Cu_3O_{7-\delta}$. The high reflectance exhibited by these samples provides further evidence that the surface of these films is of high quality.

Three distinct features appear in the spectrum; a reflectance minimum at 230 cm^{-1} and two reflectance ledges at 420 cm^{-1} and 540 cm^{-1}. As pointed out in Chapter 1, the 420 cm^{-1} ledge is a feature commonly seen in the oxide superconductors. It is very prominent in the reflectance spectrum of the $Bi_2Sr_2CaCu_2O_8$,[29]

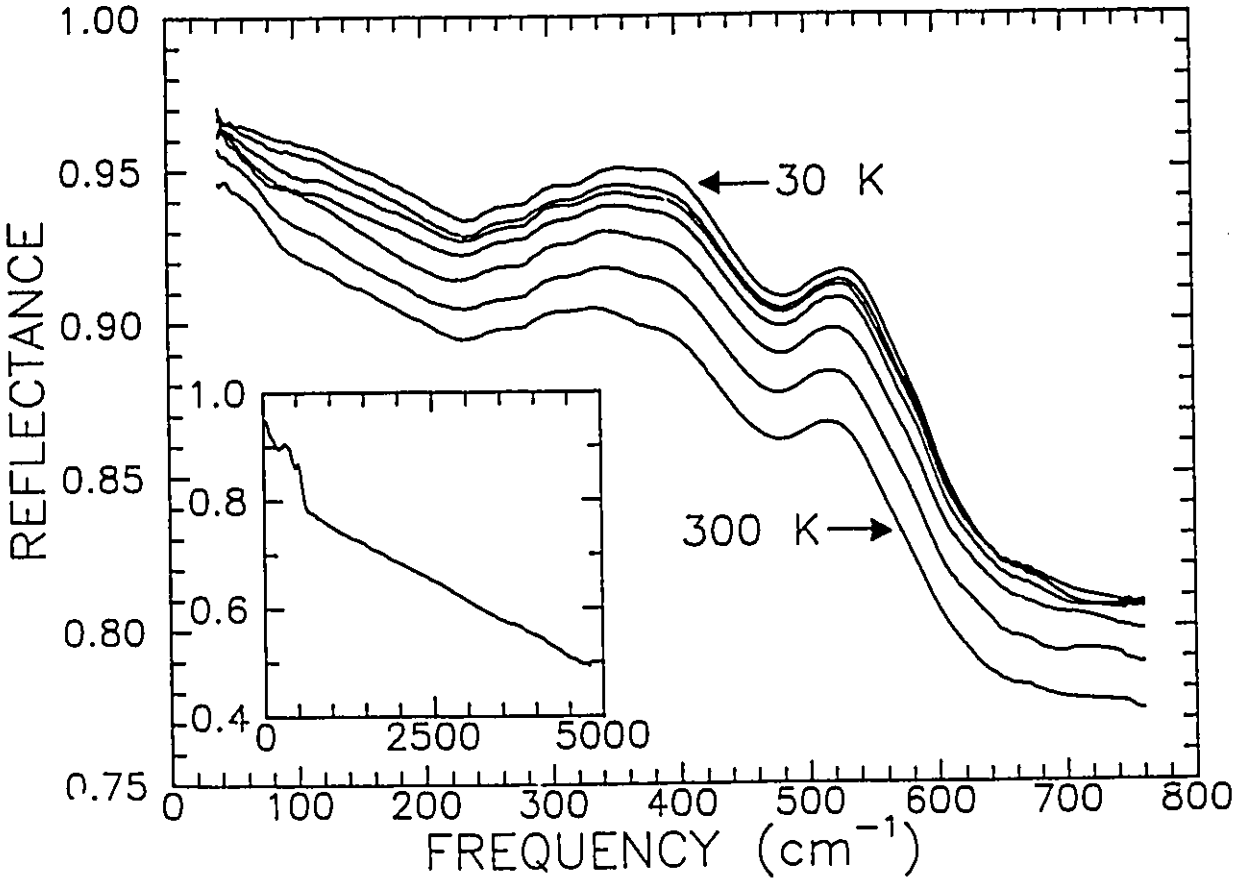

Fig. 3.2 Reflectivity versus frequency for a $Nd_{1.85}Ce_{0.15}CuO_{4+\delta}$ sample. The spectra taken at 30 K and 300 K are labelled on the graph. The intermediate spectra are for temperatures 100 K, 125 K, 150 K, 200 K and 250 K. There exists a systematic increase in the reflectance as the temperature is lowered. Measurements were also made at 60 K, 175 K, 225 K and 275 K, but they have been excluded for the sake of clarity. The inset shows that the room temperature reflectance has a linear dependence at midinfrared frequencies.

$Tl_2Ba_2CaCu_2O_8$ [30] and $Pb_2Sr_2(Y/Ca)Cu_3O_x$ [31] superconductors. The ledge is also present in $YBa_2Cu_3O_{7-\delta}$,[43] but it is often obscured by the high reflectivity associated with the free electrons and only becomes evident as the sample becomes superconducting. This has been somewhat misleading since the feature has been associated with the formation of a superconducting energy gap. The appearance of this ledge in the normal state spectra of $Nd_{1.85}Ce_{0.15}CuO_{4+\delta}$ with a T_c of 21 K and in $Tl_2Ba_2CaCu_2O_8$ with a T_c of 100 K clearly indicates that it is associated with the normal state excitation spectrum and that its position is independent of the superconducting transition temperature.

As in all the other cuprates, the midinfrared reflectance shows non-Drude behaviour. The inset to Fig. 3.2 shows the room temperature reflectance which is linear up to 5000 cm^{-1}. This linear dependence is a feature common to many of the oxide superconductors.[120] Both the absolute value and the linear dependence are consistent with the work of Cooper *et al.*[58] who performed measurements on a series of $Pr_{2-x}Ce_xCuO_{4+\delta}$ samples with x = 0, 0.04, 0.12 and 0.2.

THE OPTICAL CONDUCTIVITY

The optical conductivity offers a clearer picture of the normal state excitation spectrum. It is obtained through the model independent Kramers-Kronig transformations. To perform this calculation requires the appropriate extrapolations. A Drude model is used to extrapolate the data to zero frequency. For frequencies greater than 5000 cm^{-1} the extrapolations are based on the experimental work of Lupi *et al.*[61] and Tajima *et al.*[121] These two experiments yield data up to 40 eV. Beyond this value the reflectance is allowed to fall off according to an R^{-4} power law. This final extrapolation has virtually no influence on the values obtained for the far infrared conductivity. Figure 3.3 shows the result of this calculation. The curves clearly illustrate that the spectral weight is shifting towards lower frequencies as the temperature is lowered. This is consistent with a narrowing of the free

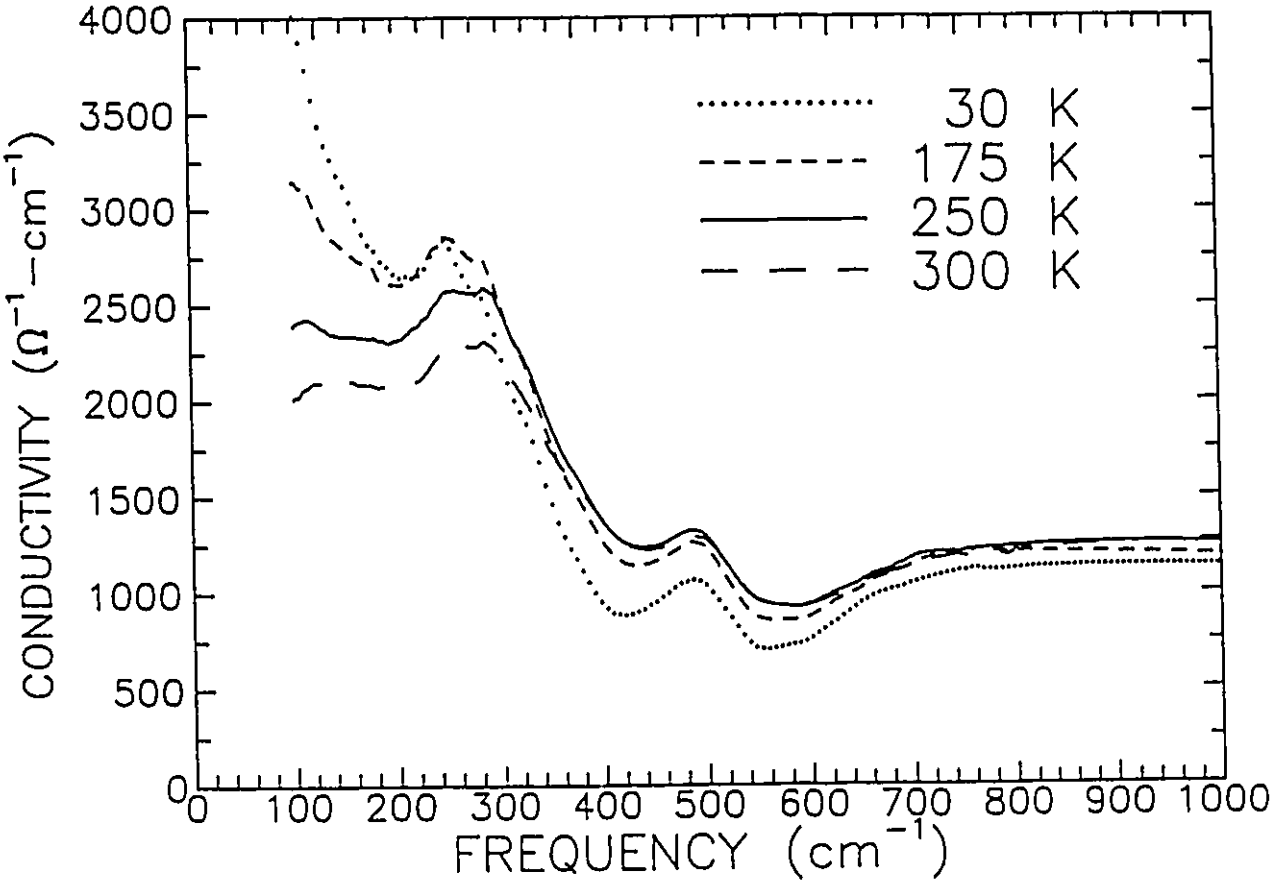

Fig. 3.3 The conductivity versus frequency for a selected group of temperatures. There is clearly a shift in the spectral weight to lower frequencies as the temperature is lowered. This shift is caused by the narrowing of the Drude peak associated with the reduced scattering rate at lower temperatures.

carrier Drude peak associated with a reduced scattering rate at low temperatures. At 300 K the Drude peak is barely discernible while at 30 K a well developed peak centered at zero frequency appears.

A fit to the prominent Drude peak displayed by the 30 K data allows its contribution to the total conductivity to be subtracted out leaving behind the features associated with other excitations (Fig. 3.4). The fact that the conductivity becomes negative near 120 cm^{-1} suggests that the Drude fit and subtraction procedure is imperfect. The result shows similarities to the equivalent plot displayed by $YBa_2Cu_3O_{7-\delta}$ (see Fig. 1.5). The spectra of both materials exhibit a broad minimum centered around 400 cm^{-1} with peaks on either side of it. The differences are that $Nd_{1.85}Ce_{0.15}CuO_{4+\delta}$ has an additional peak centered at 490 cm^{-1} and the features in $YBa_2Cu_3O_{7-\delta}$'s spectrum seem to be superimposed upon a background. Far infrared absorption measurements on detwinned single crystals with the light polarized along the a-axis still show a broad minimum centered at 400 cm^{-1},[42] but the background is not as prominent. Since the effect of the chains is minimized in this measurement, it is not too surprising that it more closely resembles the optical conductivity of $Nd_{1.85}Ce_{0.15}CuO_{4+\delta}$.

ANALYSIS

The similarities between the structures seen in the $YBa_2Cu_3O_{7-\delta}$ and $Nd_{1.85}Ce_{0.15}CuO_{4+\delta}$ spectra provide the justification for using the antiresonance model presented in Chapter I to fit the data. In summary, this model describes the optical conductivity using a Drude component to account for the free electron behaviour and phonons coupled to a broad midinfrared band to describe the remaining structure. The procedure for fitting the data begins by using the room temperature data out to 5000 cm^{-1} to fit the width, strength and center frequency of the midinfrared band. Other oxide superconductors indicate that these parameters are not strongly temperature dependent. Thus, while fitting the

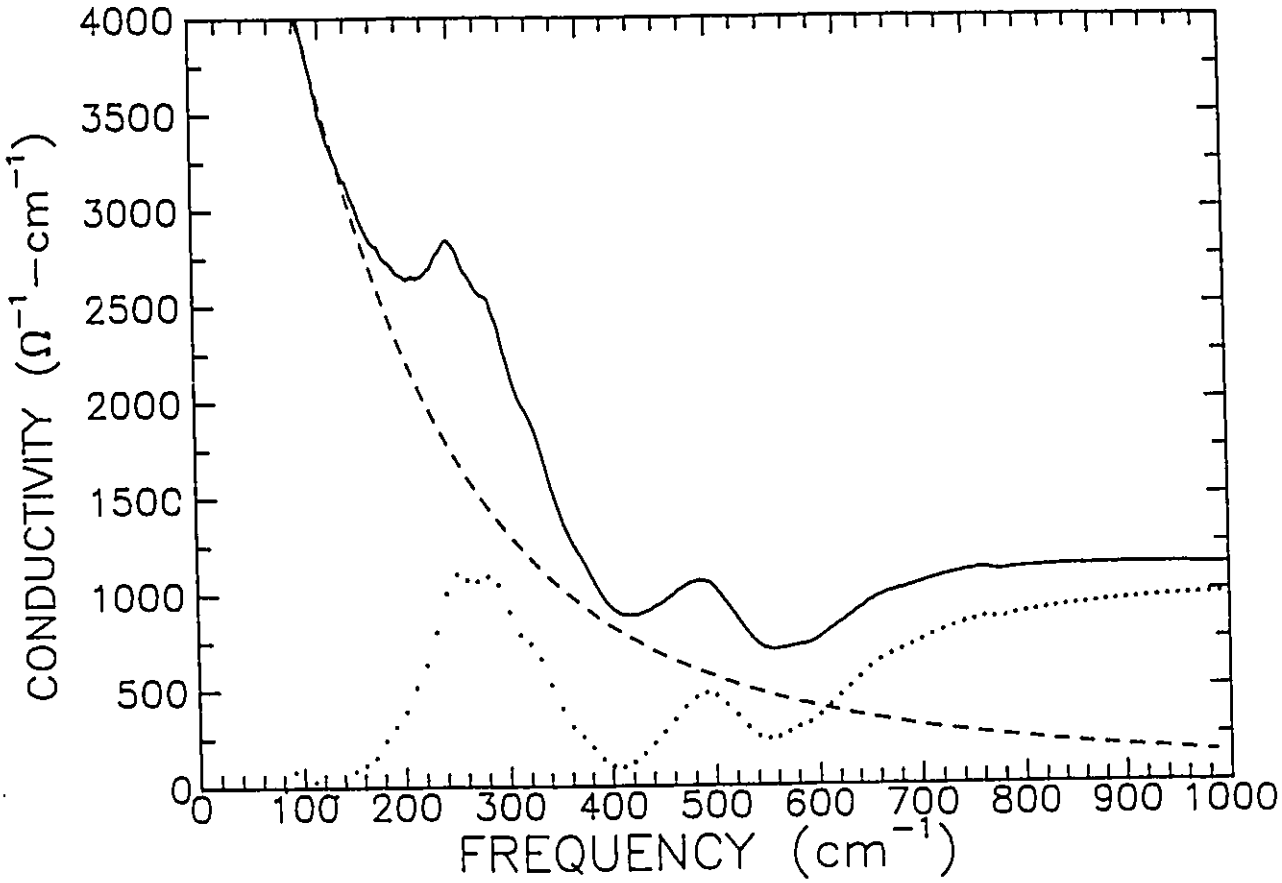

Fig. 3.4 Subtracting the Drude component (dashed) from the total conductivity (solid) leaves behind structure (dots) which can be described by phonons coupled to an electronic continuum.

far infrared data for each temperature the parameters describing the midinfrared band were not allowed to vary by more than a few percent. The model was able to adequately describe the optical conductivity at each temperature. Figure 3.5 shows the fits to the 30 K and 300 K data to give some indication of their quality.

The fits indicate that most of the temperature dependence can be accounted for by variations to the Drude term in Eqn. 1.22. Figures 3.6 and 3.7 show the values obtained for the scattering rate and the plasma frequency respectively. The plasma frequency is essentially constant, while the temperature dependence of the scattering rate shows a striking resemblance to the dc resistivity (see Fig. 2.14). The second term, which describes the coupling between phonons and a broad midinfrared band, has little temperature dependence. There is some sharpening of the structure centered around 270 cm^{-1}, but this is small in comparison to the changes associated with Drude term. The fit requires 3 phonons that are coupled to the midinfrared band. Table 3.1 lists the parameters which describe the fit to the 30 K conductivity data. It is important to note that the antiresonances (i.e. minima) appear in the optical conductivity at the phonon frequencies. The implication of the above results is that the dc resistivity is solely described by a temperature dependent free carrier scattering rate. This is consistent with the results of Kamarās *et al.*[22] on $YBa_2Cu_3O_{7-\delta}$ and Romero *et al.*[49] on $Bi_2Sr_2CaCu_2O_8$ which show a scattering rate which varies linearly with temperature and intercepts the origin of the resistivity versus temperature plot.

DISCUSSION

A temperature independent plasma frequency implies that the carrier concentration is also independent of temperature. Hall measurements on $Nd_{2-x}Ce_xCuO_{4+\delta}$ are very sample dependent. Even the sign of the Hall coefficient is in doubt. Both positive[56] and negative[55] Hall coefficients have been observed as well as reversals in its sign as the temperature is varied.[122] These optical measurements clearly

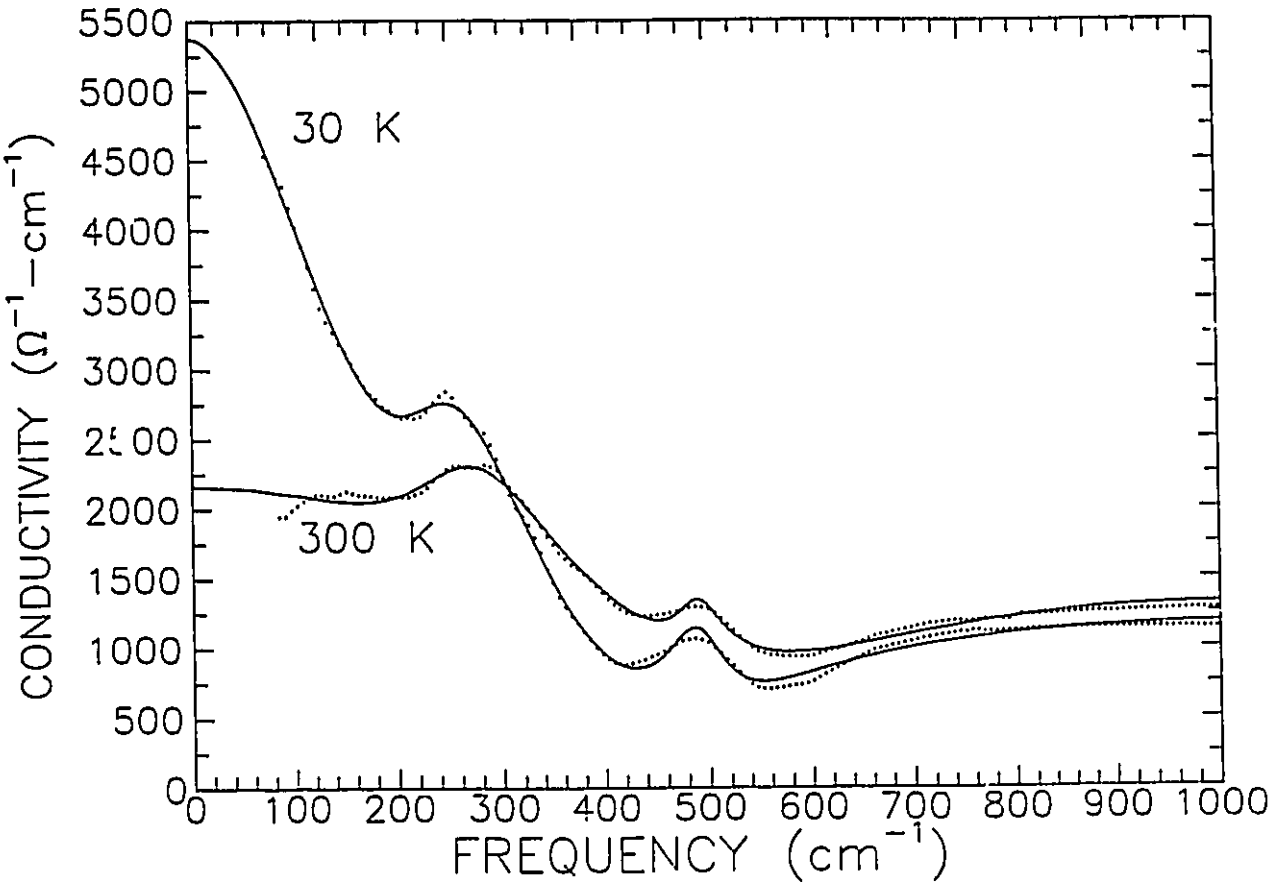

Fig. 3.5 Fits (solid) to the 30 K and 300 K optical conductivity data (dots) obtained from Kramers-Kronig analysis.

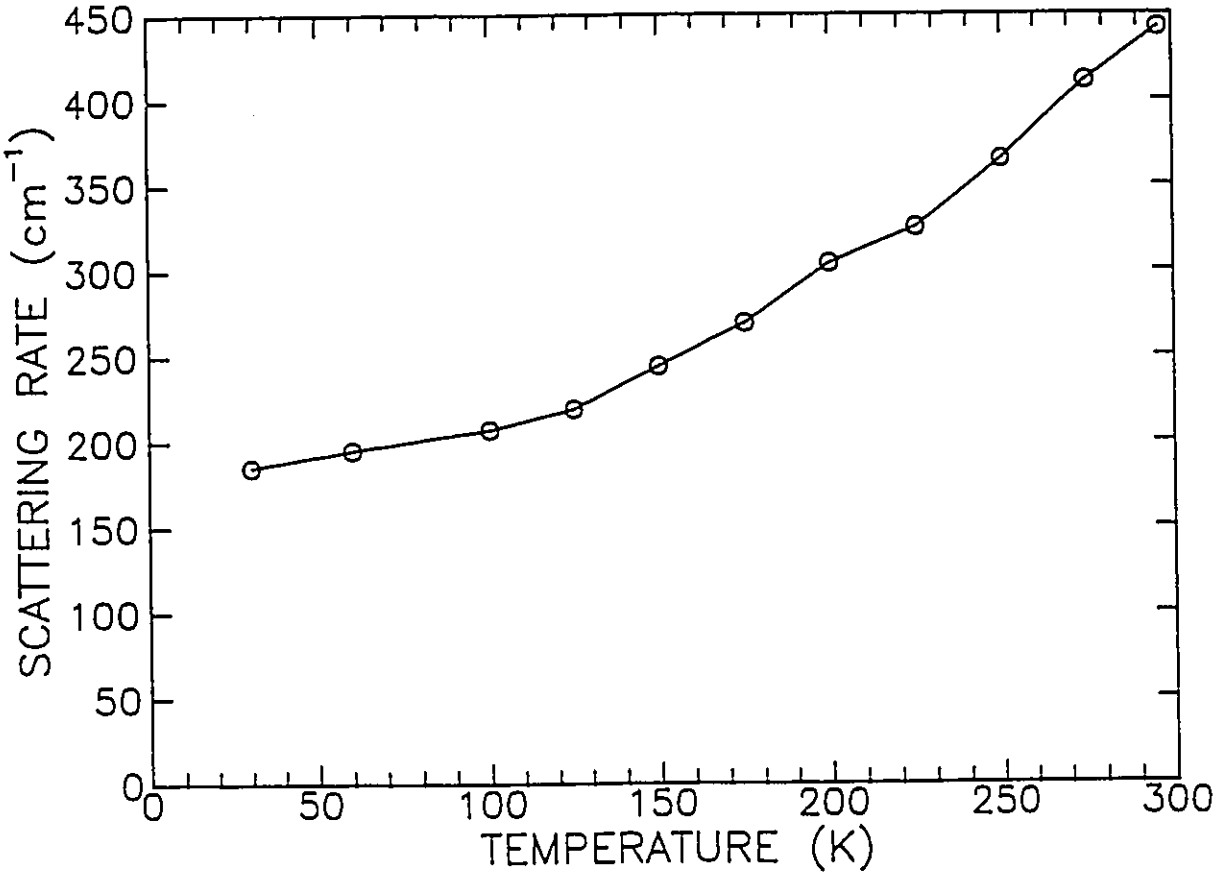

Fig. 3.6 The scattering rate as a function of temperature. Note that the scattering rate follows a temperature dependence similar to the dc resistivity.

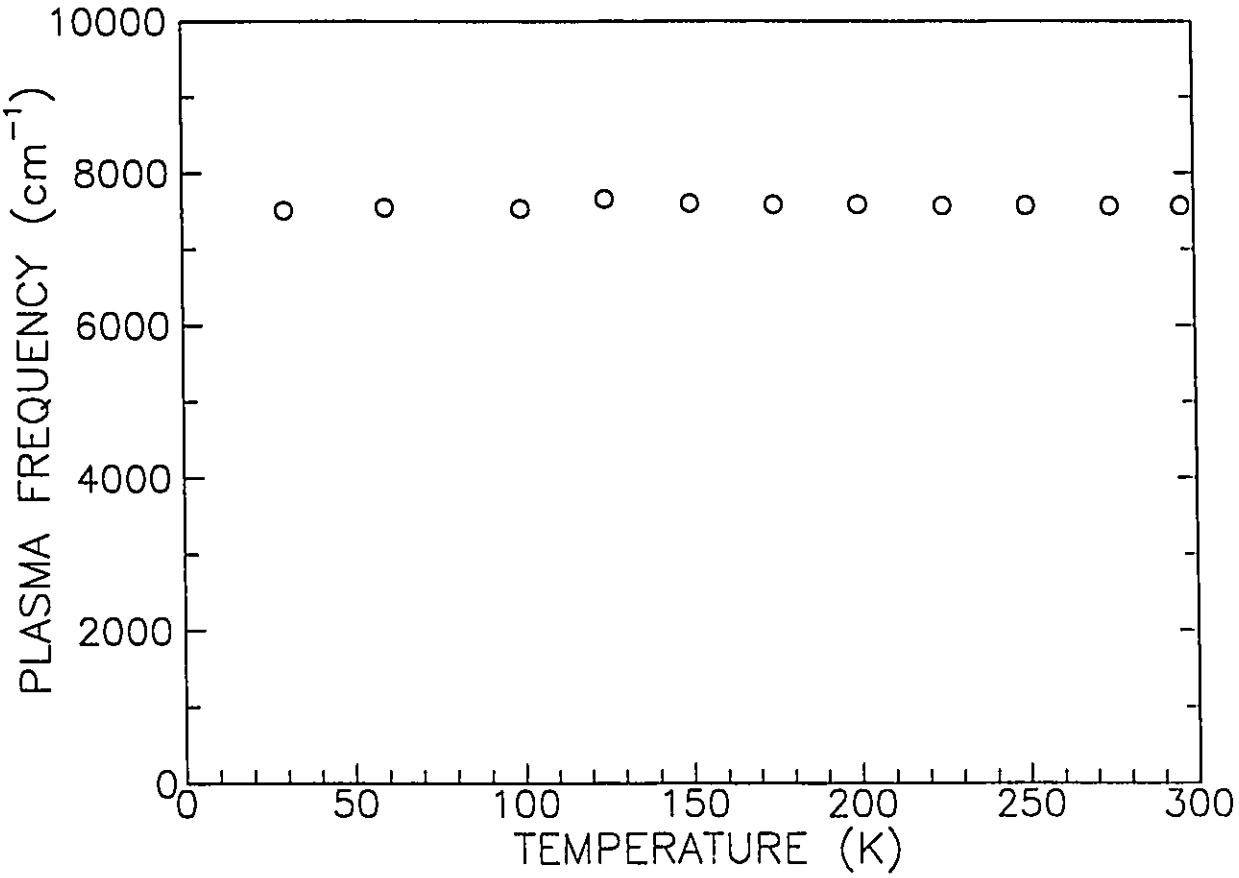

Fig. 3.7 The plasma frequency as a function of temperature. Note that the plasma frequency is temperature independent.

	ω_e	ω_{Pe}	Γ_e
mid IR band	1870	26300	10100
	ω_k	ω_{Pk}	Γ_k
phonon 1	523	729	46
phonon 2	415	786	14
phonon 3	118	564	5

Table 3.1 The fitted parameters describing the midinfrared band (position = ω_e, strength = ω_{Pe}, width = Γ_e) and the phonons (position = ω_k, strength = ω_{Pk}, width = Γ_k) which are coupled to it. All values are in units of cm^{-1}.

indicate that a naive interpretation of the Hall coefficient in terms of a carrier concentration is inappropriate. By arbitrarily setting the effective mass of the electron equal to its rest mass, the carrier concentration can be calculated using Eqn 1.14. The calculation yields a value of 6.4×10^{20} cm^{-3}. Even though it is unclear what the effective mass is for this material, the calculation serves a purpose in that it gives a reasonable value which is comparable to that obtained for the other oxide superconductors.

The values obtained from the fits are reasonable. The Drude plasma frequency of 0.94 eV, is similar tc the values obtained for all the other oxide superconductors. The scattering rate of 440 cm^{-1} at room temperature is somewhat higher than the values near 300 cm^{-1} obtained for $YBa_2Cu_3O_{7-\delta}$, but this may be the expected result since $Nd_{1.85}Ce_{0.15}CuO_{4+\delta}$ has a built in disorder from the cerium dopant and films have considerably more defects than single crystals.[103] The dc resistivity obtained from these fitted parameters using the simple Drude formula, $\rho = 4\pi\Gamma_D/\omega_{PD}^2$, shows reasonable agreement with the values obtained from the dc resistivity measurements. At 30 K the agreement is excellent. The measured resistivity is given by 0.21 mΩ – cm, compared to a value of 0.19 mΩ – cm derived from the optical conductivity. At room temperature the two values differ by 30 %.

As described in Chapter I, the partial sum rule for the optical conductivity (Eqn. 1.21) can be used to calculate the effective number of carriers per formula unit contributing to the optical properties for frequencies up to ω. Performing this calculation for energies below the charge transfer band gives $N_{eff} = 0.33$ electrons per formula unit. This value is in excellent agreement with the results obtained by Cooper *et al.*[58] on $Pr_{2-x}Ce_xCuO_{4+\delta}$ single crystals. There is also good agreement with the value extracted from the results of Abel' *et al.*[62] on $Nd_{1.85}Ce_{0.15}CuO_{4+\delta}$, but his Drude plasma frequency is equal to 1.5 eV which is significantly larger than the one obtained for these films. It should be noted that $N_{eff} = 0.15$ is the expected value if all of this spectral weight is due to the carriers introduced by

doping cerium on the neodymium site. This is obviously not the case.

COMPARISONS TO OTHER EXPERIMENTS

The phonons which give rise to the antiresonances in the optical conductivity should be directly observable by other experimental techniques. Lynn *et al.*[123] have used inelastic neutron scattering to measure the phonon density of states in superconducting $Nd_{1.85}Ce_{0.15}CuO_{4+\delta}$. Their result is shown in Fig. 3.8. The large peak in the 180 to 250 cm^{-1} region is due to a strong crystal field level. Thus, any phonon structure in this region will be hidden. The solid curve shows the phonon structures predicted by our fits to the optical conductivity. The agreement is excellent. The neutron spectrum gives peak positions at 105, 411 and 524 cm^{-1} compared with the optics results which give peak positions at 118, 415 and 523 cm^{-1}. The neutron peak at 766 cm^{-1} does not appear to couple to the electronic continuum, but this feature may also be due to a crystal field excitation.[123] Further evidence for the existence of these phonons comes from far infrared measurements on $Nd_{1.85}Ce_{0.15}CuO_{4+\delta}$ crystals with the light polarized along the c-axis.[124] Reedyk *et al.*[38] have pointed out that the minima in the ab-plane optical conductivity, seen in wide variety of oxide superconductors (including $Nd_{1.85}Ce_{0.15}CuO_{4+\delta}$), correspond to maxima in the c-axis dielectric loss function. This function peaks at frequencies corresponding to c-axis longitudinal optic phonons.

The tunneling measurements of Huang *et al.*[125] on polycrystalline $Nd_{1.85}Ce_{0.15}CuO_{4+\delta}$ show a strong resemblance to the response obtained from a traditional BCS superconductor. Both a gap-like feature with $2\Delta/k_bT_c = 3.9$ and a tunneling conductance exhibiting symmetric structure is seen. Superimposed on the smooth BCS-like conductance is a fine structure on the order of one percent. Structure such as this is seen in conventional superconductors and is attributed to an electron-phonon interaction. By applying the McMillan-Rowell[126] procedure the electron-phonon spectral density ($\alpha^2F(\omega)$) can be calculated. This

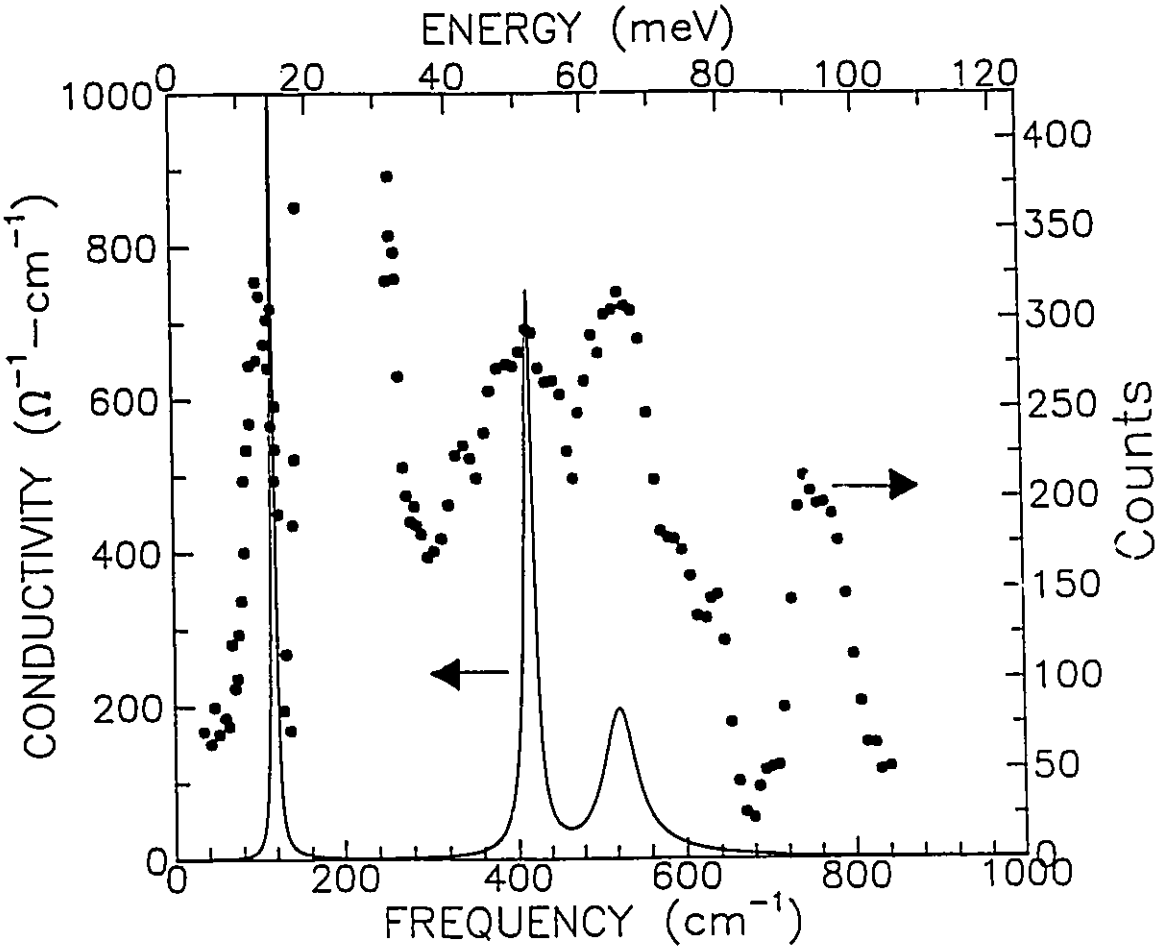

Fig. 3.8 Comparison of the phonon density of states (dots) derived from inelastic neutron scattering experiments to the phonon structure predicted by fits to the optical conductivity (solid). The gap in the neutron spectrum from 180 to 250 cm^{-1} is due to the interference with a Nd crystal field transition.

$\alpha^2F(\omega)$ function, which is proportional to the derivative of the tunneling conductance, describes the effective electron-electron interaction due to the exchange of a phonon.[127] Huang *et al.*[125] follow this straightforward procedure to extract an $\alpha^2F(\omega)$ for $Nd_{1.85}Ce_{0.15}CuO_{4+\delta}$ from which they calculate a coupling constant (λ) of the order of unity and a T_c of 20 K.

Several inconsistencies arise when comparing our interpretation of the optical conductivity and Huang *et al.'s*[125] interpretation of the structures observed in the tunneling measurements. First, one would anticipate agreement between the peaks in the $\alpha^2F(\omega)$ function found from the analysis of the tunneling spectrum and minima in the optical conductivity, since both correspond to spectral regions of strong phonon interaction. This agreement is not found (see Fig. 3.9). Second, the coupling constant they have calculated from their $\alpha^2F(\omega)$, would result in large changes to the optical conductivity as the material becomes superconducting. Specifically, the phonon structure should become sharper and shift towards higher frequency by Δ as predicted by the Holstein process.[128] In this material, as well as in other high temperature superconductors, the structure in the phonon region changes very little at T_c.

To our surprise, we found that the *tunneling conductance* shows a strong likeness to the optical conductivity. Figure 3.10 shows the comparison. The tunneling conductance has been divided by the BCS conductance to remove the gap-like feature. It was then shifted vertically and rescaled. The correspondence between the positions of the peaks and valleys in both measurements is striking. Roughly equal amplitude minima appear in both curves at 150 cm^{-1} and 400 cm^{-1}. A third minimum, seen in the optical data at 580 cm^{-1}, does not appear clearly in the tunneling data, but it is at these energies that the tunneling measurements have least sensitivity. Both measurements loose their accuracy at low frequencies. In the optical conductivity the rising Drude absorption hides weak features, while in the tunneling spectrum the BCS correction that is made to the conductivity gets larger at low energy. Thus, it is not unexpected that the poorest agreement

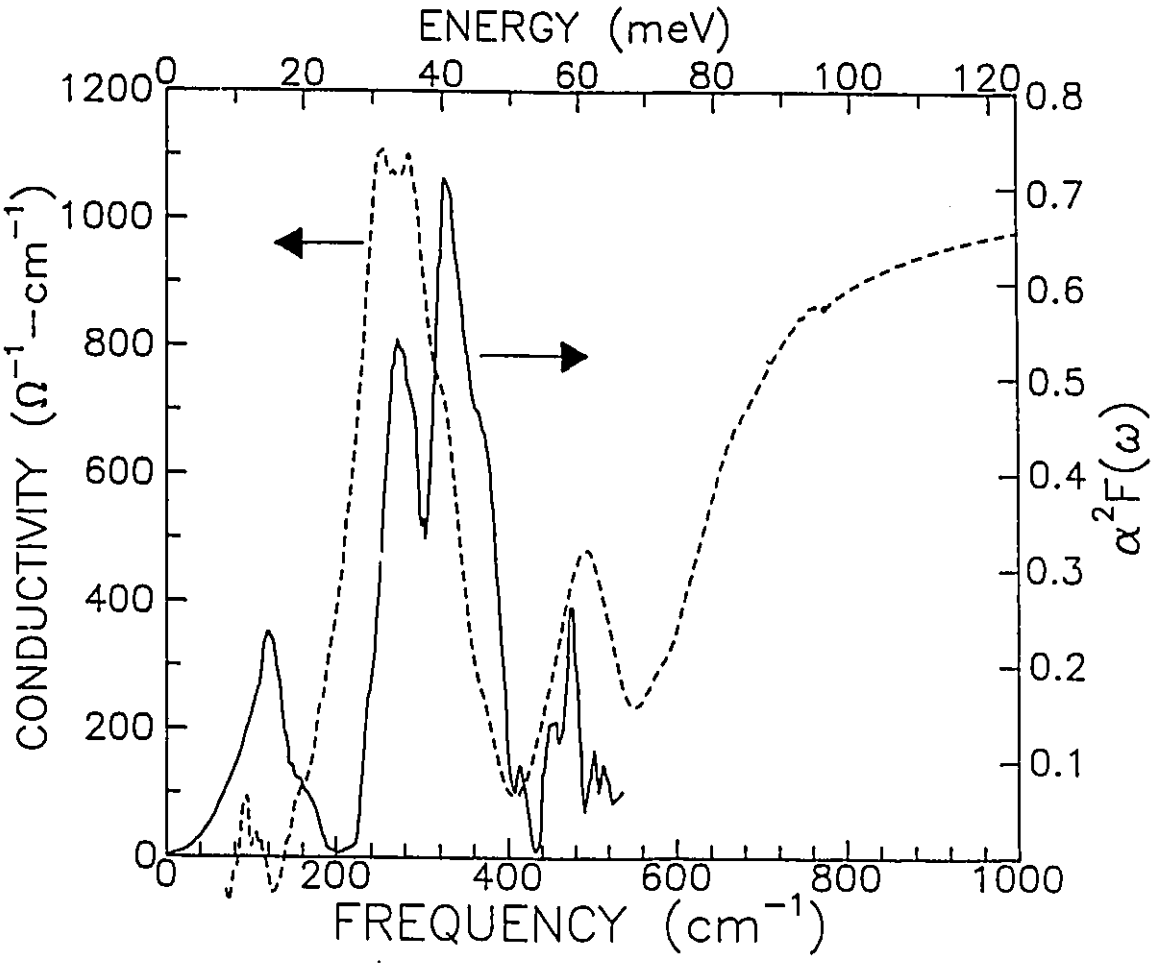

Fig. 3.9 Comparison between the optical conductivity and the $\alpha^2F(\omega)$ extracted from tunneling data. Note that there is poor agreement between the minima in the optical conductivity and the maxima in the $\alpha^2F(\omega)$ function.

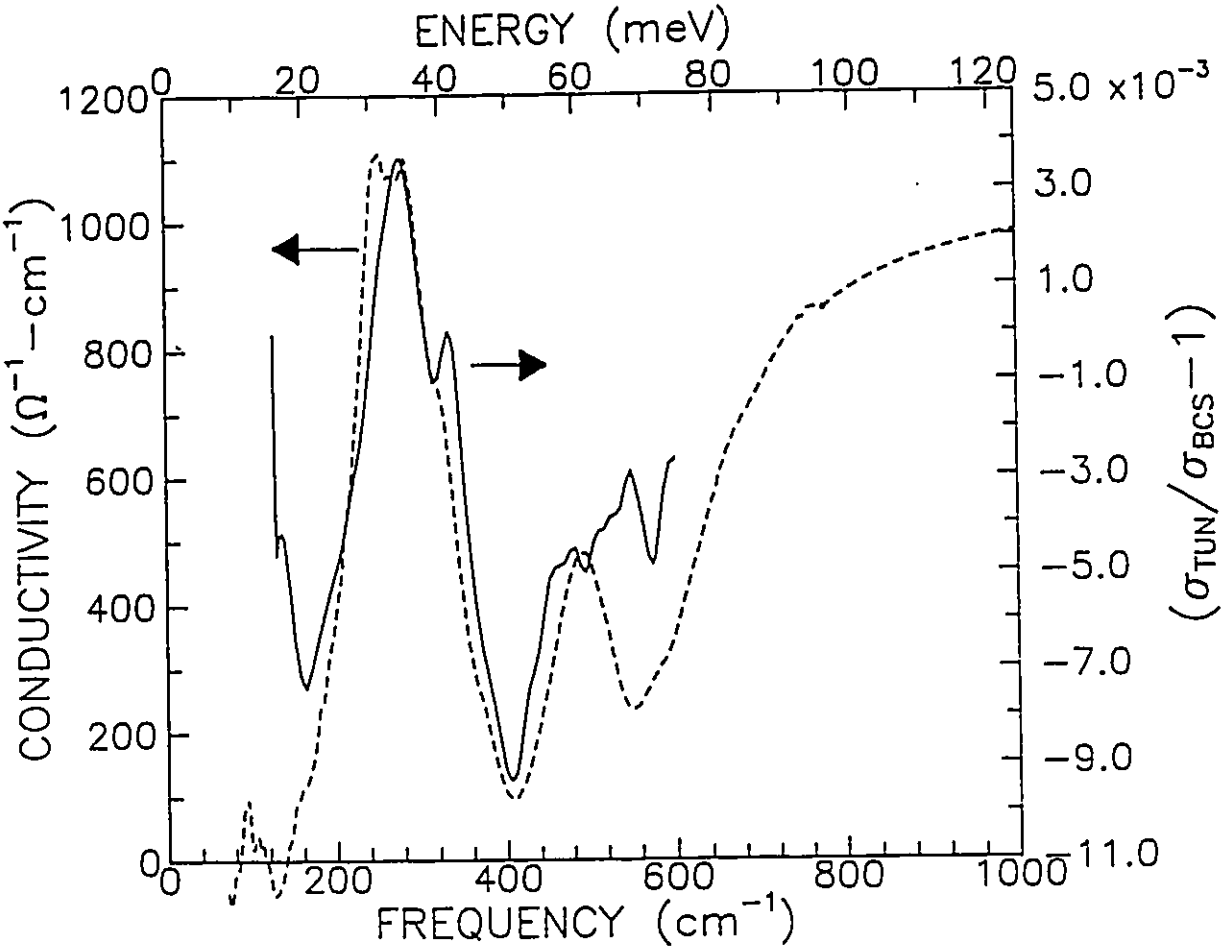

Fig. 3.10 Comparison of the tunneling conductance (solid) to the structure observed in the optical conductivity (dashed). Note that the peaks and valleys in both measurements appear at similar frequencies. The Drude contribution has been subtracted from the optical conductivity. The tunneling conductance has been divided by the BCS conductance.

is for the lowest energy feature. It should be noted that the phonon structure in the raw tunneling conductance is only of the order of one percent of the total conductance whereas the structure in the optical conductivity is of the order of 50 %.

When comparing tunneling and optical data there is some question of whether to shift the energy scale in the tunneling data by $-\Delta$. Structure due to a phonon of frequency Ω appears at an energy $\Delta+\Omega$ in a strong coupling BCS superconductor. The data in Fig. 3.10 has not been shifted. This is consistent with all of the optical work on the high-T_c superconductors where there is no evidence of an abrupt shift in the structures seen in the optical conductivity as the sample is cooled below T_c. If, as the agreement suggests, the structures in these two experiments have a common origin, then it is expected that the features in the tunneling conductance will not shift as the sample is cooled below T_c. Tunneling measurements in the normal state have not been made for $Nd_{1.85}Ce_{0.15}CuO_{4+\delta}$. Thus, at this time, there no premise for a shift in the energy scale. It should be noted that a shift would have a minimal impact on the agreement between the two curves. Such a shift would move the solid curve in Fig. 3.10 to lower frequencies by 3.7 meV (30 cm^{-1}) which would slightly reduce the quality of the agreement.

In summary, the model used to describe the optical conductivity predicts the existence of phonons that interact with the electrons at certain frequencies. Inelastic neutron scattering and c-axis far infrared measurements verified there existence. This phonon structure did not appear in the $\alpha^2F(\omega)$ derived from tunneling measurements. Instead, the tunneling conductance showed a strong likeness to the optical conductivity. At this point we do not have a clear understanding of why there is such excellent agreement between the tunneling conductance and the optical conductance. However, it does appear that the phonons observed by neutron scattering cause antiresonances in the optical conductivity and this same process somehow causes a small suppression in the electronic density of states at these same phonon energies.

CONCLUSIONS

Despite the unique properties exhibited by $Nd_{1.85}Ce_{0.15}CuO_{4+\delta}$ its far infrared optical spectra appear to exhibit many of the features common to the other cuprate superconductors. These features include the ledge in the reflectivity at 420 cm^{-1}, the linear reflectivity in the midinfrared and the development of the midinfrared band as the doping level is increased. Our analysis of the optical conductivity shows that it is comprised of two components. The first component can be described in terms of a Drude model with a temperature dependent scattering rate that closely follows the temperature dependence of the dc resistivity. The second component is relatively insensitive to temperature and has been modeled in terms of phonons which are coupled to a broad midinfrared band. It was also demonstrated that there exists a correlation between the structure in the tunneling conductance and the optical conductivity. The phonon structure predicted by fits to the optical conductivity have been observed by inelastic neutron scattering. At this time, the nature of the excitations resulting in the structures observed in the optical, tunneling and inelastic neutron scattering data are not completely understood. Nevertheless, significant progress has been made towards linking the results obtained from these three different experimental techniques.

III. THE OPTICAL PROPERTIES OF 1212 PSYCCO THIN FILMS

INTRODUCTION

An extra degree of complexity is encountered when dealing with the optical properties of 1212 PSYCCO films. The main problem originates from the fact that the films can only grow to a thickness of approximately 2000 Å before the surface morphology starts to deteriorate. This thickness is approximately the same as the skin depth for a typical oxide superconductor. Thus, some of the incident light will penetrate through the film and be reflected at the film/substrate interface. Since $LaAlO_3$ shows extensive structure in its far infrared optical properties,[129] additional features will be superimposed on the reflectance spectra of a PSYCCO film. Similar difficulties have been seen in the optical work performed on $YBa_2Cu_3O_{7-\delta}$[130] and $Bi_2Sr_2CaCu_2O_8$ [131,132] thin films. Even with this limitation it is still possible to extract a great deal of information from the resulting spectra. In this section, the reflectance spectra for PSYCCO films with the highest calcium concentration (x=0.6) are presented. These films have the highest reflectivity and as a result minimize the influence of the substrate phonons.

As was the case for $Nd_{1.85}Ce_{0.15}CuO_{4+\delta}$, the PSYCCO samples were initially screened by measuring their room temperature midinfrared reflectance. Only those films which displayed a homogeneous surface and a high reflectivity were used for far infrared temperature dependent measurements. Three samples were examined and only the results from the film with the highest reflectance will be presented here.

Reflectance measurements were made at every 10 K below 100 K and for every 25 K for temperatures ranging from 100 K to room temperature. Figure 3.11 shows the resulting spectra. As expected, the reflectance rises as the temperature is lowered. Even though the films are partially transparent their reflectance is still

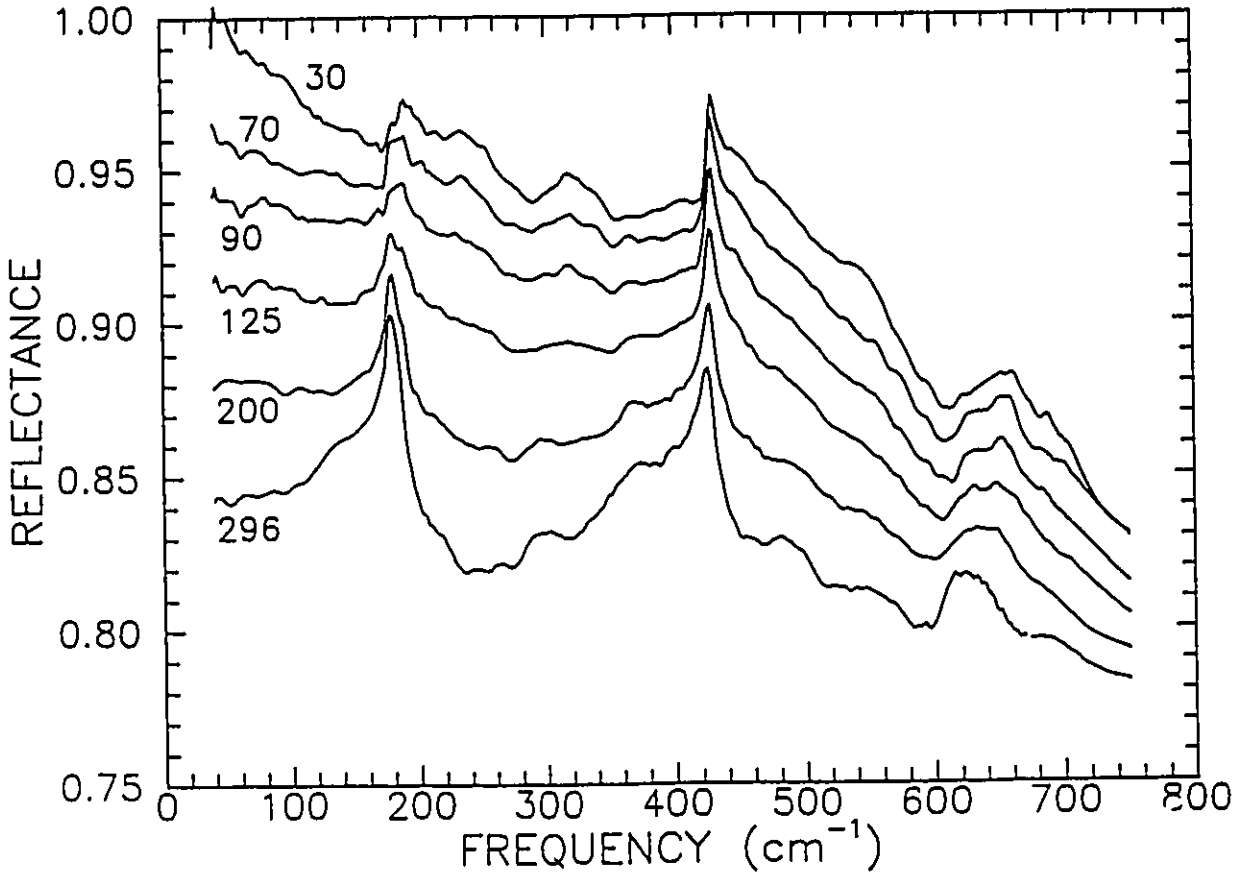

Fig. 3.11 The reflectance spectra as a function of temperature for a 1212 PSYCCO film deposited on a $LaAlO_3$ substrate. The number nearest to the spectrum gives the temperature it was recorded at. The peaks at 180, 425 and 625 cm^{-1} are due to substrate phonons. Note, that below T_c (80 K) the reflectance develops a ledge at 550 cm^{-1} as well as significant curvature at low frequencies. The spectra do not change appreciably below 30 K.

quite high. The peaks at 180, 425 and 625 cm^{-1} are due to substrate phonons. They become less prominent as the temperature is lowered. This is due to the fact that the film is becoming less transparent at lower temperatures and, as a result, the amount of light that reaches the substrate is reduced. The small peak at 320 cm^{-1}, which sharpens as the temperature is lowered, is most likely due to a Cu-O stretching mode in the PSYCCO material. This mode has been observed at similar frequencies for a wide variety of cuprates.[124]

In the normal state the reflectance systematically rises as the temperature is lowered and for all temperatures it approaches a constant value at low frequencies. Qualitatively, this is what is expected for a semi-transparent metallic film which adheres to Drude theory. As the sample enters the superconducting state the reflectance continues to rise at all measured frequencies. The ledge at 550 cm^{-1}, which is barely discernible in the 90 K and 125 K data, becomes more prominent. This is analogous to the temperature dependence of the 450 cm^{-1} ledge observed in $YBa_2Cu_3O_{7-\delta}$ and strongly suggests that they have a common origin. At low frequencies the reflectance develops significant curvature for temperatures below T_c. At 30 K the reflectance shows the presence of two ledges at 50 and 100 cm^{-1}. Below 50 cm^{-1} the reflectance appears to flatten out near the unity level. It is important to realize that the absolute value of the reflectance has an uncertainty of 1 %. Thus, it is unwise to assume that this is a superconducting energy gap without further study.

OPTICAL PROPERTIES OF THE $LaAlO_3$ SUBSTRATE

The Kramers-Kronig transformation given by Eqn. 1.5 is not valid for a semi-transparent film and therefore cannot be used to determine the optical conductivity. As a result we will rely on fits to the reflectance data to obtain quantitative information. In this section the formalism required to extract this information is presented.

The equation describing the reflectance of a semi-transparent film sitting on a substrate can be written in terms of a frequency dependent index of refraction[133] (N=n-ik) and is given by,

$$R = |r|^2 \tag{3.2}$$

where,

$$r = \frac{(r_{32} + r_{21}e^{-i2\beta_2}) + (r_{32}r_{21} + e^{-i2\beta_2})r_{13}e^{-i2\beta_1}}{(1 + r_{32}r_{21}e^{-i2\beta_2}) + (r_{21} + r_{32}e^{-i2\beta_2})r_{13}e^{-i2\beta_1}} \tag{3.3}$$

$$r_{ij} = \frac{n_i - n_j}{n_i + n_j} \tag{3.4}$$

and

$$\beta = \frac{2\pi}{\lambda} n_l d_m \tag{3.5}$$

The subscript 1 refers to substrate, 2 to the film and 3 to vacuum. λ describes the wavelength of the incident radiation in vacuum and d_m is the thickness of layer m. The substrate's optical constants were extracted from an independent measurement which is described below and its thickness, d_1, was measured. Thus, the only remaining unknown variables in the above equations are those associated with the film (n_2, k_2 and d_2). They were determined by fitting the reflectance data to models describing the optical constants.

The far infrared reflectance of $LaAlO_3$ was measured as a function of temperature (see Fig. 3.12). It shows very pronounced features associated with optic phonons. The values of n_1 and k_1 were extracted from the data by fitting it to Lorentzian oscillators. The fitted parameters for all temperatures are given in Table 3.2. Figure 3.13 shows the results for the room temperature data. A comparison between this result and the spectra given in Fig. 3.11 clearly demonstrate that it is the sharp peaks in n_1 and k_1 which give rise to the peaks in the reflectance.

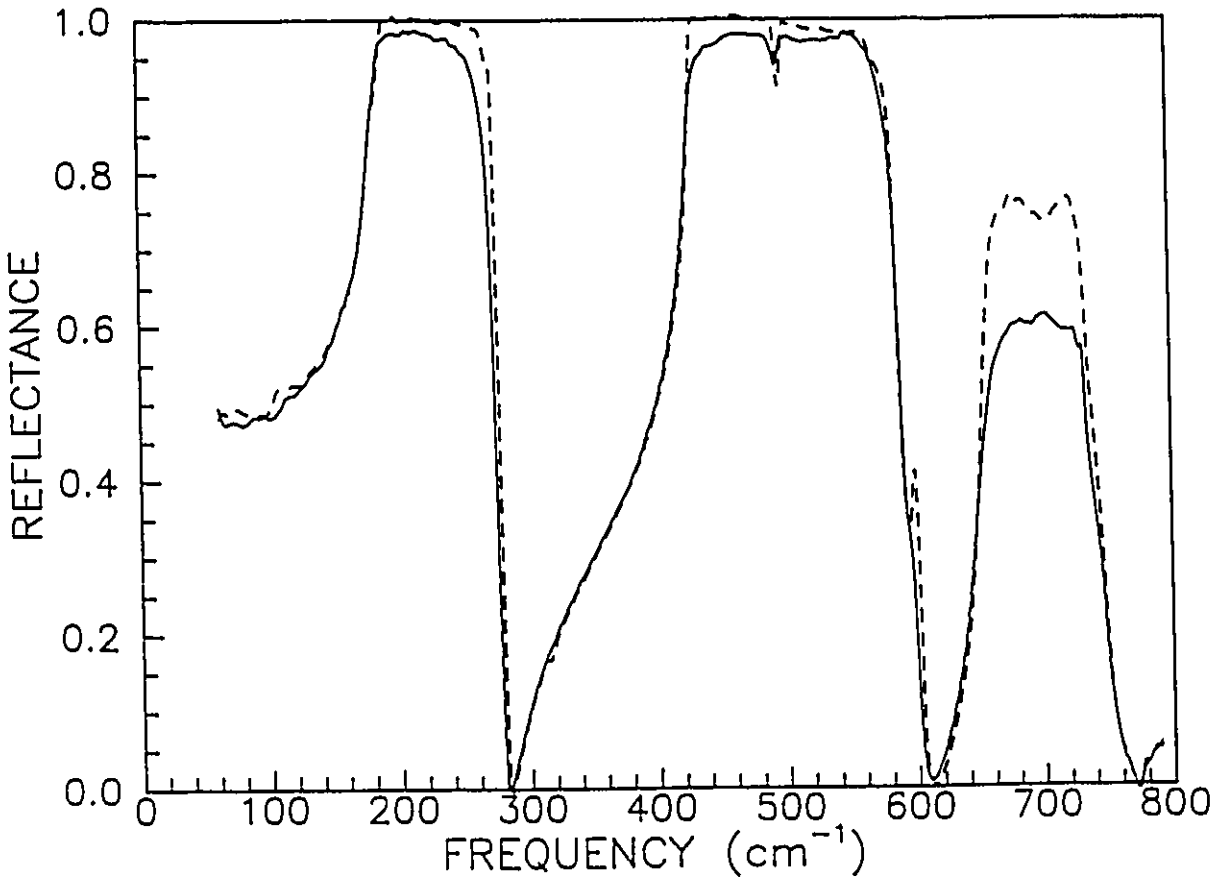

Fig. 3.12 The reflectance of the $LaAlO_3$ substrate at 50 K (dashed) and room temperature (solid).

	296 K	250 K	200 K	150 K	100 K	50 K
ω_{o1}	182	182	184	184	184	183
Γ_1	3.2	2.8	2.5	2.3	1.9	1.5
ω_{p1}	737	742	741	743	746	751
ω_{o2}	428	429	429	429	429	429
Γ_2	1.5	1.5	1.1	0.9	1.8	1.0
ω_{p2}	910	914	915	915	917	922
ω_{o3}	496	496	496	497	498	498
Γ_3	6.7	5.9	5.1	4.3	4.0	3.0
ω_{p3}	60	59	55	56	58	51
ω_{o4}	652	652	653	652	652	651
Γ_4	20	21	18	19	18	18
ω_{p4}	356	367	369	375	376	378
ω_{o5}	684	687	685	695	698	701
Γ_5	44	41	45	31	22	12
ω_{p5}	152	122	117	74	55	33
ϵ_∞	4.5	4.5	4.5	4.5	4.5	4.5

Table 3.2 The parameters describing the five Lorentzian oscillators which are used to fit the reflectance spectra of the $LaAlO_3$ substrate for various temperatures.

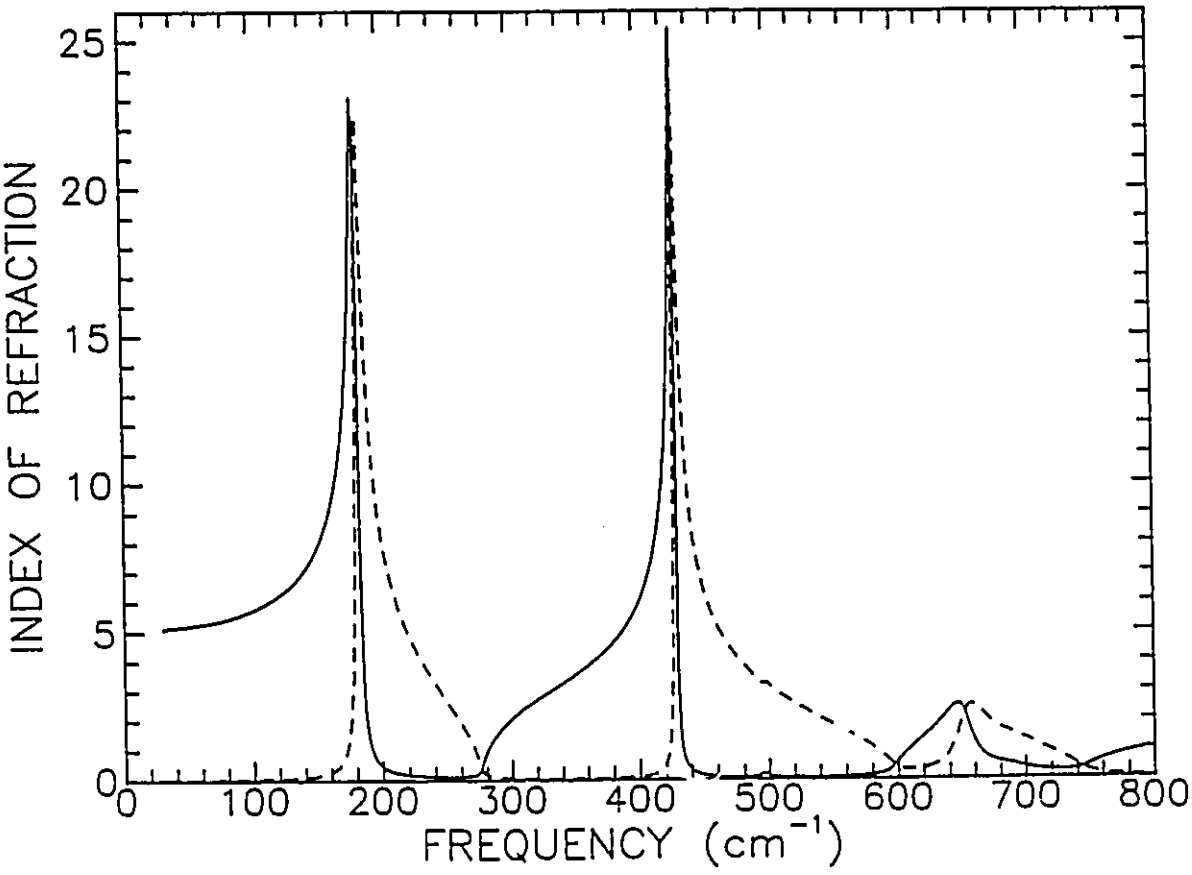

Fig. 3.13 The real (solid) and imaginary (dashed) parts of the index of refraction for the $LaAlO_3$ substrate at room temperature.

PSYCCO ANALYSIS

The normal state reflectance data of the $(Pb_{0.75}Cu_{0.25})Sr_2(Y_{0.4}Ca_{0.6})Cu_2O_7$ film was fit to the same two component model used to describe the $Nd_{1.85}Ce_{0.15}CuO_{4+\delta}$ data. Drude theory accounts for the free electron behaviour while the antiresonance model describes the bound excitations. These two components define the optical constants that yield the reflectance spectra of a two layer system given by Eqn. 3.3. Figure 3.14 shows the fits to the 90 K, 175 K and room temperature data. It is obvious that the fits to the lower temperature data, where the substrate effects play a less dominant role, are superior.

Table 3.3 lists the parameters for the 90 K data describing the broad oscillator and the three phonons which are coupled to it. The Drude component was fit with a plasma frequency of 0.98 eV and a scattering rate of 150 cm^{-1}. Both of these values are typical for an oxide superconductor. A film thickness of 2300 Å and a high frequency dielectric constant of 3.4 were also derived from the fit. Fig. 3.15 shows the conductivity which was generated from these parameters. The figure also shows the two components of the conductivity separately. It is obvious that it shares many similarities with the other oxide superconductors. Once again, a minimum near 400 cm^{-1} is present in the optical conductivity of an oxide superconductor. Fits to the remaining reflectance data yielded the temperature dependence of the fitted parameters. Only the free carrier scattering rate and the strength (ω_{pk}) of the three phonons were allowed to vary. Their temperature dependence will be described below. All other parameters showed little temperature dependence and were held constant for the fits presented here.

As was the case for $Nd_{1.85}Ce_{0.15}CuO_{4+\delta}$, much of the temperature dependence in the normal state's reflectance spectra could be accounted for by allowing the free carrier scattering rate to vary while holding the plasma frequency constant. The temperature dependence of the scattering rate is shown in Fig. 3.16. Like all of the other oxide superconductors the scattering rate shows the same temperature dependence as the dc resistivity. In fact, the dc resistivity derived from the Drude

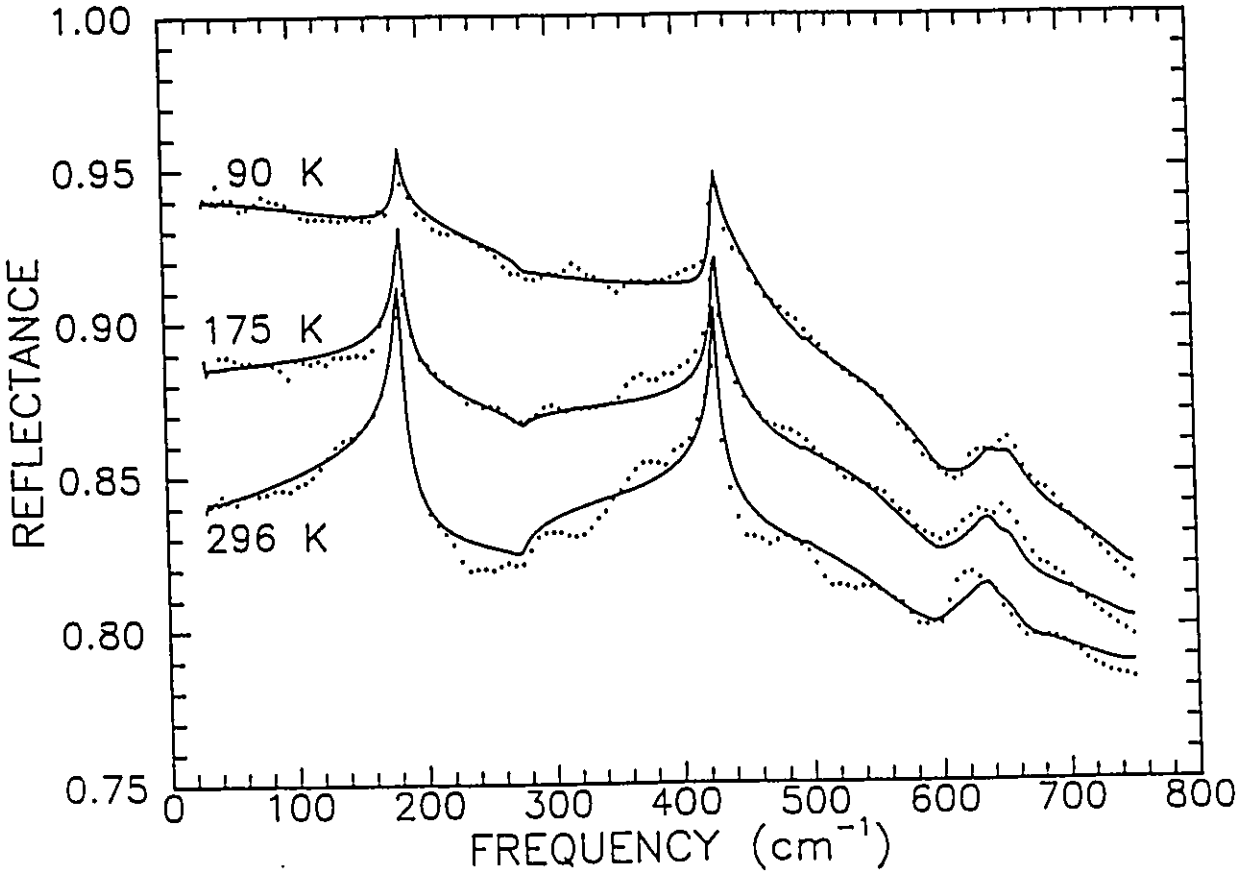

Fig. 3.14 Fits to the reflectance spectra for a 1212 PSYCCO film deposited on a $LaAlO_3$ substrate at 90 K, 175 K and room temperature. The dotted curves are the data and the solid lines are the fits.

	ω_e	ω_{Pe}	Γ_e
mid IR band	826	13540	3353
	ω_k	ω_{Pk}	Γ_k
phonon 1	437	425	75
phonon 2	559	373	120
phonon 3	643	264	20

Table 3.3 The fitted parameters describing the midinfrared band (position = ω_e, strength = ω_{Pe}, width = Γ_e) and the phonons (position = ω_k, strength = ω_{Pk}, width = Γ_k) which are coupled to it. All values are in units of cm^{-1}.

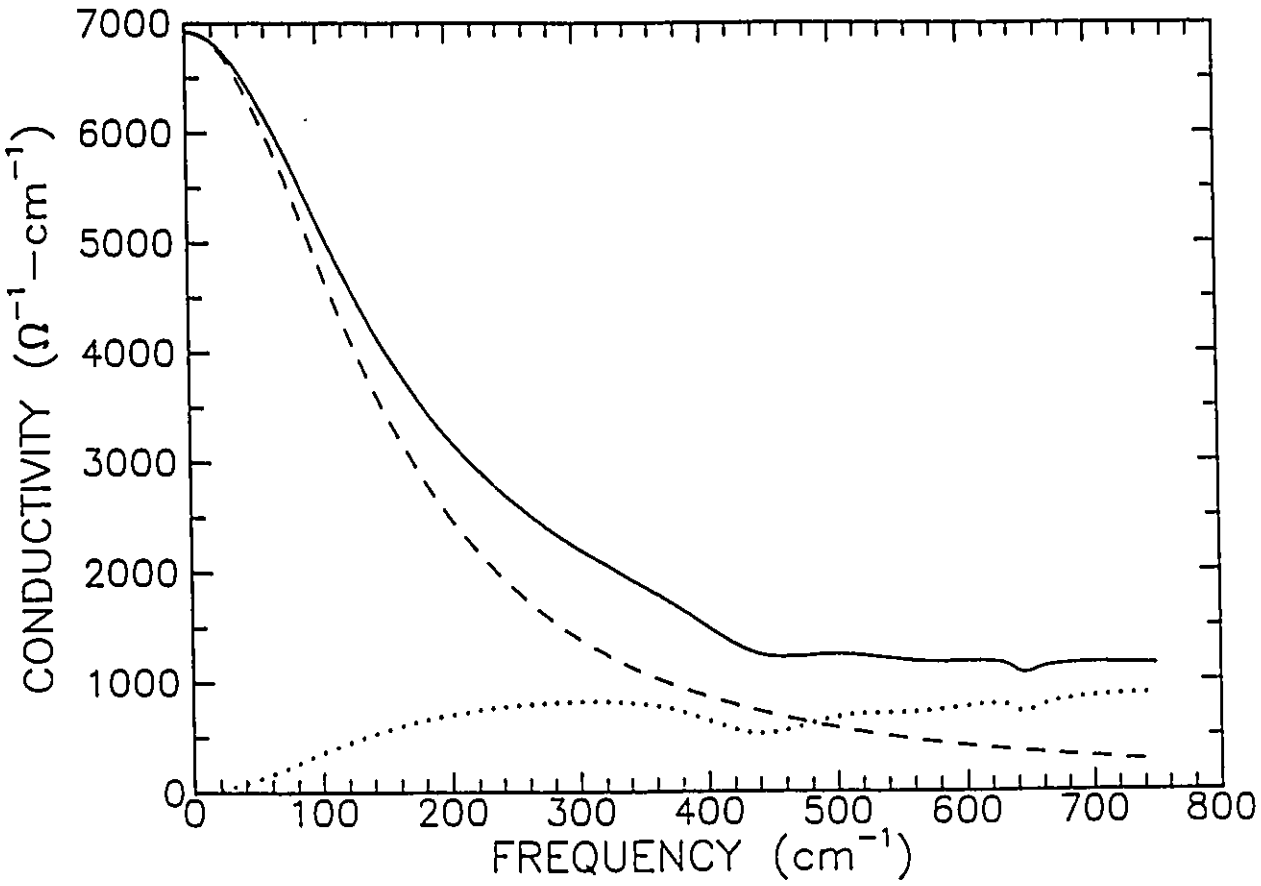

Fig. 3.15 The conductivity for the 90 K normal state data obtained from fits to the reflectance spectum. The solid line shows the total conductivity while the dashed and dotted curves show the conductivity obtained from the Drude and antiresonance model respectively.

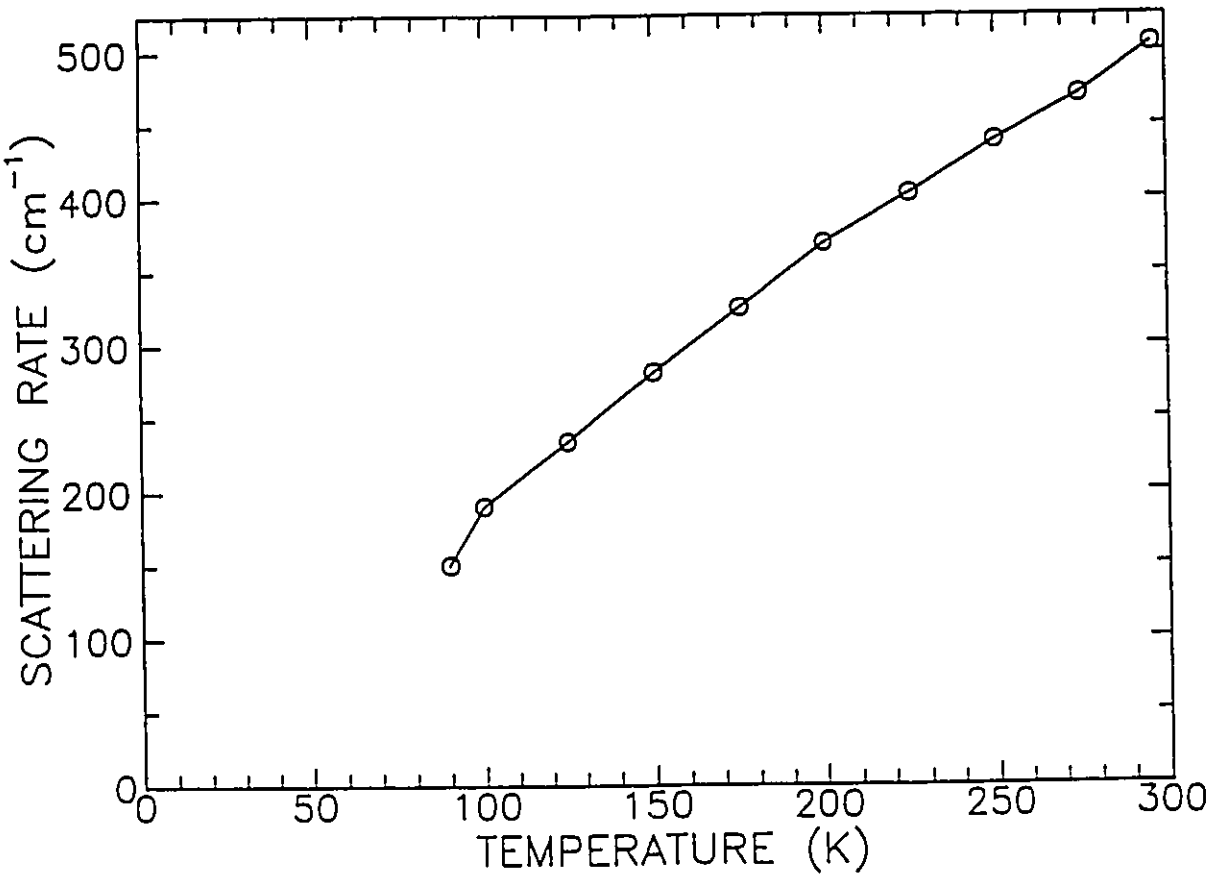

Fig. 3.16 The free carrier scattering rate as a function of temperature for a 1212 PSYCCO film.

parameters match the measured values extremely well. Figure 3.17 shows the comparison. The ability to obtain accurate values for the dc resistivity from these optics measurements is, to a large extent, due to the fact that the measurement was made on a partially transparent film. It exhibits far greater sensitivity to changes in the scattering rate. A simple comparison between the reflectance spectra obtained for the opaque $Nd_{1.85}Ce_{0.15}CuO_{4+\delta}$ film (Fig 3.2) and the partially transparent $(Pb_{0.75}Cu_{0.25})Sr_2(Y_{0.4}Ca_{0.6})Cu_2O_7$ film (Fig. 3.11) demonstrates this point. Both materials have similar scattering rates and plasma frequencies, but at the lowest frequency measured the reflectance varies by nearly 10 % between room temperature and 90 K for the $(Pb_{0.75}Cu_{0.25})Sr_2(Y_{0.4}Ca_{0.6})Cu_2O_7$ film compared to only a few percent for the $Nd_{1.85}Ce_{0.15}CuO_{4+\delta}$ film. Ultimately, it is the size of the response in the reflectivity to changes in the optical constants which determine how accurately they can be determined. Thus, in this case, the partially transparent film has been used to obtain more accurate information.

The three phonons, which are coupled to the broad oscillator, give rise to structure in the reflectance spectra. The highest frequency phonon is responsible for the ledge in the reflectance at 550 cm^{-1}. The effects of the phonons with center frequencies of 437 cm^{-1} and 643 cm^{-1} are made less obvious by the substrate phonons at similar frequencies. The 437 cm^{-1} phonon raises the level of the reflectance for frequencies ranging from 280 to 480 cm^{-1} while the phonon at 643 cm^{-1} broadens the substrate's highest frequency feature. There is absolutely no question that all three phonons are required to maintain the quality of the fit. The temperature dependence of ω_{pk} for the three phonons is shown in Fig. 3.18. Only the 437 cm^{-1} phonon shows a strong temperature dependence. Its strength increases linearly over the entire temperature range. The strength of the other two phonons show little change, although there is some indication that they are weakening at low temperatures. The coupled phonon in $YBa_2Cu_3O_{7-\delta}$ centered at 420 cm^{-1} also shows a strong temperature dependence while the phonons at 225 and 620 cm^{-1} show comparatively little variation with temperature.[34] Thus, it ap-

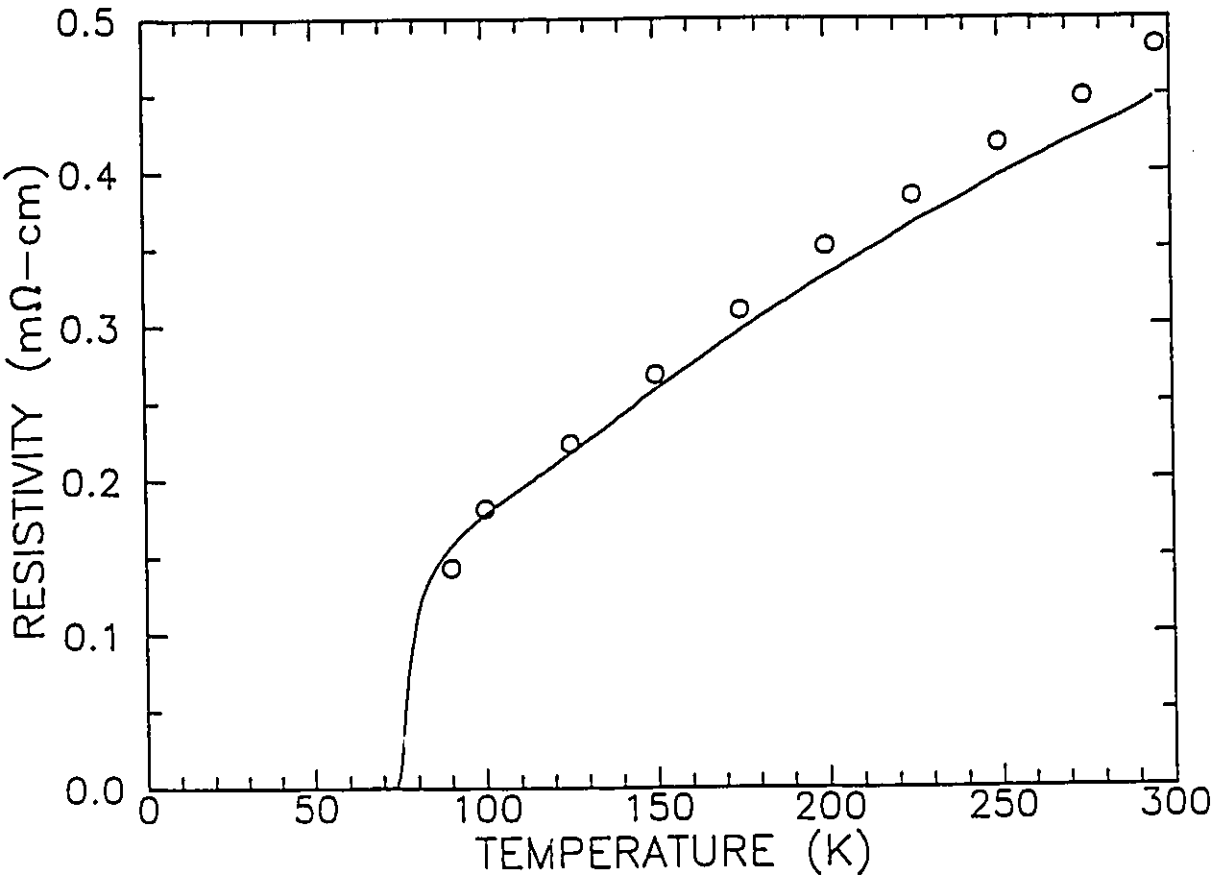

Fig. 3.17 A comparison of the dc resistivity as obtained from transport (solid) and optical (circles) measurements.

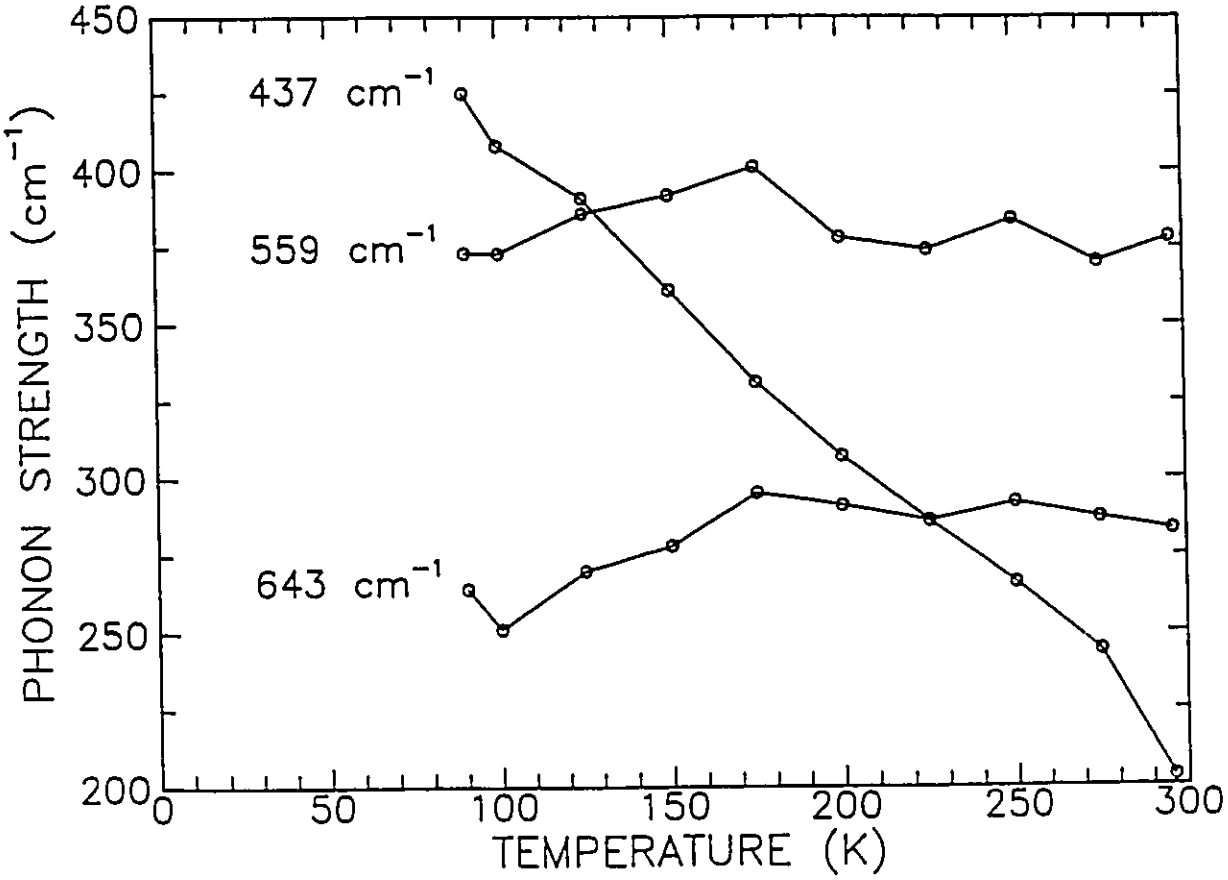

Fig. 3.18 The temperature dependence of the strengths of the three phonons centered at 437, 559 and 643 cm^{-1}. Only the 437 cm^{-1} phonon shows a substantial temperature dependence.

pears that this phonon behaves differently from the other coupled phonons in the high-T_c materials. Since we are relying on fits to specific models to extract these quantities, it is difficult to determine the temperature dependence of the phonon strengths below T_c. In this case, a suitable model describing the superconducting condensate is unavailable.

Past attempts at modeling the superconducting state's far infrared optical properties have resorted to two fluid models. One fluid describes the superconducting condensate while the second fluid describes a normal component. The condensate is modeled with a delta function at zero frequency while the normal component is described by a Drude model. The scattering rate of the normal component quickly collapses as the sample is cooled leaving only the delta function component at the lowest temperatures. This model was successfully used to described the far infrared transmission measurements performed on $Bi_2Sr_2CaCu_2O_8$ single crystals and the results were used as evidence for a collapsing scattering rate which placed the material in the clean limit.[49] The easiest test to determine if this model adequately describes the reflectance spectra of $(Pb_{0.75}Cu_{0.25})Sr_2(Y_{0.4}Ca_{0.6})Cu_2O_7$ is to allow all of the Drude peak's spectral weight to collapse into the delta function at zero frequency. This should yield the relectance spectra for temperatures well below T_c. Figure 3.19 shows a comparison of the 30 K data to the calculated spectra expected if the material is in the clean limit. It is obvious that there are substantial differences between the two results. In fact, all of our attempts to use a two fluid model to fit superconducting state's reflectance spectra have failed. It is impossible to obtain the curvature in the reflectance spectra below 170 cm^{-1} using this model.

The fact that the reflectance is lower than the clean limit demands suggests that part of the Drude spectral weight has not collapsed into the delta function. This implies that $(Pb_{0.75}Cu_{0.25})Sr_2(Y_{0.4}Ca_{0.6})Cu_2O_7$ is not in the clean limit. In an attempt to quantify the distribution of the spectral weight, we have fit the reflectance curves to three components. The first component is a delta function

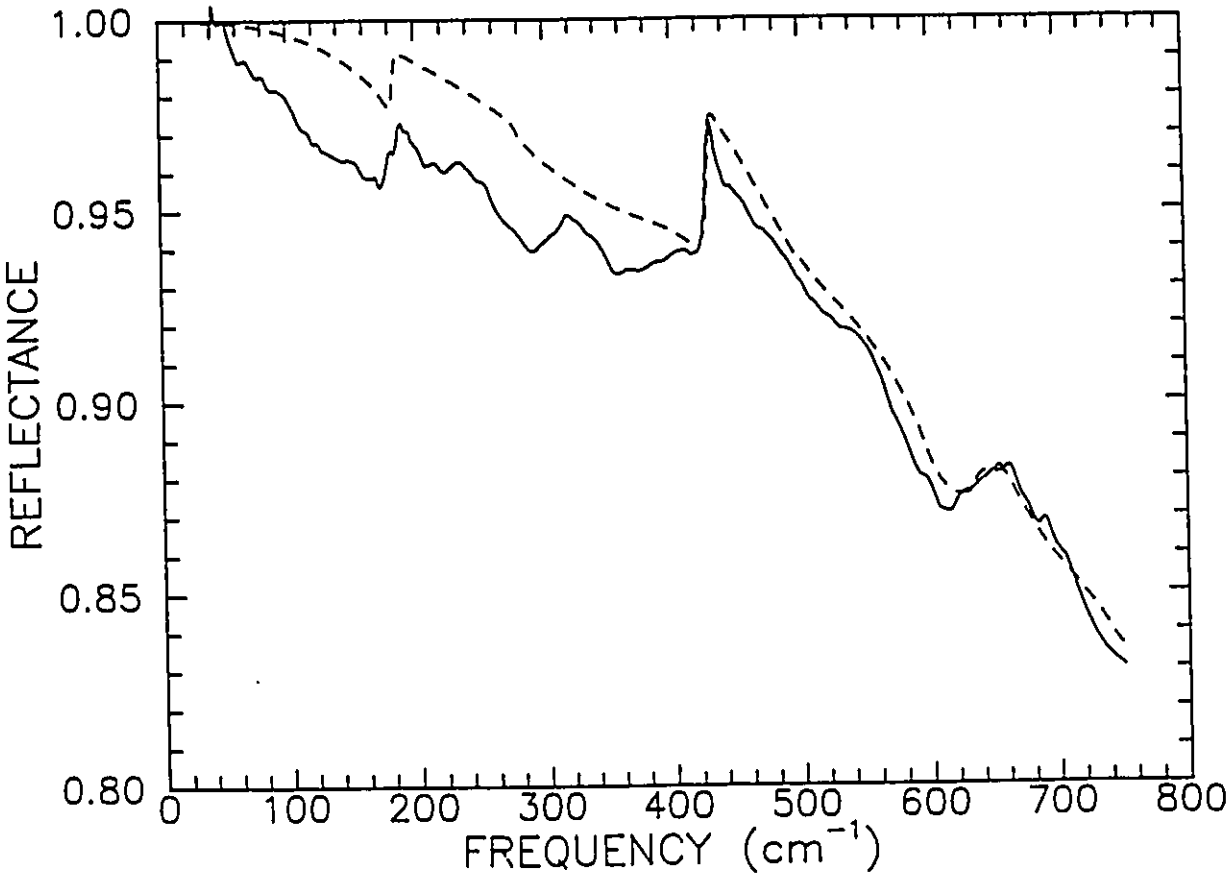

Fig. 3.19 A comparison of the 30 K reflectivity data for a 1212 PSYCCO film deposited on a $LaAlO_3$ substrate compared to the expected result if the film is in the clean limit.

(approximated by an oscillator with a narrow width and centered at zero frequency) which is used to describe the superconducting condensate. The structure observed in the normal state which is associated with the coupled phonons is still present in the superconducting state. The second component uses the parameters given in Table 3.3 to describe this structure. These parameters are all fixed in the fits and any further temperature dependence is not taken into account. Any such temperature dependence would have a minor effect on the results presented below. The final component uses four oscillators to fit any remnants of the normal state Drude peak that have not condensed into the delta function. The oscillators only provide an easy means of fitting the data. It is not our intention to imply that there is a physical process attached to each of these oscillators. It is only the cumulative conductivity that provides a rough estimate of the actual conductivity needed to describe the data.

Figure 3.20 compares the optical conductivity of the oscillator component to the 90 K normal state Drude component. As temperature is lowered oscillator strength is continuously lost from what is left of the Drude component. At all temperatures in the superconducting state the conductivity drops dramatically at low frequencies. Both of these tendencies are exhibited by a dirty limit BCS superconductor. It should be noted that the data cannot be fit to BCS theory because it does exhibit the very pronounced ledge in the reflectance which is characteristic of a BCS energy gap. However, the data strongly points towards gap-like structure at low frequencies with $2\Delta/k_bT_c \leq 1.4$. The accuracy of the reflectivity data is not sufficient to determine whether or not there is a true gap with zero conductivity up to a specific frequency.

According to the oscillator strength sum rule (Eqn. 1.20) the area beneath the conductivity versus frequency curve is proportional to the square of the plasma frequency. Figure 3.21 shows the temperature dependence of this quantity for both the oscillator and delta function components. The sum of the squares of the two components should be constant if, as expected, the oscillator strength that

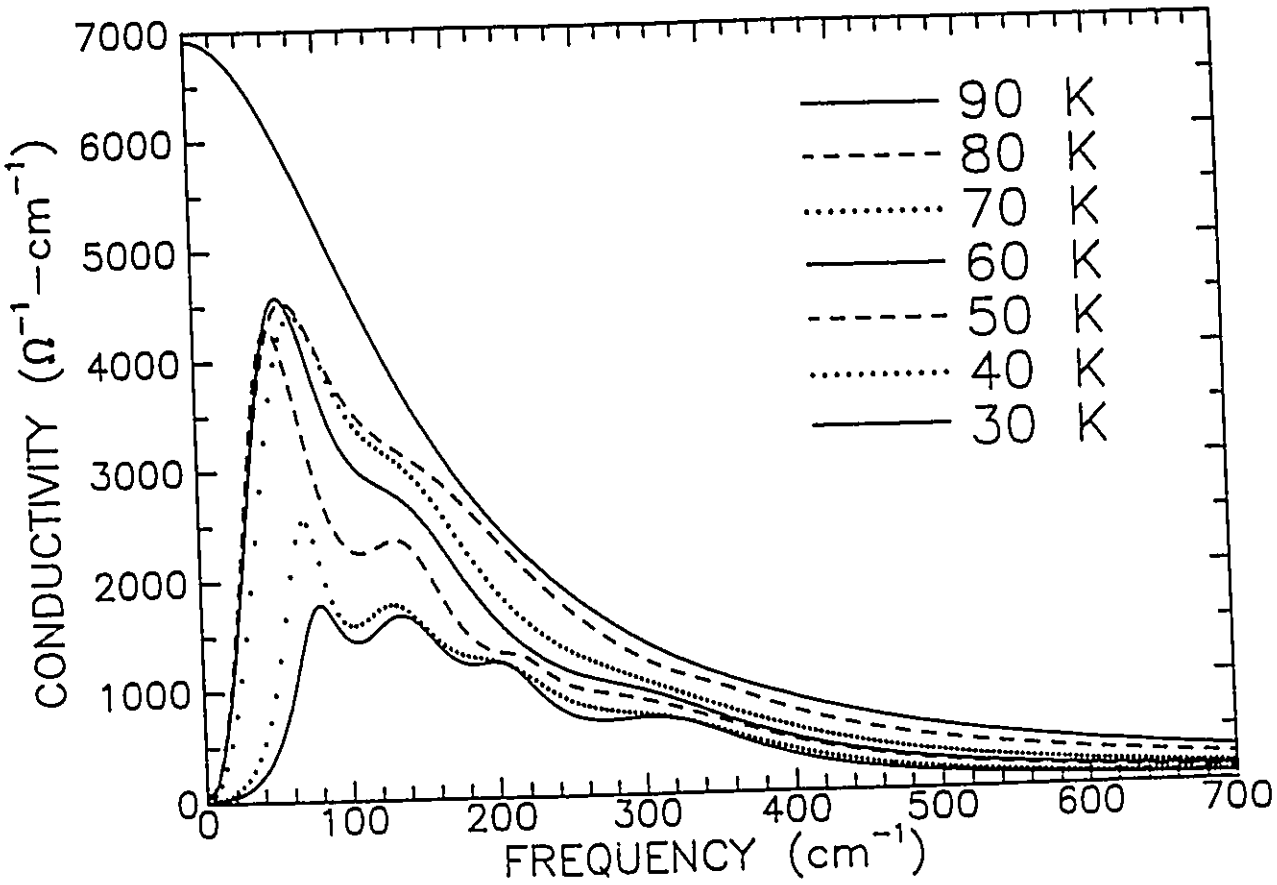

Fig. 3.20 The upper curve shows the normal state Drude component of the optical conductivity for a PSYCCO film at 90 K. As the sample is cooled below T_c much of the oscillator strength condenses into the delta function at zero frequency. The lower curves show the remnants of the Drude peak that have not condensed. A gap-like structure appears at low frequencies.

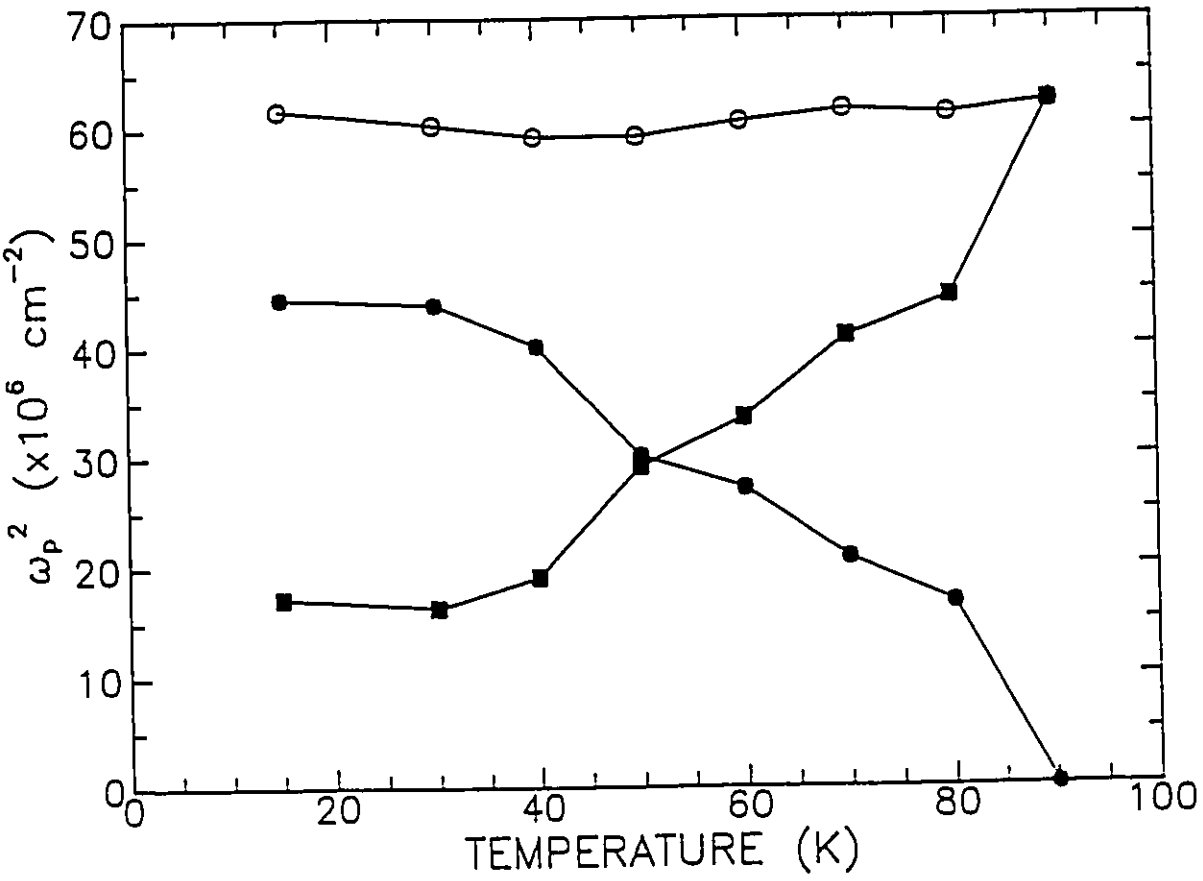

Fig. 3.21 The square of the plasma frequency versus temperature for the delta function (closed circles) and oscillator (squares) components. Note that the sum of the squares of the two components (open circles) is constant.

is lost from the Drude peak ends up in the delta function. The same figure also shows that this requirement is fulfilled. This provides further justification that the fitting procedure used yields an optical conductivity which is approximately correct.

CONCLUSIONS

The work presented here represents the first optical measurements performed on the 1212 PSYCCO superconductor. In the normal state its optical properties are very much like those of the other oxide superconductors. The optical conductivity can be divided into two components. The first component can be described by a Drude model with a scattering rate that closely follows the temperature dependence of the dc resistivity. The second component is described by three phonons which are coupled to a broad midinfrared band. One of the phonons, which is centered at 437 cm^{-1}, shows a linear increase in its strength as temperature is lowered. Below T_c the PSYCCO material behaves differently from the other oxide superconductors. Only a portion of the oscillator strength from the normal state Drude peak ends up in the delta function at zero frequency. Our attempts to model the remaining oscillator strength seem to indicate the presence of a gap-like structure below 80 cm^{-1}. It is obvious that more work is required, but these initial experiments have exposed the intriguing possibility of studying an oxide superconductor which is not in the clean limit.

CHAPTER IV
FINAL REMARKS

In order to obtain a detailed understanding of these high-T_c materials it is necessary to compare as many compounds as possible. These comparisons will expose the common features allowing the emergence of the behaviour needed to induce high temperature superconductivity. It is unwise to rely too heavily on the experiments performed on $YBa_2Cu_3O_{7-\delta}$ because if one of these cuprates is going to be different from the rest it will most likely be $YBa_2Cu_3O_{7-\delta}$ with its unusual chain layer. If this is the case, a tremendous amount of effort has gone into studying the exception rather than the rule. The work presented here has encompassed both sample processing and fundamental research on two superconductors which have received far less attention than the other cuprates. Rather than reiterate the conclusions made in Chapters II and III this work will be concluded by speculating on some future work that is within reach.

PULSED LASER DEPOSITION

Perhaps, the growth of PSYCCO films by pulsed laser deposition offers the most potential for future work. There exists a wide variety of chemical substitutions which have the potential to increase T_c. Liu *et al.*[134] have synthesized polycrystalline PSYCCO samples with a nominal composition of $(Pb_{.5}Cu_{.5})Sr_2(Y_{.5}Ca_{.5})Cu_2O_7$ and a T_c of 66 K. By substituting various rare earth atoms on the yttrium site they were able to vary T_c from 60 K (Tm) to 72 K (Nd). A similar increase in the superconducting transition temperature in our PSYCCO films would give them a T_c equal to that of $YBa_2Cu_3O_{7-\delta}$. A second possibility for increasing T_c is the partial substitution of lead by indium. With this substitution Liu *et al.*[135] were able to increase T_c from 45 to 60 K in polycrys-

talline samples with a nominal composition of $(Pb_{.75}Cu_{.25})Sr_2(Y_{.5}Ca_{.5})Cu_2O_7$. It has also been reported that the replacement of the (Pb,Cu) layer by a (Pb,Cd) layer yields T_c's as high as 92 K.[136] The superconducting transitions for both the indium and cadmium substitutions were poor implying that the samples were not homogeneous. Still, these results give a starting point for future studies using the pulsed laser deposition technique. It has also been suggested that a partial substitution of calcium by sodium could yield a higher T_c.[137] The reasoning behind this substitution was that calcium has a 2+ oxidation state while sodium has a 1+ oxidation state. Thus, each time the substitution is made a carrier is added. Figure 2.10 clearly shows that it is advantageous to increase the number of carriers if a higher T_c is desired. The fact that sodium and calcium atoms have similar radii makes this substitution possible.

In our investigations of $(Pb_{0.75}Cu_{0.25})Sr_2(Y_{1-y}Ca_y)Cu_2O_7$ we observed the onset of superconductivity at temperatures as high as 125 K for a target composition with y = 1. The transitions were broad and the x-ray patterns yielded little information. Thus, we feel that the superconductivity is due to a new phase which comprises a small portion of the total film volume. Obtaining a new phase with a T_c in excess of 120 K that does not contain the toxic element thallium is an intriguing possibility. In the isolation of this phase it may prove advantageous to use two targets. One target would be comprised of the volatile PbO component while the second target would contain the non-volatile elements in stoichiometric proportions. With a single target it is difficult to vary such growth parameters as the substrate temperature, growth rate and the oxygen pressure without altering the amount of lead in the film. Two targets would allow you to freely vary these growth parameters while compensating for excesses or deficiencies in the lead content with the PbO target. This approach has been used by Dubowski[138] to deal with the volatile cadmium component in the laser deposition of $Cd_{1-x}Mn_xTe$.

The surface morphology exhibited by the PSYCCO films is worthy of more attention. In Chapter II it was speculated that the surface morphology, which is

characterized by an array of squares, was due to the differences between the lattice constants of the film and substrate. If the PSYCCO films are grown on a substrate with a smaller lattice mismatch then the squares should become larger. The best test of this hypothesis would be to deposit a PSYCCO film on a PSYCCO single crystal. In this scenario, the lattice match would be perfect and the squares should be eliminated.

With a properly chosen substrate it may be possible to grow untwinned a-axis PSYCCO films. The substrate must have an orthorhombic crystal structure whereby the c-axis of the film prefers to lie along either the a- or b-axis of the substrate. It is far more difficult to obtain this situation for $YBa_2Cu_3O_{7-\delta}$ films since the b-axis is three times the length of the c-axis. Thus, there is no reason for preferential alignment.

$Nd_{1.85}Ce_{0.15}CuO_{4+\delta}$ provides a clear illustration of the problems encountered in the growth of n-type oxide superconductors. Excess oxygen in the crystal structure can reduce the carrier concentration causing a degradation of the superconducting properties. In this work we removed the excess oxygen by high temperature vacuum anneals. The annealing time was optimized to yield the best superconducting properties for a specific sample thickness. This process is unreliable and time consuming. The implementation of an *in situ* non-destructive characterization technique to monitor the anneal would be beneficial. It is obvious that the film is undergoing extensive changes during the anneal as it is transformed from a insulator to a metal. Something as simple as measuring the reflectance of the film at a single laser frequency may provide enough information to determine the optimum anneal time. In fact, a $Nd_{1.85}Ce_{0.15}CuO_{4+\delta}$ film which has been annealed for an excessive period of time is transparent.

In this work we have only investigated one of the possible doping configurations for the Nd_2CuO_4 compound. By varying the Nd/Ce ratio the properties of this compound are dramatically altered. Laser deposition could be used to deposit these samples by simply producing a series of targets with the appropri-

ate neodymium and cerium concentrations. It should also be possible to increase the superconducting transition temperature to 27 K by flourinating the films.[139] Recently, Smith *et al.*[140] have produced polycrystalline pellets of a new n-type superconductor with a composition of $Sr_{1-x}Nd_xCuO_2$. This compound could only be produced by annealing the pellets under a hydrostatic pressure of 25 kbar. It may be possible to mimic their high pressure growth by thin film deposition through the use of a substrate with a lattice parameter that is slightly smaller than that of the $Sr_{1-x}Nd_xCuO_2$ compound.

The highest recorded superconducting transition temperature has not gone up in years. It has become increasingly obvious that the discovery of higher T_c's will require more stringent processing conditions than the simple "shake and bake" approach that was utilized so successfully in the past. The work presented here has demonstrated the ease with which superconducting thin films of $(Pb_{0.75}Cu_{0.25})Sr_2(Y_{1-y}Ca_y)Cu_2O_7$ and $Nd_{1.85}Ce_{0.15}CuO_{4+\delta}$ were grown in comparison to their polycrystalline counterparts. This success shows the power and versatility of the laser deposition process and suggests that it may be extremely useful in the discovery of new superconducting materials.

OPTICAL PROPERTIES

The quality of optical measurements is, to a large extent, determined by the limitations set forth by the samples. Meaningful measurements are only possible if high quality samples are available. If small crystals are used, then the experimental analysis is limited by the poor signal to noise ratio. If films are used, then the signal is greatly enhanced due to their large optically smooth surfaces. The optical measurements performed here on 1212 PSYCCO, as well as similar work done on $YBa_2Cu_3O_{7-\delta}$[130] and $Bi_2Sr_2CaCu_2O_8$,[131,132] demonstrates the main limitation of thin film work. This is the distortions to the reflectivity spectra that arise when the light partially penetrates the film and interacts with the substrate.

This invalidates the Kramers-Kronig relation given by Eqn. 1.5 and forces one to rely on fits to the data using specific models. Thus, subtle features which are not described by the model may be lost in the data analysis. The best solution to this problem is to establish the growth mechanisms limiting the deposition of thicker films and then develop methods to frustrate this process.

The optical measurements performed here on $Nd_{1.85}Ce_{0.15}CuO_{4+\delta}$ do not provide a complete picture. The most obvious shortcoming is the absence of data for temperatures below T_c. These measurements are potentially revealing. The low transition temperature of this material combined with the large scattering rate just above T_c could result in a dirty limit superconductor. If this is the case, then gap structure should be visible. Alternatively, the scattering rate could collapse in a manner similar to that seen in $YBa_2Cu_3O_{7-\delta}$[47] and $Bi_2Sr_2CaCu_2O_8$[49] offering little information about the energy gap. This would be a dramatic effect which would significantly alter the reflectivity even for frequencies as high as 1000 cm^{-1}.

It should pointed out that single bounce reflectance measurements do not provide the best test for a superconducting energy gap. This technique has an uncertainty of 1 % in the absolute value of the reflectance. Thus, trying to determine if a material has unity reflectance is, in some sense, futile. At best, a sample which is cooled below T_c will show a rise in its reflectance at low frequencies followed by the onset of absoption giving rise to a ledge in the reflectance at higher frequencies. In this scenario, one can conclude that the reflectance spectrum is consistent with the formation of an energy gap. Absorption, transmission or multibounce reflectance measurements all provide superior accuracy, but they are far more demanding from both the technical and sample processing viewpoints. Samples which are subject to single bounce reflectance measurements and show features consistent with the formation of an energy gap should be exposed to the more stringent requirements set forth by these alternative experimental techniques.

A measurement of the superconducting state optical properties of $Nd_{1.85}Ce_{0.15}CuO_{4+\delta}$ would also allow for a more complete comparison of the struc-

tures observed in the tunneling conductance and the optical conductivity. In tunneling spectroscopy, it is customary to subtract Δ from the energy scale since structure due to a phonon of frequency Ω in a strongly coupled BCS superconductor appears at energy $\Delta + \Omega$. The agreement between the optical and tunneling conductivity shown in Fig. 3.10 was obtained without shifting the energy axis even though the tunneling data were obtained from the superconducting state while the optical measurements were taken in the normal state. Within the model that we have used, no shift is anticipated. It would be informative to refute or verify this prediction. A measurement of the normal state tunneling conductance may prove equally instructive.

Further optical measurements on the 1212 PSYCCO material could be informative. Here, only a single stoichiometry with the optimum calcium concentration was examined. A measurement of a series of samples with varying carrier concentrations could provide interesting comparisons to similar measurements performed on the LSCO, NCCO and YBCO systems. If the 1212 PSYCCO material behaves like these other systems it would be possible to monitor the formation of the midinfrared band while adjusting T_c to any desired value between zero and 86 K.

The fact that the Drude component does not completely condense into the delta function presents an opportunity to observe structure in the superconducting state that is not present for a superconductor in the clean limit. The gap-like structure observed in the reflectance spectra of $(Pb_{0.75}Cu_{0.25})Sr_2(Y_{0.4}Ca_{0.6})Cu_2O_7$ is worthy of more study. An obvious test of whether this is a superconducting energy gap is to measure the reflectance of PSYCCO films with reduced T_c's to see if the structure moves to lower frequencies. To do this will require that the reflectance data be extended to lower frequencies than those presented here. Until such a test is performed any gap assignments should be viewed with great caution.

CONCLUSION

Since the discovery of high temperature superconductors in 1986, great strides have been made in the understanding of these very complex materials. Nevertheless, a determination of the mechanisms governing superconductivity has eluded researchers. Forty-six years elapsed between the discovery of superconductivity by Kamerlingh Onnes and the announcement of BCS theory by Bardeen, Cooper and Schrieffer. It appears that a theory describing the high-T_c superconductors may prove equally challenging.

REFERENCES

1. H. Kamerlingh Onnes, Comm. Physical Lab., Univ. of Leiden, Suppl. 34b to 133-144, (1911).

2. J.R. Gavaler, Appl. Phys. Lett 23, 480 (1973).

3. J.G. Bednorz and K.A. Müller, Z. Phys. B 64, 189 (1986).

4. H. Takagi, S. Uchida, K. Kitazawa and S. Tanaka, Jap. J. Appl. Phys. Lett. 26, L123 (1987).

5. M.K. Wu, J.R. Ashburn, C.J. Torng, P.H. Hor, R.L. Meng, L. Gao, Z.J. Huang, Y.Q. Wang and C.W. Chu, Phys. Rev. Lett. 58, 908 (1987).

6. R.J. Cava, B. Batlogg, R.B. van Dover, D.W. Murphy, S. Sunshine, T. Siegrist, J.P. Remeika, E.A. Rietmann, S. Zahurak and G.S. Espinosa, Phys. Rev. Lett. 58, 1676 (1987).

7. H. Maeda, Y. Tanaka, M. Fukutomi, and T. Asano, Jap. J. Appl. Phys. Lett 27, L209 (1988).

8. Z.Z. Sheng and A.M. Hermann, Nature 332, 138 (1988)

9. R.J. Cava, B. Batlogg, J.J. Krajewski, L.W. Rupp, L.F. Schneemeyer, T. Siegrist, R.B. van Dover, P. Marsh, W.F. Peck Jr., P.K. Gallagher, S.H. Glarum, J.H. Marshall, R.C. Farrow, J.V. Waszczak, R. Hull and P. Trevor, Nature 336, 211 (1988).

10. Y. Tokura, H. Tagaki and S. Uchida, Nature 337, 345 (1989).

11. F.W. Wooten, Optical Properties of Solids. New York: Academic Press 1972.

12. E.D. Palik, Handbook of the Optical Constants of Solids. Orlando: Academic Press Inc., 1985.

13. R.R. Joyce and P.L. Richards, Phys. Rev. Lett. 24, 1007 (1970).

14. G. Brändli and A.J. Sievers, Phys. Rev. B 5, 3550 (1972).

15. B. Farnworth and T. Timusk, Phys. Rev. B 14, 5119 (1976).

16. J. Bardeen, L.N. Cooper and J.R. Schrieffer, Phys. Rev. 108, 1175 (1957).

17. R.E. Glover III and M. Tinkham, Phys. Rev. 104, 844 (1956).

18. R.E. Glover III and M. Tinkham, Phys. Rev. 108, 243, (1957).

19. D.C. Mattis and J. Bardeen, Phys. Rev. 111, 412 (1958).

20. G.A. Thomas, J. Orenstein, D.H. Rapkine, M. Capizzi, A.J. Millis, R.N. Bhatt, L.F. Schneemeyer and J.V. Waszczak, Phys. Rev. Lett. 61, 1313 (1988).

21. T. Timusk, S.L. Herr, K. Kamarās, C.D. Porter, D.B. Tanner, D.A. Bonn, J.D. Garrett, C.V. Stager, J.E. Greedan and M. Reedyk, Phys. Rev. B 38, 6683 (1988).

22. K. Kamarās, S.L. Herr, C.D. Porter, N. Tache, D.B. Tanner, S. Etemad, T. Venkatesan, E. Chase, A. Inam, X.D. Wu, M.S. Hedge and B. Dutta, Phys. Rev. Lett. 64, 84 (1990).

23. S.L. Cooper, G.A. Thomas, J. Orenstein, D.H. Rapkine, M. Capizzi, T. Timusk, A.J. Millis, L.F. Schneemeyer and J.V. Waszczak, Phys. Rev. B 40, 11358 (1989).

24. K.F. Renk, H. Eschrig, U. Hoffman, J. Keller, J. Schültzmann and W. Ose, Physica C 165, 1 (1990).

25. Z. Schlesinger, R.T. Collins, F. Holtzberg, C. Feild, G. Koren and A. Gupta, Phys. Rev. B 41, 11237 (1990).

26. J. Orenstein, G.A. Thomas, A.J. Millis, S.L. Cooper, D.H. Rapkine, T. Timusk, L.F. Schneemeyer and J.V. Waszczak, Phys. Rev. B 42, 6342 (1990).

27. K.F. Renk, B. Gorshunov, J. Schültzmann, A. Prückl, B. Brunner, J. Betz, S. Orbach, N. Klein, G. Müller and H. Piel, Europhys. Lett. 15, 661 (1991).

28. K. Kamaräs, C.D. Porter, M.G. Doss, S.L. Herr, D.B. Tanner, D.A. Bonn, J.E. Greedan, A.H. O'Reilly, C.V. Stager and T. Timusk, Phys. Rev. Lett 60, 969 (1988).

29. M. Reedyk, D.A. Bonn, J.D. Garrett, J.E. Greedan, C.V. Stager, T. Timusk, K. Kamaräs and D.B. Tanner, Phys. Rev. B 38, 11981 (1988).

30. C.M. Foster, K.F. Voss, T.W. Hagler, D. Mihailović, A.J. Heeger, M.M. Eddy, W.L. Olson, and E.J. Smith, Sol. St. Comm. 76, 651, (1990).

31. M. Reedyk, T. Timusk, J.S. Xue and J.E. Greedan, Phys. Rev. B 45, 7406 (1992).

32. B. Renker, F. Gompf, E. Gering, D. Ewert, H. Rietschel and A. Dianoux, Z. Phys B73, 309 (1988).

33. W. Reichardt, N. Pyka, L. Pintschovius, B. Hennion and G. Collin, Physica C 162-164, 464 (1989).

34. T. Timusk and D.B. Tanner, Physica C 169, 425 (1990).

35. T. Timusk, C.D. Porter and D.B. Tanner, Phys. Rev. Lett. 66, 663 (1992).

36. U. Fano, Phys. Rev. 124, 1866 (1961)

37. Ran Liu, M. Cardona, B. Gegenheimer, E.T. Heyen and C. Thomsen, Phys. Rev. B 40, 2654 (1989).

38. M. Reedyk and T. Timusk, (submitted).

39. M.J. Rice, Phys. Rev. Lett. 37, 36 (1976).

40. R.T. Collins, Z. Schlesinger, F. Holtzberg and C. Field, Phys. Rev. Lett. 63, 422 (1989).

41. T. Pham, H.D. Drew, S.H. Moseley and J.Z. Liu, Phys. Rev. B 41, 11681 (1990).

42. T. Pham, M.W. Lee, H.D. Drew, U. Welp and Y. Fang, Phys. Rev. B 44, 5377 (1991).

43. Z. Schlesinger, R.T. Collins, D.L. Kaiser and F. Holtzberg, Phys. Rev. Lett. 59, 1958 (1987).

44. J. Schützmann, W. Ose, J. Keller, K.F. Renk, B. Roas, L. Schultz and G. Saemann-Ischenko, Europhys. Lett. 8, 679 (1989).

45. R.A. Hughes, T. Timusk, S.L. Cooper, G.A. Thomas, J.J. Yeh and M. Hong, Phys. Rev. B 40, 5162 (1989).

46. L. Forro, G.L. Carr, G.P. Williams, D. Mandrus and L. Mihaly, Phys. Rev. Lett. 65, 1941 (1990).

47. D.A. Bonn, P. Dosanjh, R. Liang, W.N. Hardy, (submitted).

48. D.B. Romero, G.L. Carr, D.B. Tanner, L. Forro, D. Mandrus, L. Mihaly, and G.P. Williams, Phys. Rev. 44, 2818 (1991).

49. D.B. Romero, C.D. Porter, D.B. Tanner, L. Forro, D. Mandrus, L. Mihaly, G.L. Carr and G.P. Williams, Phys. Rev. Lett. 68, 1590 (1991).

50. M.A. Subramanian, J. Gopalakrishnan, C.C. Torardi, P.L. Gai, E.D. Boyes, T.R. Askew, R.B. Flippen, W.E. Farneth, and A.W. Sleight, Physica C 157, 124 (1989).

51. J.Y. Lee, J.S. Swinnea and H. Steinfink, J. Mater. Res. 4, 763 (1989).

52. X.X. Tang, D.E. Morris and A.P.B. Sinha, Phys. Rev. B 43, 7936 (1991).

53. T. Maeda, K. Sakuyama, S. Koriyama, H. Yamauchi and S. Tanaka, Phys. Rev. B 43, 7866 (1991).

54. T. Rouillon, J. Provost, M. Hervieu, D. Groult, C. Michel and B. Raveau, Physica C 159, 201 (1989).

55. H. Tagaki, S. Uchida and Y. Tokura, Phys. Rev. Lett. 62, 1197 (1989).

56. Z.Z. Wang, T.R. Chien, N.P. Ong, J.M. Tarascon and E. Wang, Phys. Rev. B 43, 3020 (1991).

57. C.C. Tsuei, A. Gupta and G. Koren, Physica C 161, 415 (1989).

58. S.L. Cooper, G.A. Thomas, J. Orenstein, D.H. Rapkine, A.J. Millis, S. Cheong, A.S. Cooper and Z. Fisk, Phys. Rev. B 41, 11605, (1990).

59. Ji-Guang Zhang, Xiang-Xin Bi, E. McRae, P.C. Eklund, B.C. Sales and M. Mostoller, Phys. Rev. B 43, 5389 (1991).

60. K. Hirochi, S. Hayashi, H. Adachi, T. Mitsuyu, T. Hirao, K. Setsune and K. Wasa, Physica C 160, 273 (1989).

61. S. Lupi, P. Calvani, M. Capizzi, P. Maselli, W. Sadowski and E. Walker, Phys. Rev. B (to be published).

62. E.V. Abel', V.S. Bagaev, D.N. Basov, O.V. Dolgov, A.F. Plotnikov, A.G. Poiarkov and W. Sadovsky, Sol. St. Comm. 79, 931 (1991).

63. S. Uchida, T. Ido, H. Takagi, T. Arima, Y. Tokura and S. Tajima, Phys. Rev. B 43, 7942 (1991).

64. S.H. Wang, Q. Song, B.P. Clayman, J.L. Peng, L. Zhang and R.N. Shelton, Phys. Rev. Lett. 64, 1067 (1990).

65. L. Degiorgi, S. Rusiecki and P. Wachter, Physica C 161, 239 (1989).

66. D.A. Bonn, J.E. Greedan, C.V. Stager, T. Timusk, M.G. Doss, S.L. Herr, K. Kamarās, C.D. Porter, D.B. Tanner, J.M. Tarascon, W.R. McKinnon and L.H. Greene, Phys. Rev. B 35, 8843 (1987).

67. M.S. Sherwin, P.L. Richards and A. Zettl, Phys. Rev. B 37, 1587 (1987).

68. S.D. Brorson, A. Kazeroonian, J.S. Moodera, D.W. Face, T.K. Cheng, E.P. Ippen, M.S. Dresselhaus and G. Dresselhaus, Phys. Rev. Lett. 64, 2172 (1990).

69. D. Dijkkamp, T. Venkatesan, X.D. Wu, S.A. Shaheen, N. Jisrawi, Y.H. Min-Lee, W.L. McLean and M. Croft, Appl. Phys. Lett. 51, 619 (1987).

70. X.D. Wu, A. Inam, T. Venkatesan, C.C. Chang, E.W. Chase, P. Barboux, J.M. Tarascon and B. Wilkens, Appl. Phys. Lett. 52, 754 (1988).

71. A. Inam, X.D. Wu, T. Venkatesan, S.B. Ogale, C.C. Chang and D. Dijkkamp, Appl. Phys. Lett. 51, 1112 (1987).

72. D.B. Geohegan, D.N. Mashburn, R.J. Culbertson, S.J. Pennycook, J.D. Budai, R.E. Valiga, B.C. Sales, D.H. Lowndes, L.A. Boatner, E. Sonder, D. Eres, D.K. Christen and W.H. Christie, J. Mat. Res. 3, 1169 (1988).

73. D.S. Misra and S.B. Palmer, Physica C 176, 43 (1991).

74. W. Kautek, B. Roas and L. Schultz, Thin Solid Films, 191, 317 (1990).

75. D.B. Geohagen, J. Mater. Educ. 12, 383 (1990).

76. G. Koren, R.J. Baseman, A. Gupta, M.I. Lutwyche and R.B. Laibowitz, Appl. Phys. Lett. 56, 2144 (1990).

77. H. Dupendant, J.P. Gavigan, D. Givord, A. Lienard, J.P. Rebouillat and Y. Souche, Applied Surface Science, 43, 369 (1989).

78. T. Venkatesan, X.D. Wu, A. Inam and J.B. Wachtman, Appl. Phys. Lett. 52, 1193 (1988).

79. S.R. Foltyn, R.C. Dye, K.C. Ott, E. Peterson, K.M. Hubbard, W. Hutchinson, R.E. Muenchausen, R.C. Estler and X.D. Wu, Appl. Phys. Lett. 59, 595 (1991).

80. A. Cohen, P. Allenspacher, M.M. Brieger, I. Jeuck and H. Opower, Appl. Phys. Lett. 59, 2186 (1991).

81. O. Eryu, K. Murakami, K. Masuda, A. Kasuya and Y. Nishina, Appl. Phys. Lett. 54, 2716 (1989).

82. M.G. Norton and C.B. Carter, Journal of Crystal Growth, 110, 641 (1991).

83. W.Y. Lee, J. Salem, V. Lee, T. Huang, R. Savoy, V. Deline and J. Duran, Appl. Phys. Lett. 52, 2263 (1988).

84. T. Venkatesan, E.W. Chase, X.D. Wu, A. Inam, C.C. Chang and F.K. Shokoohi, Appl. Phys. Lett. 53, 243 (1988).

85. M. Aslam, R.E. Soltis, E.M. Logothetis, R. Ager, M. Mikkor, W. Win, J.T. Chen and L.E. Wenger, Appl. Phys. Lett. 53, 153 (1988).

86. M.R. Rao, E.J. Tarsa, L.A. Samoska, J.H. English, A.C. Gossard, H. Kroemer, P.M. Petroff and E.L. Hu, Appl. Phys. Lett. 56, 1905 (1990).

87. M. Naito, R.H. Hammond, B. Oh, M.R. Hahn, J.W.P. Hsu, P. Rosenthal, A.F. Marshall, M.R. Beasley, T.H. Geballe and A. Kapitulnik, J. Mat. Res. 2, 713 (1987).

88. X.D. Wu, R.C. Dye, R.E. Muenchausen, S.R. Foltyn, M. Maley, A.D. Rollett, A.R. Garcia and N.S. Nogar, Appl. Phys. Lett. 58, 2165 (1991).

89. P. Merchant, R.D. Jacowitz, K. Tibbs, R.C. Taber and S.S. Laderman, Appl. Phys. Lett. 60, 763 (1992).

90. R.W. Simon, C.E. Platt, A.E. Lee, G.S. Lee, K.P. Daly, M.S. Wire, J.A. Luine and M. Urbanik, Appl. Phys. Lett. 53, 2677 (1988)

91. M. Mukaida, S. Miyazawa, M. Sasaura and K. Kuroda, Jap. J. Appl. Phys. 29, L936 (1990).

92. S. Miyawzawa, Appl. Phys. Lett. 55, 2230 (1989).

93. C.C. Chang, X.D. Wu, R. Ramesh, X.X. Xi, T.S. Ravi, T. Venkatesan, D.M. Hwang, R.E. Meunchausen, S. Foltyn and N.S. Nogar, Appl. Phys. Lett. 57, 1814 (1990).

94. R. Ramesh, A. Inam, D.M. Hwang, T.D. Sands, C.C. Chang and D.L. Hart, Appl. Phys. Lett. 58, 1557 (1991).

95. C. Gerber, D. Anselmetti, J.G. Bednorz, J. Mannhart and D.G. Schlom, Nature, 350, 279 (1991).

96. M. Hawley, I.D. Raistrick, J.G. Beery and R.H. Houlton, Science 251, 1587 (1991).

97. H.U. Krebs, C. Krauns, X. Yang and U. Geyer, Appl. Phys. Lett. 59, 2180 (1991).

98. J.M. Triscone, O. Fischer, O. Brunner, L. Antognazza, A.D. Kent and M.G. Karkut, Phys. Rev. Lett. 64, 804 (1990).

99. Q. Li, X.X. Xi, X.D. Wu, A. Inam, S. Vadlamannati, W.L. McLean, T. Venkatesan, R. Ramesh, D.M. Hwang, J.A. Martinez and L. Nazar, Phys. Rev. Lett. 64, 3086 (1990).

100. D.H. Lowndes, D.P. Norton and J.D. Budai, Phys. Rev. Lett. 65, 1160 (1990).

101. L. Luo, X.D. Wu, R.C. Dye, R.E. Muenchausen, S.R. Foltyn, Y. Coulter, C.J. Maggiore and T. Inoue, Appl. Phys. Lett. 59, 2043 (1991).

102. A. Inam, C.T. Rogers, R. Ramesh, K. Remschnig, L. Farrow, D. Hart, T. Venkatesan and B. Wilkens, Appl. Phys. Lett. 57, 2484 (1990).

103. R. Ramesh, C.C. Chang, T.S. Ravi, D.M. Hwang, A. Inam, X.X. Xi, Q. Li, X.D. Wu and T. Venkatesan, Appl. Phys. Lett. 57, 1064 (1990).

104. G. Linker, X.X. Xi, O. Meyer, Q. Li, and J. Geerk, Sol. St. Comm. 69, 249 (1989).

105. A. Gupta, G. Koren, R.J. Baseman, A. Segmüller and W. Holber, Physica C 162-164, 127 (1989).

106. D.H.A. Blank, D.J. Adelerhof, J. Flokstra and H. Rogalla, Physica C 162, 125 (1989).

107. J.E. Andrew, P.E. Dyer, R.D. Greenough and P.H. Key, Appl. Phys. Lett. 43, 1076 (1983).

108. J.L. Vossen, in "Adhesion Measurement of Thin Films, Thick Films and Bulk Coatings", edited by K.L. Mittal (ASTM STP), 122 (1978).

109. G. Koren, A. Gupta, R.J. Baseman, M.I. Lutwyche and R.B. Laibowitz, Appl. Phys. Lett. 55, 2450 (1989).

110. R. Ramesh, A. Inam, W.A. Bonner, P. England, B.J. Wilkens, B.J. Meagher, L. Nazar, X.D. Wu, M.S. Hedge, C.C. Chang, T. Venkatesan and H. Padamsee, Appl. Phys. Lett. 55, 1138 (1989).

111. G. Koren, A. Gupta, E.A. Giess, A. Segmüller and R.B. Laibowitz, Appl. Phys. Lett. 54, 1054 (1989).

112. J. Gao, Y.Z. Zhang, B.R. Zhao, P. Out, C.W. Yuan and L. Li, Appl. Phys. Lett., 53, 2675 (1988).

113. K.H. Wu, C.L. Lee, J.Y. Juang, T.M. Uen and Y.S. Gou, Appl. Phys. Lett., 58, 1089 (1991).

114. J.S. Horwitz, D.B. Chrisey, M.S. Osofsky, K.S. Grabowski and T.A. Vanderah, J. Appl. Phys. 70, 1045 (1991).

115. A. Gupta, G. Koren, C.C. Tsuei, A. Segmüller and T.R. McGuire, Appl. Phys. Lett. 55, 1795 (1989).

116. A. Kussmaul, J.S. Moodera, P.M. Tedrow, A. Gupta and C.C. Tsuei, IEEE Transactions on Magnetics 27, 1325 (1991).

117. J.H. Claassen, M.E. Reeves and R.J. Soulen, Jr., Rev. Sci. Instr. 62, 996 (1991).

118. S. Hayashi, H. Adachi, K. Setsune, T. Hirao and K. Wasa, Jap. J. Appl. Phys. 28, L962 (1989).

119. T.C. Huang, E. Moran, A.I. Nazzal and J.B. Torrance, Physica C 158, 148 (1989).

120. J.H. Kim, I. Bozovic, J.S. Harris, Jr., W.Y. Lee, C.B. Eom and T.H. Geballe (preprint).

121. S. Tajima, H. Ishii, T. Nakahashi, T. Takagi, S. Uchida, M. Seki, S. Suga, Y. Hidaka, M. Suzuki, T. Murakami, K. Oka and H. Unoki, J. Opt. Soc. Am. B 6, 475 (1989).

122. S. Kubo and M. Suzuki, Physica C 185-189, 1251 (1991).

123. J.W. Lynn, I.W. Sumarlin, D.A. Neumann, J.J. Rush, J.L. Peng, and Z.Y. Li, Phys. Rev. Lett. 66, 919 (1991).

124. S. Tajima, T. Ido, S. Ishibashi, T. Itoh, H. Eisaki, Y. Mizuo, T.Arima, H. Takagi and S. Uchida, Phys. Rev. B 43, 10496 (1991).

125. Q. Huang, J.F. Zasadzinski, N. Tralshawala, K.E. Gray, D.G. Hinks, J.L. Peng and R.L. Greene, Nature 347, 369 (1990).

126. J.M. Rowell and W.L. McMillan, Phys. Rev. Lett. 16, 453 (1966).

127. E.L. Wolf, *Principles of Electron Tunneling Spectroscopy* (Oxford University Press, New York, 1985).

128. P.B. Allen, Phys. Rev. B 3, 305 (1971).

129. P. Calvani, M. Capizzi, F. Donato, P. Dore, S. Lupi, P. Maselli and C.P. Varsamis, Physica C. 181, 289 (1991).

130. D. van der Marel, H.U. Habermeier, D. Heitmann, W. König and A. Wittlin, Physica C 176, 1 (1991).

131. A.M. Rao, P.C. Eklund, G.W. Lehman, D.W. Face, G.L. Doll, G. Dresselhaus and M.S. Dresselhaus, Phys. Rev. B 42, 193 (1990).

132. P. Calvani, M. Capizzi, S. Lupi, P. Maselli and E. Agostinelli, Physica C 180, 116 (1991).

133. L. Ley, in Topics in Applied Physics, edited by J.D. Joannopoulos and G. Lucovsky (Springer-Verlag, New York, 1984) p. 61.

134. H.B. Liu and D.E. Morris, Phys. Rev. B 44, 5369 (1991).

135. R.S. Liu, S.F. Hu, I. Gameson, S.D. Obertelli, P.P. Edwards, D.A. Jefferson, T. Rouillon, M. Hervieu, C. Michel, D. Groult, J. Provost and B. Raveau, Physica C 190, 99 (1991).

136. T.P. Beales, C. Dineen, W.G. Freeman, S.R. Hall, M.R. Harrison, D.M. Jacobson and S.J. Zammattio, Superconductor Science and Technology, 5, 47 (1992).

137. J. Greedan (private communication)

138. J.J. Dubowski, J. Cryst. Growth 101, 105 (1990).

139. A.C.W.P. James, S.M. Zahurak and D.W. Murphy, Nature 338, 240 (1989).

140. M.G. Smith, A. Manthiram, J. Zhou, J.B. Goodenough and J.T. Markert, Nature 351, 549 (1991).